Quaternary evolution of the Corinth Rift and its implications for the Late Cenozoic evolution of the Aegean

Rolando Armijo, B. Meyer, G. C. P. King, Alexis Rigo, D. Papanastassiou

Geophys. J. Int. (1996) **126,** 11–53

Quaternary evolution of the Corinth Rift and its implications for the Late Cenozoic evolution of the Aegean

R. Armijo,[1] B. Meyer,[1] G. C. P. King,[2] A. Rigo[1] and D. Papanastassiou[3]

[1] *Institut de Physique du Globe de Paris, CNRS-URA* 1093, 4 *place Jussieu,* 75252 *Paris Cedex* 05, *France*

[2] *Institut de Physique du Globe,* 5 *rue Descartes,* 67084 *Strasbourg, France*

[3] *National Observatory of Athens,* PO Box 20048, 11810 *Athens, Greece*

Accepted 1995 December 22. Received 1995 December 2; in original form 1995 June 26

SUMMARY

We present geological and morphological observations at different scales to constrain rates of faulting and the distribution of deformation in the seismically active Aegean region. We focus first on the 130 km long Corinth Rift, an asymmetric graben where a flight of terraces of marine origin are uplifted. We show that the edges of the terraces lie in the footwall of the normal fault bounding the Corinth Rift and correspond to sea-level highstands of late Pleistocene age. Using a detailed analysis of aerial and SPOT imagery supported by field observations, we have mapped 10 terrace platforms and strandlines ranging in elevation from 10 to 400 m over distances of 2 to 20 km from the fault. The elevation of the terraces' inner edges was estimated at 172 sites with an error of ± 5 m. This data set contains a precise description of the uplift and flexure of 10 different palaeohorizontal lines with respect to the present sea level. To date the deformation, we correlate the Corinth terraces with late Pleistocene oxygen-isotope stages of high sea-level stands and with global sea-level fluctuations. Using a thick elastic plate model consistent with our current understanding of the earthquake cycle and a boundary-element technique we reproduce the geometry of the shorelines to constrain both mechanical parameters and the slip on the fault. We show that the seismogenic layer behaves over the long term as if its elastic modulus were reduced by a factor of about 1000. All the terraces are fitted for fault slip increasing in proportion to terrace age, and the component of regional uplift is found to be less than 0.3 mm yr^{-1}. The best fits give a slip rate of 11 ± 3 mm yr^{-1} on the main rift-bounding fault over the last 350 kyr. Other geological and morphologic information allows us to estimate the total age of the main fault (≈ 1 Ma) and to examine the mechanical evolution of the Corinth Rift. The minimum observed sediment thickness in the Gulf places an extreme check on the results of the modelling and a lower bound on slip rate of 6–7 mm yr^{-1} (40 per cent less than estimated with modelling). Even this slip rate is nearly 10 times higher than for comparable features in most of the Aegean and elsewhere in the world.

At a larger scale, the spacing and asymmetry of the rift systems in the Aegean suggest strain localization in the upper mantle, with slow extension starting 15 Myr ago or earlier. The more recent (1 Myr), rapid phase of rifting in Corinth partly reactivated this earlier phase of extension. The younger faulting in Corinth appears to result from its present location in the inhomogeneous stress field (process zone) of the south-westward propagating tip of the southern branch of the North Anatolian Fault. We extend these relations to propose a mechanical model for the Late Cenozoic evolution of the Aegean. As the Arabia/Europe collision progressed in eastern Turkey it caused Anatolia to move to the west and the North Anatolian Fault to propagate into the Aegean, where the early slow extension started to be modified about 5 Ma ago. The process of propagation dramatically increased the activity of some but not all of the earlier rifts. The model we present is compatible with tectonic observations, as well as with the seismicity, the palaeomagnetic rotations and the displacement field now observed with GPS and SLR.

1 INTRODUCTION

We examine aspects of the evolution of the Aegean from the Late Tertiary to the Present using a combination of geological, geomorphic, geodetic and seismic information. The overall purpose of the study is to understand the mechanical processes occurring at scales ranging from a few kilometres to several hundred kilometres. We are guided by two concepts in our interpretation of the present activity and geological history of the region. The first is that geological structures must evolve in a way that is consistent with our understanding of the earthquake cycle. We therefore treat the crust as behaving as an elastic plate overlying a viscoelastic lower crust. This is a simplification, since non-Newtonian flow must occur in the lower crust and it may retain significant long-term strength. The second concept is that faults evolve by a process of propagation. At smaller scales the processes can be restricted to the crust, but at larger scales the rupture propagation process must involve the upper mantle. Among other observations, this strongly supports the view that localization processes are important in the mechanical behaviour of the continental lithosphere.

The Aegean region is one of the most active extensional continental regions in the world (e.g. McKenzie 1972, 1978; Mercier, Sorel & Vergely 1977; Le Pichon & Angelier 1981; Angelier *et al.* 1982; Jackson & McKenzie 1988), yet many of the most stretched areas are under the sea and thus difficult to observe (Fig. 1). Although its bottom has long since subsided below sea level, the Gulf of Corinth is probably the most prominent rift in the region that is accessible to detailed surface observation. The geological record of vigorous Quaternary normal faulting in the Gulf of Corinth (Sébrier 1977) and the high level of historical and instrumental seismicity (Papazachos & Papazachos 1989; Papazachos & Kiratzi 1992; Ambraseys & Jackson 1990) attest to a high rate of extension. Present deformation retrieved from re-measurement, in 1988, of old geodetic benchmarks (installed during 1890–1900) across the Gulf region suggest an average N–S extension rate of the order of 10 mm yr^{-1} (Billiris *et al.* 1991). Geological observations indicate that the southern coast is subject to uplift whereas the northern coast subsides (Sébrier 1977).

As a first step in this study we have examined the regional morphology using SPOT satellite images. This allows us to revise the abundant geological literature and to clarify the tectonic environment of the Corinth Rift, as well as to evaluate the degree of activity of the different faults, and to describe the general features of the rifting process (Fig. 2).

Second, we have focused on a flight of terraces, about 30 km long and up to about 400 m high south and west of the city of Corinth (Fig. 2). Relevant observations of geological structures to constrain the evolution of large normal faults are rare because markers of deformation scaling with crustal thickness are generally hidden by sediments on one side of the fault and eroded on the other side. Appropriate age constraints (in the range 10^4–10^5 years) are also usually limited. To study the mechanical changes near growing faults it is crucial, however, to have reliable descriptions of the fault-bounded structures in areas with high slip rates which none the less have low erosion and sedimentation rates, and where the initial geometry of the markers is unequivocal. We show that this is the case for the Corinth terraces, which lie on the footwall of the major normal fault bounding the Corinth Rift. Based on detailed mapping of the terraces supported by stratigraphic evidence and U/Th dates, we correlate these features with the worldwide chronology of Pleistocene sea level change, which allows us to deduce rates of tectonic uplift.

Third, we employ the terrace data to constrain a mechanical model of the deformation of the footwall of the main fault of the Corinth Rift. We use a thick elastic plate model and a boundary-element technique to reproduce the fault slip and the flexed geometry of the strandlines (King & Ellis 1990), taking into account the permanent deformation associated with the seismic cycle, as well as that related to erosion and sediment load (King, Stein & Rundle 1988; King & Ellis 1990). This allows us to deduce slip rates on the main Corinth Rift Fault over the last 350 ka.

Fourth, using longer-term morphological features and some terrace data in other fault segments we examine the mechanics of the Corinth Rift as a whole. This is done by comparing slip and slip rates averaged over different spans of time, on different segments of the Rift. The problems of fault segmentation, scaling and propagation are addressed.

Finally, we compare the main features of the Corinth Rift with those of other similar rifts in the Aegean and elsewhere in the world. A geodynamic model for the evolution of the Aegean is proposed, taking into account the Corinth data as well as the constraints on the timing of major regional events, the geometry and kinematics of the major fault systems such as the North Anatolian Fault, the known palaeomagnetic rotations, and the current overall motion deduced from the geodesy (GPS and SLR).

2 SEISMICITY, TECTONIC SETTING, AND OVERALL MORPHOLOGY

2.1 The Gulf of Corinth

Although several large earthquakes have destroyed cities in the Gulf of Corinth in the past, few of these earthquakes have provided reliable information about the faults that produced them. Probably the most famous is the historical earthquake of 373 BC, after which, legend relates, the ancient city of Heliki was swallowed by the sea. The area of Heliki and Aigio was also damaged by the earthquake of 1861 December 26. After this later shock, Julius Schmidt (1881) described the submersion of several square kilometres of the coastal plain, the widespread opening of fissures, and the existence of a continuous break (*Spalt*) near the mountain front. The break was 2 m wide and followed closely (for about 13 km from modern Heliki eastwards to the coast of the Gulf) the trace of the fault now mapped both in the field and using the SPOT imagery (Fig. 2). Some segments of a 1–2 m high scarp visible at some places along the fault trace may be interpreted as remnants of the original break observed by J. Schmidt (Mouyaris, Papastamatiou & Vita-Finzi 1992; Rigo 1994). Other ancient cities of the Gulf of Corinth have suffered from earthquakes (e.g. Delfi in 348 BC, 279 BC; Corinth in 77, 543, 580, 1858), but it is difficult to associate any of these events with a rupture on a particular fault (Papazachos & Papazachos 1989; Ambraseys & Jackson 1990). The instrumentally recorded seismicity in the Gulf of Corinth is also intense (Ambraseys & Jackson 1990; Papazachos & Kiratzi 1992) (Fig. 1), and includes six events with magnitude (Ms) greater than 6 (Corinth, 1928, Ms 6.3; Eratini, 1965, Ms 6.4; Antikyra, 1970,

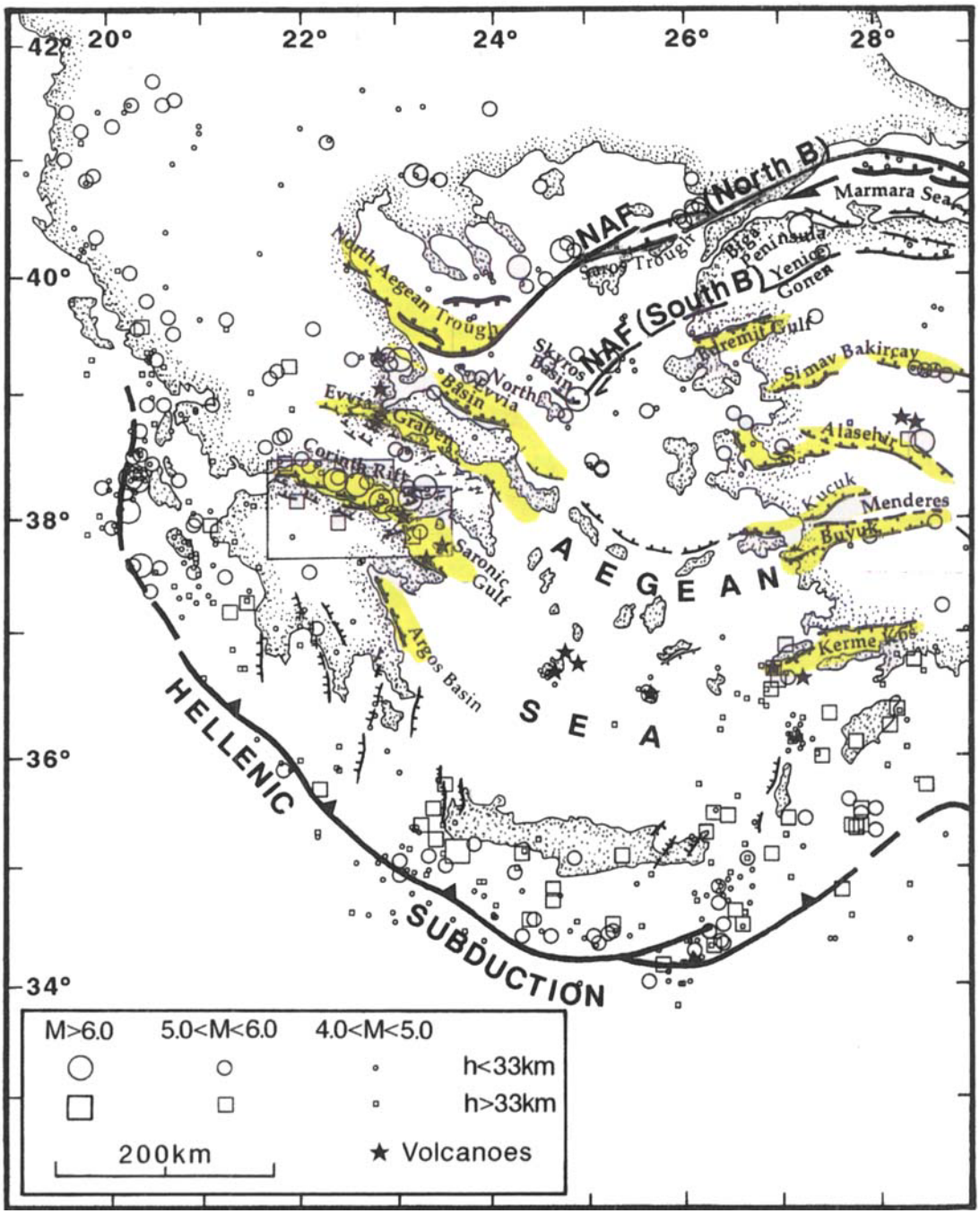

Figure 1. Tectonic framework and 1965–1992 seismicity of the Aegean region (from the NEIC catalogue). The box outlines the location of the Corinth Rift system mapped in more detail in Fig. 2. The main extensional basins discernible on and near the land margins of the Aegean are outlined in yellow. NAF indicates the two branches (North and South) of the North Anatolian Fault.

Ms 6.2; Corinth, Perahora, and Kaparelli, 1981, Ms 6.7, 6.4 and 6.2). The sequence formed by the 1981 events and their aftershocks was extensively studied, providing the best seismotectonic information in the region (Jackson *et al.* 1982; King *et al.* 1985). Rupture on two major onshore faults (Pisia and Kaparelli) was well documented (Jackson *et al.* 1982), but there has been controversy about whether the first shock ruptured part of the Pisia Fault or an offshore fault between Perahora Peninsula and Xylokastro (Fig. 2) (Taymaz, Jackson & McKenzie 1991; Hubert *et al.* 1996).

Almost all of the focal mechanisms and surface rupture in the Gulf of Corinth correspond to normal faulting, with an extension directed roughly N–S (Jackson *et al.* 1982). This is consistent with the overall rift structure, which is outlined by a prominent topographic depression trending ≈ESE–WNW across the NNW–SSE-trending fabric of the Hellenic mountain belt. The large normal faults that bound the Rift cut the fold–thrust tectonic units of the belt, which include mainly Mesozoic and Tertiary phyllites, ophiolites, unmetamorphosed flysh, and thick platform carbonates (IGME 1983). The youngest sediments involved in the fold–thrust deformation of the units in the central part of the Gulf (Pindos units) are of Miocene age

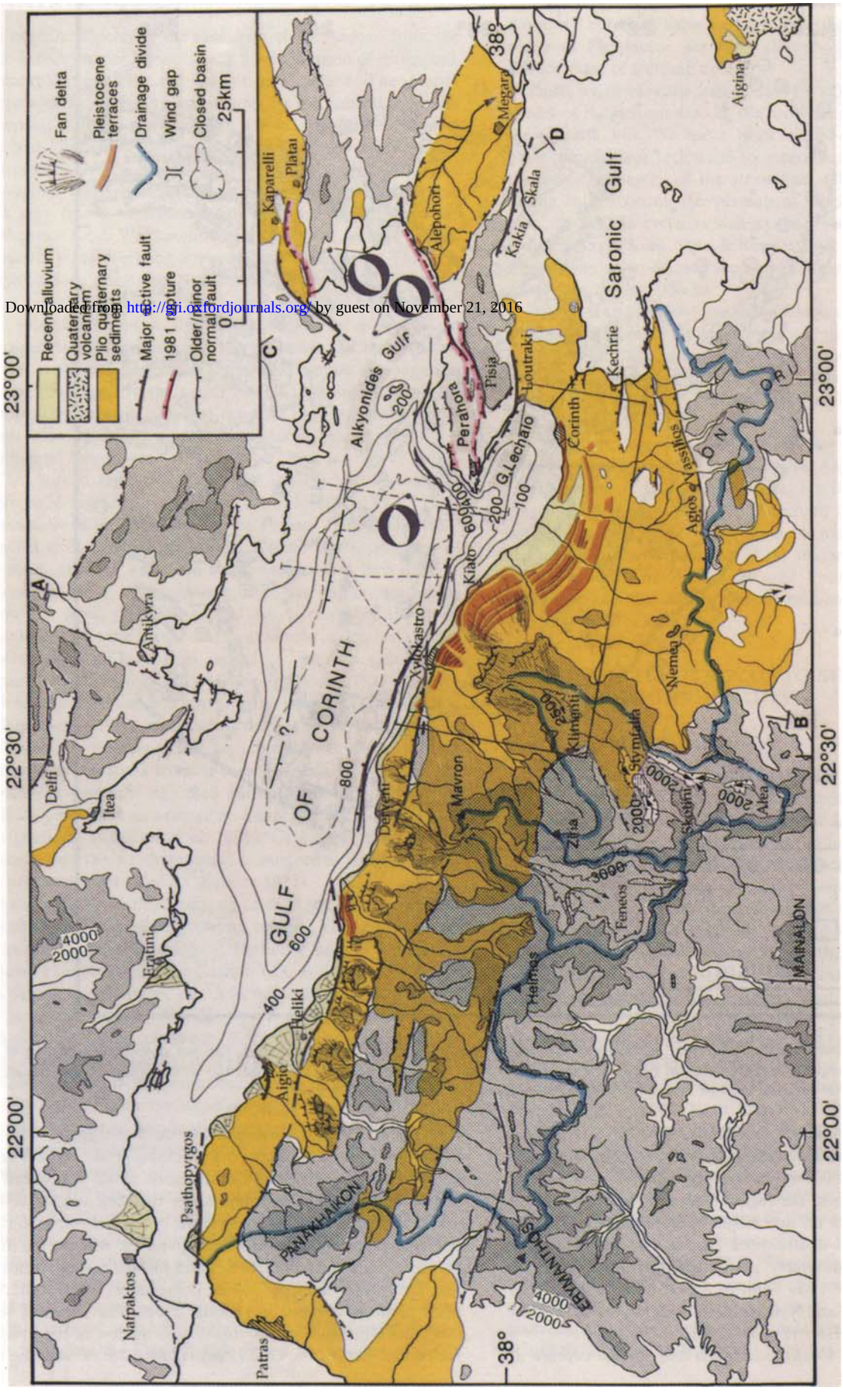

Figure 2. Active tectonics in the Gulf of Corinth. The topography (in feet) is from DMAAC (1984); the bathymetry (in metres) is taken from Perissoratis *et al.* (1986) for the eastern Gulf and from UNESCO (1981). The geology is modified from IGME (1983) and Dufaure & Zamanis (1980). The fault plane solutions of the 1981 shocks are from Taymaz *et al.* (1991). The active faulting is compiled with panchromatic SPOT satellite imagery (scenes with K/J coordinates 087/273, 088/273, 089/273, 089/274, 090/273 and 090/274). The box outlines the location of the Corinth terraces mapped in Fig. 4. A–B and C–D represent the traces of sections shown in Figs 13(a) and 23. Three traces of seismic sections that cross offshore faults north and east of Xylokastro are also indicated [from Brooks & Ferentinos (1984) and Higgs (1988)]. The karst plains of Feneos, Klimenti, Stymfalia, Skotini and Alea form the two catchments with reversed drainage on both sides of Ziria mountain.

(IGME 1983), but the E–W normal faults also cut younger, unfolded sediments of Plio–Pleistocene age (Fig. 2). This indicates that the Gulf of Corinth Rift formed mainly during the Quaternary. It also implies that the extensional deformation and topography mostly postdate and overprint, almost orthogonally, the fabric and topography of the Hellenic belt.

The overall form of the Gulf of Corinth is that of an asymmetric half-graben with an uplifted southern footwall and downward flexed northern hanging wall, with minor antithetic faulting. This is seen at first glance by looking at the shape of the coastline, which is sharp and linear in the south, and sinuous, with many peninsulas, in the north (Fig. 2). The asymmetry is also evident in the seismic profiles (Brooks & Ferentinos 1984; Higgs 1988). A series of three main en échelon normal fault segments bound the high relief along the southern coast and enter the sea in the east (Psathopyrgos, Heliki, and Xylokastro faults, Fig. 2). These fault segments, with lengths between 15 and 25 km, have an average strike of N90–105°E, and a northward dip of about 50° near the surface (Fig. 2). The westernmost fault segment of the Gulf of Corinth bounds a narrow strait that opens, to the south-west, into the Gulf of Patras. The eastern extremity of the Gulf of Corinth, site of the three shocks in 1981, is more complex. There the main active normal fault segments strike more north-eastwards and cut obliquely across both structures and the relief. Like the main fault segments of the south coast of the Gulf of Corinth, the faults dip north, with the exception of the Loutraki and the Kaparelli faults (Fig. 2). The latter faults dip south, like the small antithetic faults seen on some parts of the northern coast of the Gulf, and like other inferred offshore faults (Brooks & Ferentinos 1984; Perissoratis, Mitropoulos & Angelopoulos 1986; Higgs 1988) (Fig. 2).

Another feature is the increasing width of the Gulf from west to east, from a minimum of about 5 km north of the Psathopyrgos Fault, to a maximum of about 30 km north of the Xylokastro Fault (Fig. 2). The bathymetry outlines this progressive eastward width and depth increase (Fig. 2), which also coincides with an increase of the sediment infill (Heezen, Ewing & Johnson 1966; Brooks & Ferentinos 1984). This suggests that the amount of extension across the central-eastern part of the Gulf is greater than at its western end. Restoration of the topography and structural relief associated with normal faulting on simplified sections across the Gulf of Corinth provides a crude estimate of the total extension. Taking into account the youngest deformation within the present rift shoulders only, restored sections suggest about 2 km and 7 km of N–S to NNE–SSW extension north of the Psathopyrgos and the Xylokastro faults, respectively (Rigo 1994). This young deformation, as argued below, may be of Pleistocene age (1–2 Ma?), which implies fast extension rates, of at least 3–4 mm yr^{-1}, across the most active parts of the Rift system. The difference in the amount of young extension in front of the Psathopyrgos and the Xylokastro faults, separated by 60 km, may account for about 4° to 6° of the clockwise rotation of the Peloponnesus with respect to central Greece. We discuss the implications of fast extension rates and of rotations later.

The geometry of faulting in the Gulf of Corinth seems to have changed since the rifting process started. Plio–Pleistocene lacustrine, fluvial sands and silts, and fan delta conglomerates interbedded with marine marls are uplifted to elevations reaching 1756 m on the southern shoulder of the Rift (Mt Mavron, Fig. 2). This suggests both a fast slip rate on the major faults at the present Rift edge, and a change from subsidence and sedimentary deposition near to sea level, to uplift (Keraudren 1970, 1971; Dufaure 1977). The former region of sedimentation appears to have occupied a wider area delimited by other normal faults with attitudes very similar to those at the present Rift edge (Fig. 2). Most of these faults are located north of limestone massifs like Erymanthos, Helmos, Ziria, and Onia (Fig. 2). These faults outline the southern edge of the Plio–Pleistocene basin. Other faults form secondary fault steps, or grabens, such as the Demestiha depression, between the Erymanthos and Panakhaikon mountains (Fig. 2). There is evidence of synsedimentary and Pleistocene displacement on many of the faults within the uplifted part of the basin (Dufaure 1977; Doutsos & Piper 1990), but these faults generally lack, on the SPOT imagery and in the field, clear morphological evidence of young, Holocene, activity. Consequently, both the seismicity (Fig. 1) and the morphology suggest that these faults are older, and less active, than the faults at the present Rift edge. This indicates, in turn, that both the normal fault activity and the southern edge of the evolving Corinth Rift have migrated northwards. The overall migration of the Rift edge has been about 25–30 km, and possibly involved jumps in the late Pliocene or in the early Quaternary. The older fault strand that is closest to the present Rift edge is 5–10 km to the south, in the western half of the Gulf. Much like the faults of the present edge, the older faults have en échelon segments similar to the presently active faults (e.g. south of the Psathopyrgos and Heliki faults, and east-north-east of Mavron mountain, Fig. 2). Conversely, some offshore faults seen in the seismic profiles (Brooks & Ferentinos 1984), for instance north of the Xylokastro Fault (Fig. 2), may be starting to create a new rift edge, a few kilometres north of the present one.

Erosional and sedimentary environments also appear to have migrated northwards, together with fault migration in the same direction. River incision has revealed a set of conspicuous northward-fed fan deltas emplaced on top of the uplifted block, south of the Heliki Fault (Fig. 2). Sedimentary conditions observed in these incised fan deltas are probably very similar to those in fan deltas now being deposited north of the faults that form the present edge of the Gulf (Ori 1989), for instance north of the Heliki Fault (Fig. 2).

The northward migration of the southern edge of the Gulf of Corinth Rift has modified the regional drainage. The present catchment north of the watershed represented in Fig. 2 has a flow directed northwards, into the Gulf, which is consistent with the regional inner slope created by the Rift. Some parts of this large catchment, however, display evidence of a recent drainage reversal (Dufaure 1977; Bousquet, Dufaure & Péchoux 1977). This is seen in the central part of the catchment, at the two now internally drained basins that supply water to the plains of Feneos, west of the Ziria mountains, and to the plains of Klimenti, Stymfalia, Skotini, and Alea, east and south of the Ziria mountains (Fig. 2). The two basins have similar areas in map view ($\approx 250\ km^2$) and funnel shapes with valleys that widen southwards, towards the mountains, where the water now sinks into the karst. The shape of these catchments and other smaller-scale morphological indicators (river terrace dip, tributary angles, direction of sediment transport, etc.) testify that long-term equilibrium was attained mainly under northward-directed flow (Dufaure 1977). The outlets originally connecting these catchments with the main Gulf basin are now

wind gaps, at elevations of 800–1200 m, carved across mountain shoulders that are topped by massive Plio–Pleistocene conglomerates such as the Mavron Oros (Fig. 2). These wind gaps and shoulders overlook the present Rift edge. The wind gap north of the Klimenti karst plain is very clear in the SPOT images (Fig. 3) and in the topography (Fig. 4). It is cut into northward-fed fan delta sediments including marine marls with nanoplankton fauna of the NN20 zone, and was thus probably deposited sometime after 450 000 yr BP (Keraudren & Sorel 1987). We suggest, therefore, that the drainage reversal occurred here later, probably when the Xylokastro Fault had moved sufficiently to uplift the fan delta deposits and tilt the present Rift shoulder southwards. The topography of the two catchments with reversed drainage furnish constraints on the slip of the Xylokastro Fault. We discuss such constraints later.

2.2 Faulting evolution at the eastern extremity of the Gulf

The geometry of faulting at the eastern extremity of the Gulf of Corinth also seems to have changed since the rifting process started, but in a different way. Fault activity appears to have migrated northwards, as in the western and central parts of the Rift, but the orientation of the faults has also changed. The newer fault steps here are oblique to the older faults and basins (Fig. 2), a geometry that has given rise to the recently deformed palaeogeographic markers we examine in detail. The relations between the major fault-bounded structures are summarized here.

On the southern shoulder of the present Rift, the ≈N70°E striking Agios Vasilios Fault marks approximately the southern edge of the basin filled with Plio–Pleistocene sediments, which connects with the Saronic Gulf (Fig. 2). The parallel Kechrie Fault bounds one of the major secondary steps within this basin (Fig. 2), and many other (≈E–W striking) minor intrabasinal faults are well exposed and described in the Corinth Canal area (Collier 1990). North and north-east of these faults, the basins formed by the Gulf of Lechaio–Corinth Isthmus and by the Alkyonides Gulf–Megara plain have an oblique trend controlled by fault segments striking about N120°E. These segments include the prominent south-dipping Loutraki and Kakia Skala faults, which display evidence of Holocene activity (Armijo, Lyon-Caen & Papanastassiou 1992), and the faults with smoother morphology, probably inactive, on both flanks of the Megara Basin (Leeder, Seger & Stark 1991) (Fig. 2). The sediment infill, mainly lacustrine with marine transgressions, indicates that these two WNW–ESE, oblique-trending basins communicated with the Gulf of Corinth and with the Saronic Gulf and the Aegean. There is evidence that a sea-way existed in the upper Pleistocene between the Gulf of Corinth and the Saronic Gulf, through the Gulf of Lechaio and the Corinth Isthmus (Collier *et al.* 1992). The Gulf of Corinth was thus connected with the Saronic Gulf and the Aegean through the two oblique grabens, the Gulf of Lechaio–Corinth Isthmus and the Alkyonides Gulf–Megara plain. The oblique tectonic trend of these grabens coincides, at a much larger scale, with the WNW–ESE-trending pattern of Plio–Quaternary volcanic centres at the islands of Methana and Aigina in the Saronic Gulf, and of small Pliocene centres located a few kilometres east and north of the Corinth Canal (Fig. 2). These volcanoes represent the north-westernmost extremity of the main Aegean volcanic belt (Fig. 1).

The major and most active normal faults at the edge of the present Corinth Rift are situated north of the basins of Lechaio–Corinth Isthmus and Megara, in continuity with the main en échelon normal fault segments that bound the high relief along the southern coast of the Gulf (Fig. 2). Consequently, the two WNW–ESE-trending basins, as well as the folded structure of the Perahora Peninsula, are truncated by the newly formed, north-dipping, N70–90°E-striking faults. The latter faults are chiefly the eastward, offshore extension of the Xylokastro Fault, the Pisia, and the Alepohori (or Skinos–Psatha) faults (Fig. 2). The abrupt changes in the bathymetry of the eastern extremity of the Gulf, which contrasts with the gradual depth decrease towards its western extremity (Fig. 2), suggests a dramatic structural change both in space and time associated with recent fault propagation along the new rift edge. However, the overall westward tapering of the amount of cumulative extension across the Rift suggests mostly westward propagation. That the present eastern Corinth Rift edge is now along a new trend, across the older palaeogeography and structure, is corroborated by the occurrence of the three large shocks that broke successively eastwards along the new faults in 1981 (Jackson *et al.* 1982; King *et al.* 1985) (Fig. 2). The observation that active normal faults striking E–W to ENE–WSW cut older normal faults now striking WNW–ESE is consistent with the constant orientation of principal stresses (≈N–S extension) superimposed over a clockwise-rotating region. This agrees, in turn, with the overall Miocene–Present clockwise rotation of the Peloponnesus and central Greece suggested by palaeomagnetism (Kissel & Laj 1988).

Truncation of the basins of Lechaio–Corinth Isthmus and Alkyonides–Megara by the new faults has important structural consequences. In the uppermost fluviatile deposits in the Megara Basin there is evidence for north-westward palaeocurrents, while the top surface of the basin now slopes south-east (Bentham *et al.* 1991). This gives support to the view that the whole basin is being uplifted and tilted south-eastwards on top of the footwall of the normal fault offshore of Alepohori (Leeder *et al.* 1991; Collier *et al.* 1992) (Fig. 2). The presence, along the coast facing the Alkyonides Gulf near Alepohori, of a set of three raised marine cliffs, with the highest containing dated corals at 25–35 m, and of a raised biogenic notch at 2 m, documents uplift of the order of 0.3 mm yr^{-1} (Collier *et al.* 1992). This is interpreted to be mainly an effect of footwall uplift (Collier *et al.* 1992). A similar rate of uplift is deduced from coral samples in the area of the Corinth Isthmus, but it is interpreted to be the result of background tectonic uplift of the Peloponnesus (Collier *et al.* 1992). However, as argued above, this area appears to lie on top of the uplifted southern shoulder of the Corinth Rift, as does the rest of the Gulf of Lechaio (Fig. 2). We continue this discussion later.

Uplift of the smooth topography of the southern coast of the basin formed by the Gulf of Lechaio and the Corinth Isthmus is marked by a flight of emergent terraces about 30 km long and up to 400 m high (Fig. 2). Some workers have interpreted their step-like appearance to be primarily a consequence of normal faulting of a few original marine terraces (Depéret 1913; Freyberg 1973; Vita-Finzi & King 1985; Doutsos & Piper 1990). However, the arcuate form and parallelism of edges of these surfaces both to each other and to the present coast (seen best in the SPOT imagery) (Fig. 3) seems to leave little doubt that their origin is dominantly non-tectonic and that the inner edges of the terraces are sea-level

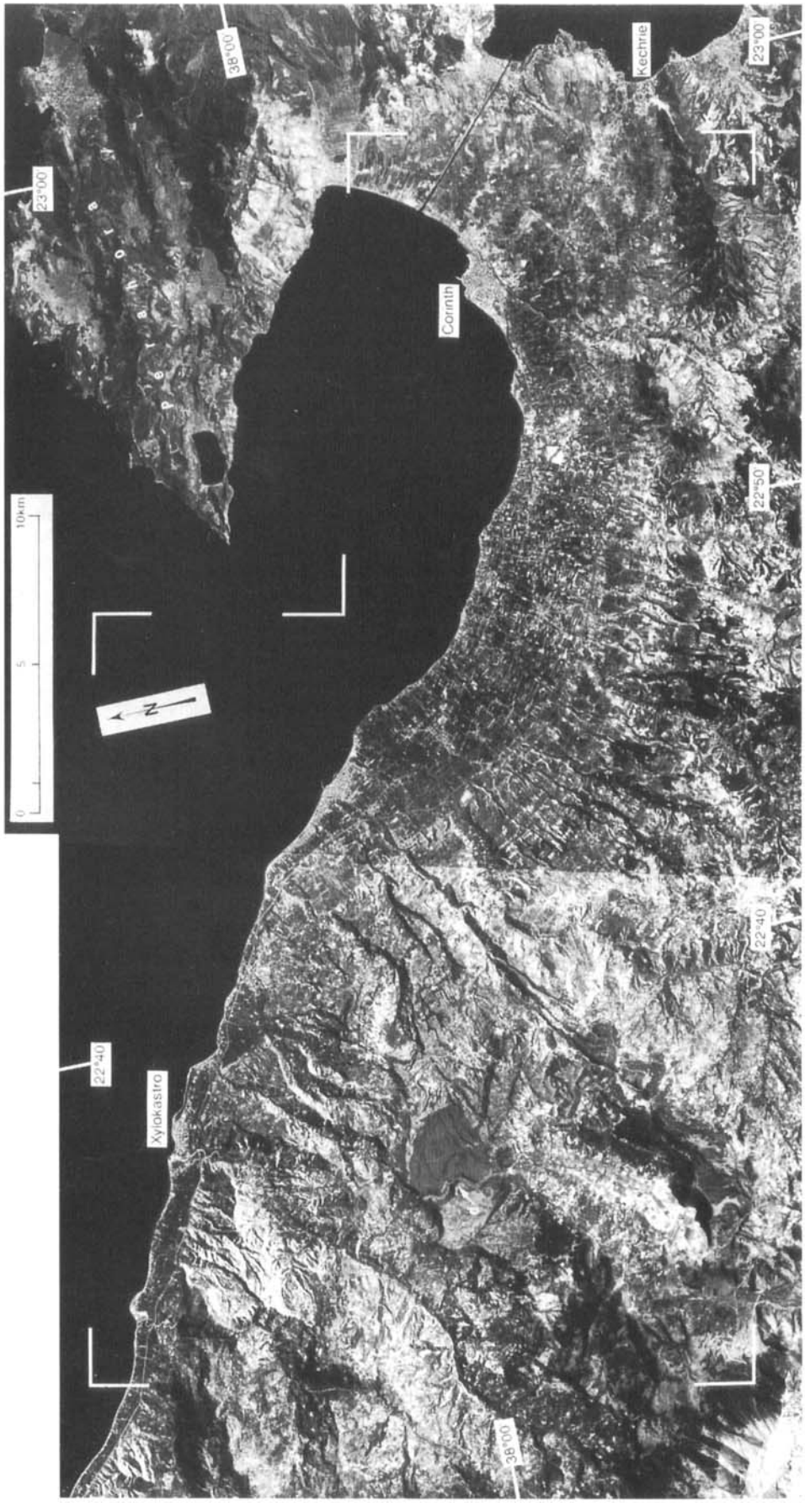

Figure 3. SPOT mosaic of the Xylokastro–Corinth area. The white corners outline the area mapped in Fig. 4. The white arrowed '**d**' indicates the wind gap in a canyon, which is evidence for drainage reversal (see text).

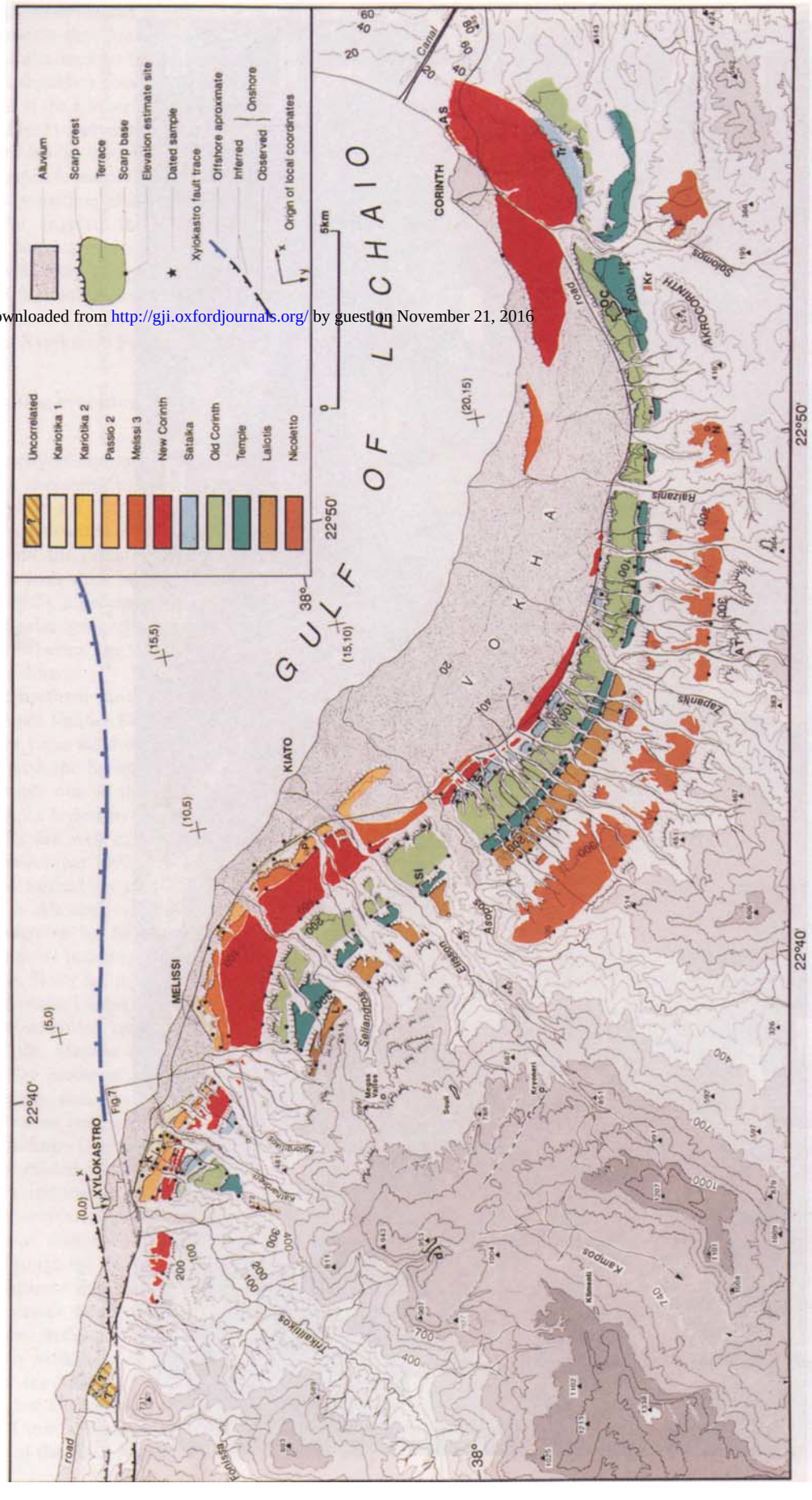

Figure 4. Map of the deformed marine terraces and palaeo-shorelines between Corinth and Xylokastro. The contours are based on the interpretation of high-resolution panchromatic SPOT images and 1:35 000 scale aerial photographs. The elevation estimates along palaeo-shorelines are at the sites indicated near the base of the cliffs (black dots) and are referred to local coordinates (x, y) in km (see Table 1). The white dots are for the estimates where the cliffs are ill-defined. The topography (in m) is from HAGS (1975a,b, 1976). The light shade covers the area between 400 and 700 m elevation, the medium shade between 700 and 1000 m, and the dark shade between 1000 and 1300 m. The frame indicates the location of Fig. 7. AS is Agios Spiridon; Tr, Tripos; OC, Old Corinth; T, Temple; Kr, Kranion; N, Nicoletto; F, Fortikia; AT, Agia Trias; S, Sataika; P, Passio; Si, Sikyon; L, Laliotis; K, Kariotika. The letter '**d**' indicates the wind gap in the canyon connecting the Klimenti catchment with the main Gulf Basin through the Trikalitikos river, as in Fig. 3.

strandlines of late Pleistocene age, as proposed and documented by Sébrier (1977), Dufaure & Zamanis (1980), and Keraudren & Sorel (1987). In addition, as noticed by these authors, the edges of the terraces vary in elevation and appear to be higher in sections located to the north-west, i.e. closer to the trace of the Xylokastro Fault (Fig. 2). Marine or lake strandlines are generally good markers to define palaeohorizontal planes, since they correspond to a base level at the time of their formation. In the following section we describe precisely the present shape of each of the strandlines, which are found to be flexed, tilted, and uplifted, in order to characterize the total deformation absorbed by the footwall of the Xylokastro Fault.

3 THE CORINTH TERRACES

3.1 Earlier work

The terraces south of the Gulf of Lechaio and the Corinth Isthmus have been cut and deposited in a region of relatively modest topography. This topography corresponds to the dominant occurrence in the former basin of the thick, soft Corinth Marls, which are mainly of freshwater lacustrine to brackish facies and of loosely determined Plio–Pleistocene age (Freyberg 1973; Sébrier 1977; Collier 1990) (Fig. 2). They are interbedded with some marine marls and shoreface sands and conglomerates. Marine fossil assemblages found near Souli suggest that part of the Corinth Marls are of middle to late Pleistocene age (Keraudren & Sorel 1987). During the excavations for the construction of the Corinth Canal, the association of fauna found in the transgressive marine sediments overlying the Corinth Marls was correlated by Depéret (1913) to the Tyrrhenian (Last Interglacial sea-level highstand). He then interpreted all the terraces south and east of the Canal to correspond to one single platform of that age, displaced by faulting (Depéret 1913). Variations on this hypothesis have been subsequently followed by many authors (e.g. Vita-Finzi & King 1985).

Sébrier (1977) described the stratigraphy of six terraces in the section south of the city of Corinth. He noted that the terrace levels differ from one another because they contain different marine fauna, represent different environments, and have different degrees of weathering. Each terrace comprises an erosion-resistant lid of caprock generally 2–6 m thick formed from well-cemented sands and conglomerates. Sébrier (1977) observed that they correspond to cycles, starting with marine transgression, generally with an angular unconformity over the underlying Corinth Marls, followed by regression, during a globally regressive process. As he could see no clear trace of faulting between the different platforms he suggested that the terrace cycles could be associated with glacio-eustatic sea-level fluctuations in the Pleistocene. Samples of molluscs collected at two different levels, New Corinth and Old Corinth, at about 20 m and 60 m elevation, respectively, gave U/Th dates of 49 ka $\pm$ 20 and 235 ka (+40, −30) (Sébrier 1977). He did not assign much confidence to these dates, and, based rather on the stratigraphical and palaeontological evidence, proposed that only the New Corinth terrace corresponds to the Tyrrhenian.

Dufaure & Zamanis (1980) made detailed sedimentological observations across the edges of the terraces and space correlations. Their work includes the first overall map of the terraces, although schematic and without topography. They observed that the terraces split into a greater number of platforms towards the West, and suggested that strong vertical uplift favours a multiplication of platforms. Dufaure & Zamanis (1980) defined four prominent sets of terraces (see Fig 4): the very high Old Red levels at 600 m elevation near Souli, of possible marine origin; the Ancient marine levels at 200–300 m elevation south of Corinth; the Middle marine levels, including the Old Corinth and Temple levels of Sébrier (1977); and finally the Tyrrhenian levels, including the New Corinth terrace. They suggested a minimum of eight 'certainly marine levels, without the Holocene one', and possibly a maximum of 11 levels south of Kiato and Xylokastro. They observed that some terraces have a simple structure corresponding to a single transgressive–regressive deposition cycle. An example of this is the Temple level, with basal conglomerate, beach sands, and finally the eolian sands of 'Poros' facies, used for the Temple construction. Other terraces, like Old Corinth, have a more complex structure, with two sequences of conglomeratic layers followed by marls and sands. Dufaure & Zamanis (1980) inferred a gradual increase in elevation of the terraces towards the Mavron Oros (Fig. 2), with 'transverse', anticlinal and synclinal undulations.

The correlations in space of Dufaure & Zamanis (1980) are slightly modified in the schematic map by Keraudren & Sorel (1987). These authors described four profiles across the terraces between Xylokastro and Corinth, with elevations measured with an altimeter. They correlated the terraces' profiles with highstand sea-level stages of the oxygen-isotope chronology, neglecting absolute sea-level differences from stage to stage which are known from studies of absolute sea-level variation to have been as large as 40–50 m (e.g. Chappell & Shackleton 1986). This correlation led them to propose a decrease of the uplift rate with time, and to suggest that the sea level is constant for all highstand stages and substages. Precise mapping of the terraces together with proper use of the absolute sea-level variation has caused us to revise their views while accepting that the processes involved in the formation of the terraces are essentially the same.

Some authors have disputed that all the terraces are of marine origin because most of the Corinth Marls underlying the terraces are of lacustrine facies and because of the relative thinness of the prograded transgressive sequences (Doutsos & Piper 1990). This feature may be an effect of the rapid uplift in the area, which prevents the margins of the basin from efficient sediment accumulation, as we show later in this paper. The marine fauna associated with beach facies in the caprock of the terraces (Sébrier 1977; Dufaure & Zamanis 1980) rule out a lacustrine origin for the 10 terraces and shorelines discussed in this paper. A lacustrine environment isolated from the open sea almost certainly prevailed in the Gulf of Corinth, however, during periods of low sea-level stands (Collier 1990; Doutsos & Piper 1990). These are not recorded by visible terraces.

Doutsos & Piper (1990) made a sedimentological description of the terraces and interpreted the surface morphology to be the result of complex relationships between active normal faulting and sedimentary processes. They mapped many parallel short normal fault segments (2–4 km long) interrupted by an orthogonal, 15 km long 'transfer fault' that parallels the Elisson valley (their Fig. 3). We have not been able to see in the SPOT imagery or in the field this mechanically improbable

fault geometry. West of the Asopos and Elisson rivers (Fig. 4) the terraces lie upon marls and increasing amounts of conglomerate (Dufaure & Zamanis 1980). These conglomerates correspond to a sequence of large fan deltas fed from the Ziria mountains to the SW (Fig. 2). That the marine terraces outline the convex shape of the youngest, more distal fan of this sequence, between the Asopos and the Agiorgitikos rivers, militates against a tectonic origin for the terrace edges (Figs 2, 3 and 4). In addition, we suspect that many of the synsedimentary faults seen in sections within the fan deltas are growth faults associated with gravitational collapse during the sedimentation processes, rather than true normal faults related to tectonic extension. We have visited the field sections where Doutsos & Piper (1990) claim that four major normal faults (F_9, F_{10}, F_{11} and F_{12}) cut and offset the terrace platforms, by up to 60 m. As noted by these authors, minor, discontinuous normal faults are seen in many places within the underlying marls and sands, often showing synsedimentary displacement of less than a few metres and with variable NW–SE to E–W strike, but very few of these faults offset the caprock, so that no recent, continuous scarp can be observed at the surface. In the absence of any direct, compelling observation of faulting in the collapsed debris slopes of the valleys, and having carefully scrutinized the geometry of the main contacts in map view with the SPOT imagery and aerial photographs, we conclude that they correspond very closely to inner edges and cliffs of terraces of different age, as formerly proposed by Sébrier (1977), Dufaure & Zamanis (1980) and Keraudren & Sorel (1987), and not to faults.

Collier (1990) and Collier *et al.* (1992) described six marine transgressive cycles in the Corinth Canal section. They dated with U/Th techniques *Acropora sp.* coral samples from the Canal, and two samples collected in raised terraces south of Alepohori and Corinth (Figs 2 and 4). Collier *et al.* (1992) interpreted these dates as correlating with interglacials of isotope stages 5, 7 and 9 of the marine record, and deduced minimum average rates of uplift of 0.3 mm yr^{-1} for the Corinth Isthmus and of 0.44 mm yr^{-1} south of the town of Corinth. The U-series dates obtained by these authors cast doubt on the ^{14}C dates reported by Vita-Finzi & King (1985) for bivalve samples in the Isthmus, in Perahora and in the terraces south of Corinth, whose ages would be mostly beyond the dating range of the radiocarbon method.

3.2 Methodology and correlation in space

It is now generally agreed that flights of marine terraces result from the interplay of the rate of global sea-level change and the rate of tectonic uplift (e.g. Chappell 1974; Lajoie 1986; Valensise & Ward 1991). Periodic glacio-eustatic global sea-level changes are very rapid. During the last deglaciation, at the end of the Pleistocene, the absolute sea-level rise was about 150 m in 12 ka or less, implying an average rate of more than 12 mm yr^{-1} (Chappell & Shackleton 1986). Most observed rates of long-term coastal tectonic uplift in the world, however, are less than 2 mm yr^{-1} (Lajoie 1986). A rising coast can thus record, much as a moving strip chart, the Pleistocene sequence of brief but still sea-level highstands, which are marked in the coastal landscape as a series of terraces and strandlines. Strandlines may also form during sea-level lowstands but they are usually destroyed by wave erosion and covered by sediments deposited during subsequent sea-level highstands (e.g. Lajoie 1986; Collier 1990). The terraces are generally erosional or thin depositional platforms that slope seawards very gently ($\leq 10°$) (see Fig. 5). They have a landward margin, or inner edge marked by the shoreline angle, at the base of the coeval palaeo-sea-cliff, and a seaward eroded edge at the top of the next, younger sea cliff (Fig. 5). A series of such platforms and cliffs resembles a flight of stairs carved into the coastal topography (see Fig. 6). The lines at the inner edges of the terraces are therefore precise marks of abandoned marine shorelines, formed horizontally, at sea level.

Based on the previous field descriptions of Sébrier (1977) and Dufaure & Zamanis (1980), we mapped 10 terrace platforms that are readily identified in some type-sections, and that can be correlated in space with confidence for several kilometres. For instance, the distinct eolian sands of 'Poros' facies of the Temple terrace are the same as those quarried to construct the ancient city of Sikyon, about 15 km north-west of the Temple site on the same terrace (Fig. 4). The use of SPOT satellite high-resolution panchromatic imagery (pixel size = 10 m) (Fig. 3) and of 1:35 000 scale aerial photographs (Fig. 7a) allowed us to extend the terrace correlations across the stream and river valleys and to trace the main features on the 1:5000 scale topographic maps of the Hellenic Army Geographical Service (HAGS) 1975a, 1975b, 1976, which have contours every 4 m (Fig. 7b). We carefully checked in the field the reliability of all the correlations. For each identified terrace we traced the contours of two edges that are very distinct in the morphology: the seaward outer edge, at the top of the scarp that forms the younger sea cliff, and the landward inner edge, at the slope break angle that marks the base of the coeval sea cliff. In spite of cliff degradation, as shown below, the basal slope break angle generally appears to approximate closely the actual shoreline angle (Fig. 5). We finally summarized all the observations on the 1:50 000 scale topographic maps (Fig. 4). Precise estimates of shoreline angle elevation at selected sites (Figs 4 and 7b) are listed in Table 1 and shown in Fig. 8. Our correlation of the terraces in space appears to be consistent with the main features of the schematic maps published by Dufaure & Zamanis (1980) and by Keraudren & Sorel (1987), although it is difficult to be certain because their maps lack topographic information. Some manifest inconsistencies arise, however, with the map by Dufaure & Zamanis (1980) in the area south of Xylokastro, and with the elevation of the terraces in the profiles by Keraudren & Sorel (1987). We attribute these inconsistencies to errors in correlations by the former, and to inaccuracies in the elevation estimates by the latter.

The terraces in the area near Akrocorinth and the Kechrie Fault have been subject to a different and more complex deformation regime than the terraces to the west and north-west, as noted by Vita-Finzi & King (1985) . Nevertheless, for the sake of stratigraphical coherence with the earlier descriptions, we identified the terraces, taking as a reference the section and the local names given by Sébrier (1977) south of the town of Corinth. This section includes six levels: Agios Spiridon, New Corinth, Tripos, Old Corinth, Temple and Nicoletto (Fig. 4). We have preferred to take the Nicoletto terrace of Dufaure & Zamanis (1980) west of Akrocorinth rather than the probably equivalent Fortikia level of Sébrier (1977) decribed east of it (Fig. 4). The uppermost Agia Trias level of Dufaure & Zamanis (1980) has doubtful marine origin

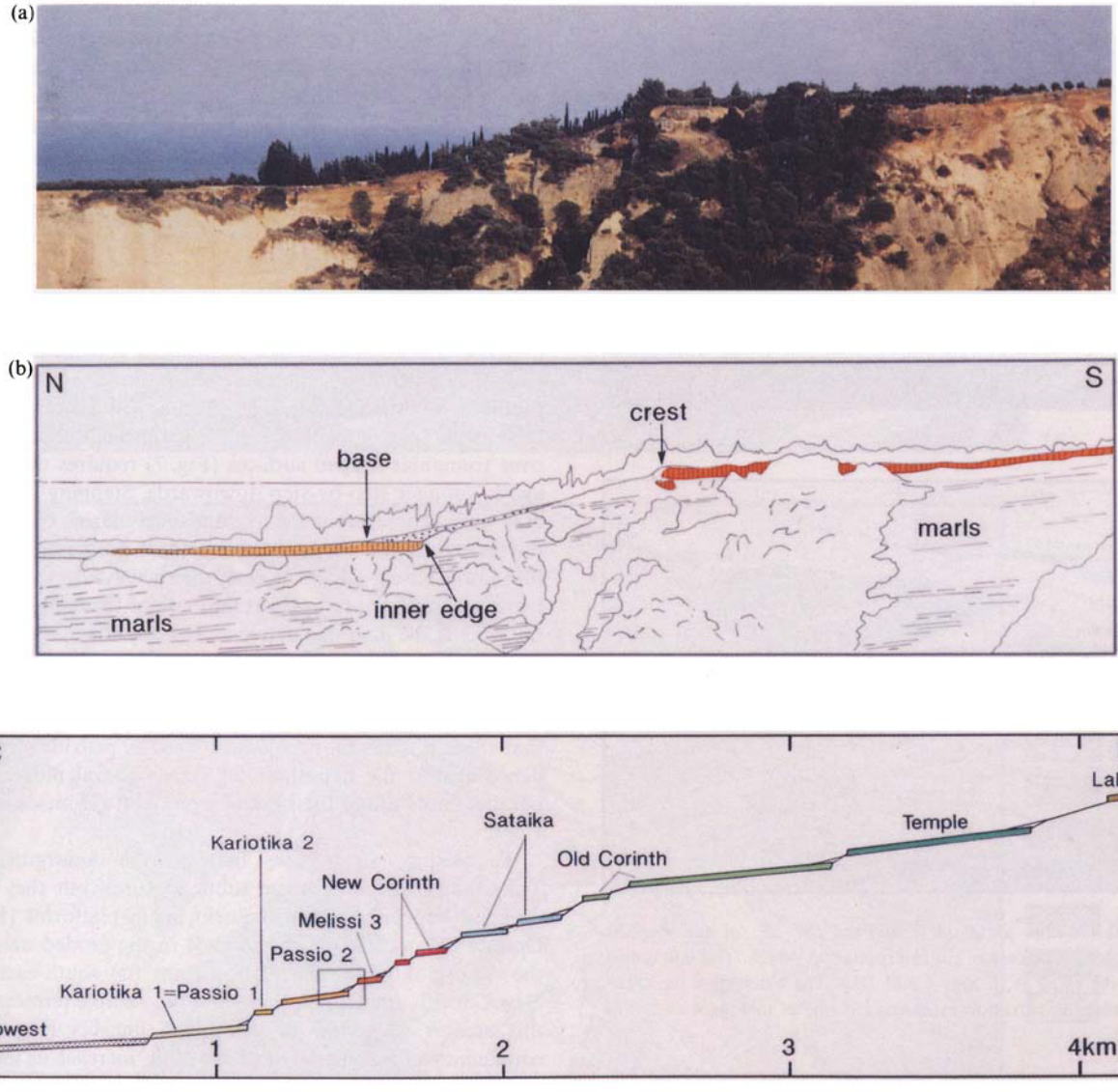

Figure 5. (a) Lateral view of the scarp between the Passio 2 and Melissi 3 terraces near Xylokastro, from the river Trikalitikos towards the east. Cypress trees about 8 m tall in the background give the scale. For location see the map in Fig. 7(b) and the box in the complete section in Fig. 5(c). (b) Interpretative sketch. The difference in elevation between the basal slope-break angle and the inner edge (shoreline angle) of the lower terrace (Passio 2) is less than 2 m. (c) Schematic section across the main stepped terraces in the Xylokastro area (see Fig. 7b for location).

and an ill-defined inner edge (Fig. 4). We have, therefore, not considered it in this study.

In the 10–12 km long stretch between the rivers Raizanis and Asopos, the correlation of the edges of the Old Corinth, Temple and Nicoletto levels is very clear (Fig. 3), as well as their north-westward elevation increase (Figs 4 and 8). The New Corinth terrace, however, is mostly covered here by the recent fan alluvium of the Vokha plain. At least two extra terrace platforms appear to intercalate progressively within the others and are increasingly better defined toward the Asopos river. One of these platforms appears immediately above the Temple level. This terrace, named here Laliotis (a village on the left bank of the Seliandros, Fig. 4), corresponds to the M3 level of Dufaure & Zamanis (1980). A string of disrupted surfaces forms a cliff above the Laliotis terrace. These terrace remnants may be equivalent to some disrupted caprock surfaces described north of Akrocorinth, at Kranion, by Sébrier (1977) (Fig. 4). Because these remnants of an intermediate level have no preserved inner edge, however, we have included them in the lower, eroded part of the ensemble mapped as the Nicoletto terrace. Correlation of the two edges of the wide New Corinth platform is found again west of the Elisson river (Fig. 4). This correlation allows us to bracket one extra terrace step inserted between the New Corinth and the Old Corinth levels. We named this terrace Sataika and tentatively correlated it, as did Dufaure & Zamanis (1980), to the Tripos terrace of Sébrier (1977).

Between the Asopos and Agiorgitikos rivers, as mentioned above, the curved, seaward-convex contours of the terraces appear to outline the shape of a fan delta. Several conglomeratic layers, interbeded within sands and marls of the delta, crop out upstream of the extension of the Laliotis terrace, towards Megas Valtos and Souli. These conglomerates form gently sloping platforms and crests (Fig. 4) that are easily confused with the sparse remnants of the Nicoletto, and perhaps older terraces, that once capped this eroded, relatively

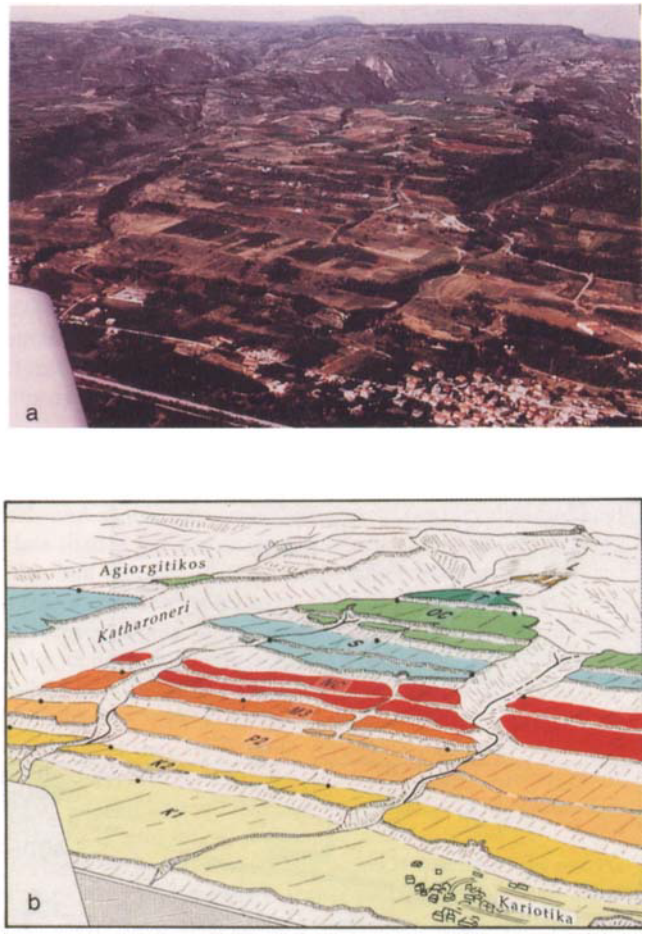

Figure 6. (a) Oblique aerial view, toward the SE, of the stepped terraces south of Xylokastro. (b) Interpretative sketch. The labels and colours are the same as in Figs 4 and 7(b). The black dots represent sites with shoreline elevation estimates (in m), as in Figs 4 and 7(b) (see Table 1).

elevated area (Dufaure & Zamanis 1980; Vita-Finzi & King 1985). We consequently do not to take these remnants into account. Three extra terrace fragments appear discontinuously within this stretch, seawards of the New Corinth level. These terraces are better defined SE of Kiato, and S of Melissi (Fig. 4). We named them, from the bottom up, Passio 1 (= Melissi 1), Passio 2 (= Melissi 2), and Passio 3 (= Melissi 3). The middle terrace is better exposed at Passio, and is the only one of the three to be continuous from Passio to Melissi, allowing for the correlation of the other two. The highest terrace, which is better exposed at Melissi, may then be correlated with the isolated platform, at about 15 m elevation, that crops out in the Vokha plain, east of the Raizanis river, and to the Agios Spiridon terrace of Sébrier (1977), both of which are located just below the New Corinth terrace (Fig. 4). That these three pairs of terraces are interrupted in the external, more exposed part of the fan delta can be reasonably attributed to smoothing of the convexity of the coastline by wave action during the subsequent sea-level highstands, which probably include the Holocene one. The same kind of process may have acted during the New Corinth highstand to erode the Sataika (Tripos) terrace, which is now lacking in the central part of the fan delta (Fig. 4).

The most impressive stretch of the flight of terraces is that between the Agiorgitikos and Trikalitikos rivers (Figs 4, 6 and 7). The very good preservation of every marine platform here is probably a result of the dominant occurrence, on the north-western side of the conglomeratic fan delta, of the same soft Corinth Marl facies (Fig. 5) that underlie the terraces south-east of the Asopos. The close association of well-preserved terrace platforms with soft underlying rocks tends to corroborate the inference of the non-tectonic origin of the platforms' edges. It is very unlikely that the nearly intact morphology of the terraces lying on soft marls south of Xylokastro (see Figs 6 and 7) could have survived a complex history including many cycles of normal faulting, scarp retreat under wave action, sedimentation, and renewed faulting, as proposed by Doutsos & Piper (1990). The geometrical arrangement and the morphology of the flanks of the parallel cliffs and platforms over triangular shaped surfaces (Fig. 7) requires that the cliff age is younger step-by-step downwards. Stepping downwards may have proceeded as the average local marine base level fell due to uplift, and as the flanking rivers progressively graded into lower base levels by incising their valleys. In this morphological process the last cliff at the base of the emerged part of the facet is the only one active at any one time. Therefore, the observed geometry and morphology in this area are consistent with the gradual, simple process of terrace formation described in other rising coasts in the world (e.g. Lajoie 1986). We argue that these pristine morphological features provide strong evidence against the hypothesis of active, coeval movement on parallel faults along the base of every cliff (Doutsos & Piper 1990).

We identify 13 terraces between the Agiorgitikos and Trikalitikos, including some subtle features, but they can be grouped into only nine prominent, main platforms (Fig. 7b). Despite the occurrence of badlands in the eroded marls near the Agiorgitikos, the correlation from the south-east of the New Corinth, the Old Corinth, and the Temple terraces across this area is very clear in the SPOT imagery (Fig. 3). The consistency of north-westward elevation increase in the measured shoreline angles of these terraces (Fig. 8) provides further confirmation to the correlation with the SPOT imagery. As mentioned above, this correlation seems to be somewhat different to that in the map by Dufaure & Zamanis (1980). It is more similar to that in the sketch map by Keraudren & Sorel (1987), despite large errors in the elevation estimates in their profile (up to about 40 m) and the misidentification of some minor platforms. Such errors could be due to the authors' lack of precise topographic maps and aerial photographs.

The correlation of the edges of the main terraces south of Xylokastro is a guideline, as elsewhere, for the correlation of sublevels and of intermediate levels within them. Our detailed map of Fig. 7(b) implies, first, that the New Corinth and the Old Corinth terraces each split into two sublevels. Second, that we can correlate the two intermediate platforms between the New and Old Corinth terraces as split from the Sataika level, which seems to have been eroded in the area of the fan delta within the Asopos and the Agiorgitikos (Fig. 4). Third, below the New Corinth levels we identified four terraces: from the bottom up, Kariotika 1 and 2, a terrace that is readily correlated with the Melissi 2 terrace (= Passio 2), and an upper, narrower level that we correlate with the Melissi 3 terrace (Figs 6 and 7). The well-exposed Kariotika 1 terrace seems to correlate adequately with the Melissi 1 level and

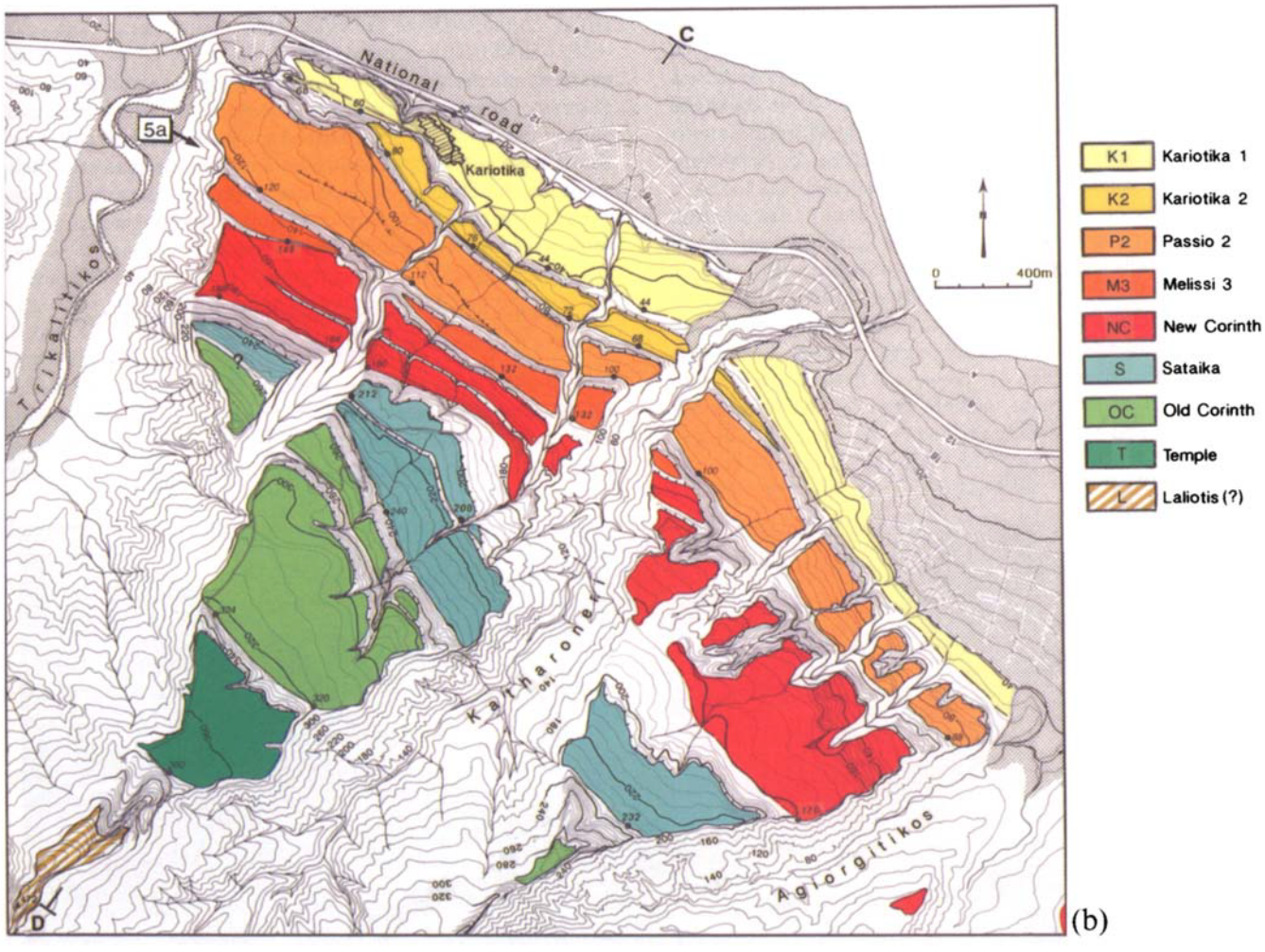

Figure 7. (a) Aerial photograph stereo pair of the area south of Xylokastro (see Fig. 4 for location). (b) Detailed map of the stepped terraces corresponding to (a). The black dots with elevation (in m) are sites with elevation estimates of the shoreline inner edge as in Fig. 4 (see Table 1). The lowest shoreline lies at the base of the cliff separating the Kariotika 1 level from the littoral platform, which is mostly covered with young alluvium. The topography is from HAGS (1980). C–D is the trace of the complete section in Fig. 5(c).

farther south-east with the Passio 1 level (Figs 4 and 8). This implies that the Kariotika 2 terrace is missing or is indistinguishable in the very populated slopes of Melissi, and that it does not exist farther south-east. Fourth, the lowest traceable shoreline lies at the base of the cliff separating the Kariotika 1 level from the littoral platform, which is mostly covered with young alluvium (Fig. 7). Although ill-defined, this lowest shoreline can be followed eastwards, across the Vokha plain,

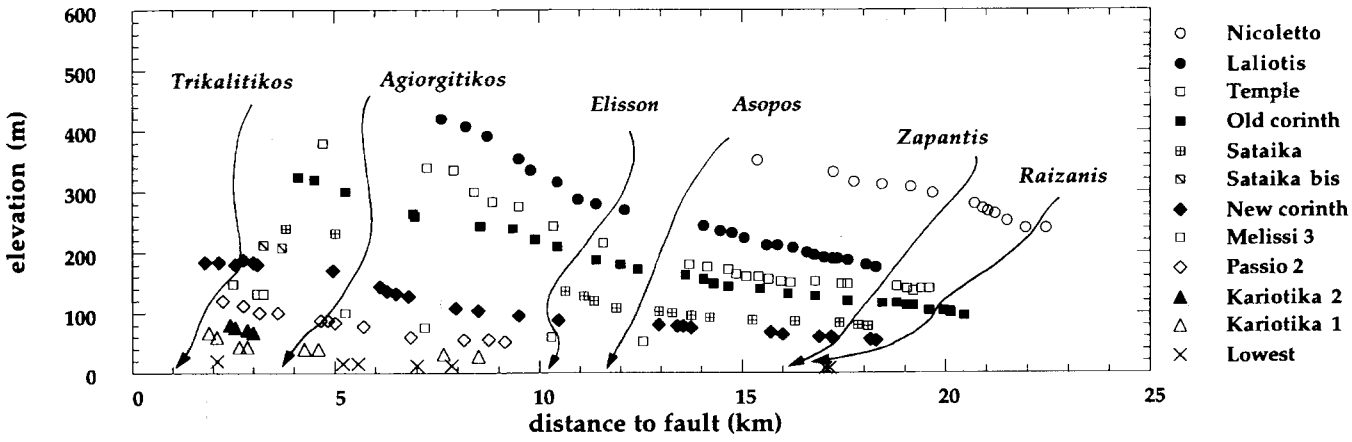

Figure 8. Plot of elevation estimates along the inner edges of the terraces (=shoreline angles) as a function of distance from the Xylokastro Fault trace (N–S projection). The complete data set is in Table 1. The uncertainties in horizontal and vertical position of the inner edges are smaller than the size of the symbols (see text). The sinuous arrows indicate the projected path of the main rivers across the terraces.

seawards of different terraces (Passio 2, Melissi 3 and New Corinth, Fig. 4). Finally, the highest platform visible above the Temple terrace may be correlated tentatively with the Laliotis level, but its shoreline edge is not defined (Fig. 4). No terrace can reasonably be mapped here above this level.

Few patches of marine platforms have been preserved from erosion in the badlands just west of the Trikalitikos river, on top of the Corinth Marls. The clearest of them, with an inner edge at 180–185 m, can be correlated with the New Corinth terrace (Figs 4 and 8). Farther north-west, some discontinuous remnants of marine platforms are visible near the coast, east of the Fonissa river (Fig. 4). However, these remnants are located north of the main onshore trace of the Xylokastro Fault (Figs 9 and 4). Because they lie on the hanging wall and very close to the fault trace, the platforms here are likely to be more intensely deformed than elsewhere. In addition, their shorelines may be vertically offset tens or hundreds of metres from those of the terraces mapped south-east of the Xylokastro Fault trace. Clearly, the correlation with 'Tyrrhenian' levels proposed by Dufaure & Zamanis (1980) is uncertain (Fig. 4). We suspect that these terrace remnants located north of the fault trace could be much older.

3.3 Deformation of the strandlines, erosion of the terraces and fault geometry

In order to constrain the present, deformed shape of the palaeohorizontal lines defined by the set of 10 mapped shorelines, we have determined the elevation (z) and the horizontal coordinates (x, y) of the inner edges of the Corinth terraces at

Figure 9. The Xylokastro Fault scarp. The view is to the east towards the Gulf of Lechaio, from the Fonissa valley (see Fig. 4 for location). The town of Xylokastro is visible on the coast in the background. The footwall limestones to the right (south) are of Jurassic age and belong to the Pindos Unit. The terraces capping the marls to the left (north) are uplifted more than 100 m above the present sea level. They are uncorrelated with terraces farther south-east in the footwall.

172 sites selected on our detailed maps (Table 1). The sites are all taken where the morphologically defined slope break angle, which marks a terrace's inner edge, is very clear. In addition, these sites are generally near valleys where the correspondence of the surface platforms with exposures in natural sections could be checked. The horizontal mislocation of the terraces' inner edges is less than about 100 m on the 1:50 000 scale maps used for the final x, y grid (Fig. 4), and the vertical uncertainty is less than ± 4 m on the 1:5000 scale maps used to determine the shoreline angle elevations (e.g. Fig. 7b). Because thin colluvium and talus onlap the base of the cliffs (Fig. 5), the elevation estimates of the shoreline angles from that of slope break angles can be slightly underestimated, by less than about 2 m. In some places where the cliff has retreated landwards under erosion, the basal slope break angle can be mislocated as much as 80 m landwards from the actual position of the terrace inner edge. This horizontal mislocation due to erosion occurs with corresponding colluvial thickening over the inner edge, which may cause an overestimation of its elevation by as much as 20 m. Dufaure & Zamanis (1980) have illustrated sections with such extreme bias in terraces near the eroded flanks of Akrocorinth, far from our estimate sites (Fig. 4). The difference in elevation that we could observe near our sites between the morphologically defined slope break angle and the shoreline angle seen in section was generally small, less than about 6 m. The maximum observed difference, within a small area, was 10 m at the inner edge of the New Corinth terrace in the Agiorgitikos valley (Figs 4 and 7b). Therefore, the total average uncertainty in horizontal coordinates of inner edge positions (x, y) is ± 100 m, and that in elevation estimates of shoreline angles (z) is $+4$ m, -10 m (Table 1). This accuracy is enough to resolve the position and the gradual decrease in elevation of each individual shoreline up to about 20 km away from the Xylokastro Fault trace (Fig. 8).

Plotted with respect to the trace of the Xylokastro Fault and its eastward offshore extension, the present shape of the shorelines strongly suggests footwall deformation associated with normal fault displacement on this fault system (Fig. 8). The shorelines in the Gulf of Lechaio appear to be tilted outwards from the present Corinth Rift edge, much like the sediments and the upper surface in the uplifted Megara Basin (Collier *et al.* 1992) (Fig. 2). The total observed decrease in elevation away from the fault is about 130 m for the New Corinth terrace, and 250 m for the Laliotis terrace, corresponding to average tilts of about 0.45° and 1.3°, respectively (Table 1). This reflects the general characteristic that the older shorelines are more uplifted and tilted than the younger ones. Another apparent feature is that the tilt of most of the shorelines is greater near the fault trace than away from it. This tilt variation produces the slightly flexed, concave upwards, shape of the shorelines (Fig. 8). At places where the shape of the shorelines is well constrained by morphological observations, the maximun tilts determined close to the fault are of the order of 1°–2° for young terraces such as Kariotika 1, Kariotika 2, and Passio 2, as well as for older terraces such as Laliotis.

Quantification of the local balance between erosion and sediment deposition is a prerequisite to the modelling of the long-term deformation of dip-slip fault-bounded structures (Stein, King & Rundle 1988). Sediment accumulation and subsidence in the hanging wall of the Xylokastro Fault is

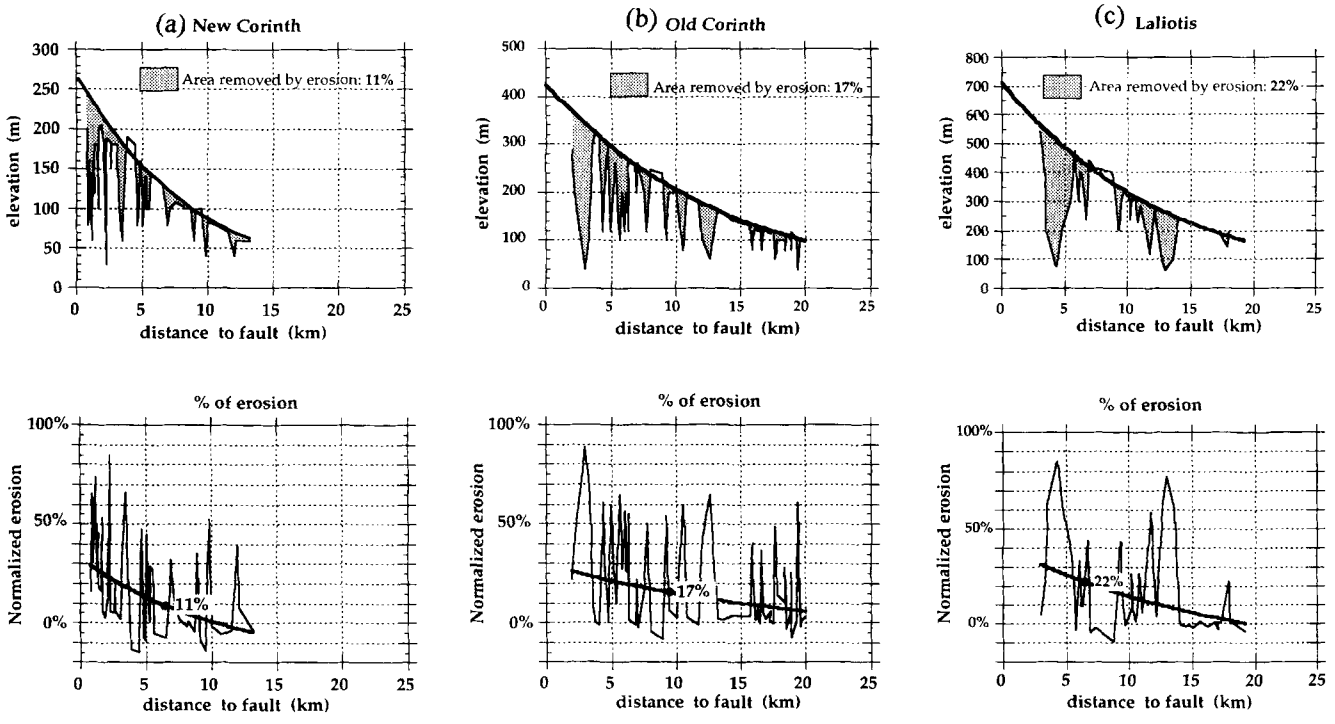

Figure 10. Erosion estimates for three different terraces, plotted as a function of distance from the master fault trace. (a) The New Corinth terrace; (b) The Old Corinth terrace; (c) The Laliotis terrace. Top: differences in elevation (shaded areas) between a hypothetical initial surface (smooth upper envelope) and the present incised surface of the terraces (saw-toothed). The erosion percentage is expressed as the section area removed with respect to the present sea level. Bottom: corresponding proportion (saw-toothed), average (smoothed curve), and mean percentage of erosion. The negative values correspond to overlaps between the observed geometry of the terraces and the hypothesized initial one.

Table 1. Elevation of uplifted shorelines in the Corinth–Xylokastro area. The origin of the coordinates (x, y) is about 38°05′N, 22°38′E (see Fig. 4). The elevations of the shoreline angles (z) are taken from 1:5 000 scale topographic maps with contours every 4 m at least (HAGS 1980). The uncertainties are ±100 m (1σ) horizontally (x, y) and +4 m, −10 m vertically (z) (see text).

Nicoletto			Laliotis			Temple			Old Corinth			Sataika			Sataika bis		
x (km)	y (km)	z (m)	x (km)	y (km)	z (m)	x (km)	y (km)	z (m)	x (km)	y (km)	z (m)	x (km)	y (km)	z (m)	x (km)	y (km)	z (m)
5.4500	15.375	352	2.3000	7.6000	420	−0.450	4.700	380	−0.1500	4.1000	324	0.6500	3.8000	240	0.50000	3.2500	212
6.9000	17.250	332	3.7000	8.2000	408	3.2750	7.2500	340	0.25000	4.5000	320	1.6000	5.0000	232	0.90000	3.7000	208
7.4500	17.750	316	4.2500	8.7250	392	4.2000	7.9000	336	1.0500	5.2500	300	8.2500	10.650	136			
8.4500	18.450	312	4.8000	9.5000	354	5.7750	8.4000	300	3.6000	6.9000	264	8.5000	11.100	128			
8.6000	19.150	308	5.0750	9.8000	336	5.4000	8.8500	284	4.0000	6.9500	260	8.6250	11.350	120			
9.2500	19.675	298	5.2750	10.450	316	5.8750	9.5000	276	5.9000	8.5500	244	8.8500	11.900	108			
11.600	20.700	280	5.6250	10.950	288	6.3000	10.350	244	6.4000	9.3500	240	9.4000	12.950	102			
12.625	20.900	272	5.8500	11.400	280	6.9500	11.575	216	6.6500	9.9000	222	9.5500	13.275	100			
13.000	21.025	268	6.2500	12.100	270	7.8500	13.700	180	6.9500	10.450	210	9.7500	13.750	96			
13.500	21.200	264	7.2500	14.050	244	8.1000	14.150	176	7.2500	11.400	188	10.000	14.200	92			
14.250	21.500	252	7.5000	14.450	236	8.4000	14.650	172	7.6500	12.000	180	10.400	15.250	88			
15.500	21.950	240	7.6500	14.750	232	8.6000	14.850	164	7.9250	12.425	172	11.550	16.300	86			
17.750	22.450	240	7.9000	15.050	224	8.7750	15.100	160	8.2500	13.600	162	13.200	17.400	84			
			8.3000	15.600	212	9.0250	15.400	160	8.5000	14.050	156	13.600	17.850	80			
			8.5000	15.875	212	9.3000	15.650	156	8.7000	14.300	148	14.400	18.100	78			
			8.8000	16.250	208	9.6000	15.950	152	8.9500	14.650	144						
			9.1500	16.600	200	9.8500	16.200	150	9.5000	15.450	140						
			9.4000	16.775	196	10.450	16.800	152	10.050	16.125	132						
			9.6500	17.025	192	11.050	17.450	148	11.875	16.800	128						
			9.9000	17.225	190	11.325	17.600	148	11.950	17.600	120						
			10.075	17.350	190	13.100	18.800	144	13.025	18.450	116						
			10.400	17.600	188	13.700	19.050	140	13.775	18.800	116						
			11.050	18.050	180	14.250	19.200	136	14.450	19.050	112						
			11.500	18.300	176	14.900	19.400	140	15.000	19.200	116						
						15.600	19.600	140	16.600	19.600	104						
									17.250	19.950	104						
									17.925	20.100	102						
									18.275	20.125	100						
									19.250	20.450	96						

New Corinth			Melissi 3 = Aiyios Spiridon			Passio 2 = Melissi 2			Kariotika 2			Kariotika 1 = Melissi 1 = Passio 1			Lowest		
x (km)	y (km)	z (m)	x (km)	y (km)	z (m)	x (km)	y (km)	z (m)	x (km)	y (km)	z (m)	x (km)	y (km)	z (m)	x (km)	y (km)	z (m)
−2.9500	1.8000	184	0.100	2.5000	148	−0.500	2.2500	120	0.77500	2.4250	80	0.20000	1.9000	68	1.0250	2.1000	20
−2.2000	2.1500	184	1.000	3.1000	132	0.700	2.7500	112	0.92500	2.5500	76	0.65000	2.1000	60	6.6000	5.2000	16
−1.2750	2.5500	180	1.4000	3.2500	132	1.5500	3.1500	100	1.3000	2.8500	72	1.3000	2.6500	44	7.1750	5.5750	16
−0.15000	2.7500	188	4.0000	5.2500	100	1.9000	3.6000	100	1.6500	3.0000	68	1.6500	2.8500	44	8.6000	7.0000	12
0.35000	3.0000	184	7.9500	7.2000	76	2.8500	4.6500	88				4.1750	4.2500	40	9.2500	7.8500	12
0.55000	3.1000	180	8.1000	10.300	60	3.7750	5.0000	84				5.0000	4.6000	40	20.050	17.050	8
2.2500	4.9500	170	9.7000	12.550	52	5.1250	4.8250	88				8.7000	7.6500	32	20.600	17.050	8
3.7000	6.1000	144				7.000	5.700	78				9.2000	8.5000	28	24.350	17.150	8

4.2000	6.2750	136			
5.0000	6.5000	132	8.000	6.850	60
5.6000	6.8000	128	8.4500	8.1500	56
6.9750	7.9500	108	8.5000	8.7500	56
7.3250	8.5000	104	9.0500	9.1500	52
7.8500	9.5000	96			
8.4750	10.475	88			
9.7000	12.950	80			
9.9500	13.400	78			
10.000	13.550	78			
10.175	13.750	76			
11.275	15.700	68			
11.700	16.000	64			
12.650	16.900	60			
13.150	17.200	60			
15.100	18.150	56			
15.400	18.300	54			

difficult to evaluate because of the lack of offshore observations on the deep structure. Seismic profiling in the Gulf reveals the upper part of a sediment infill composed of a sequence of turbidites probably of Pleistocene age that are at least 1 km thick beneath the floor in the centre of the basin (Brooks & Ferentinos 1984; Higgs 1988). Projected onto the Xylokastro Fault, this observation provides a lower bound of about 2000 m for the total subsidence, below present sea level, of the basement rocks of the Pindos unit in the downthrown block (Brooks & Ferentinos 1984; Rigo 1994). Based on crude age correlations with the onshore sediments, Brooks & Ferentinos (1984) suggested that the average rate of turbidite sedimentation could be 1 mm yr^{-1}, which they regarded as a rough minimum bound.

For the later mechanical modelling, an estimate of loading and unloading by erosion and deposition of sediment is required. To evaluate the erosion on the uplifted block of the Xylokastro Fault we compare the present shape of the terraces, incised by minor streams and river valleys, with a curve that approximates their initial surface (Fig. 10). An exponential form has been used, although this is regarded as having no significance other than that it produces satisfactory looking fits to the positions of the shorelines along a N–S section (Table 1). We have taken three terraces with different elevations, and thus with different ages, that are well-defined (New Corinth, Old Corinth, and Laliotis), and explored the variation of erosion as a function of distance from the Xylokastro Fault trace (Fig. 10). Erosion is evaluated in the sections as the area removed, taking the present sea level as a reference for potential erosion of the terraces. The choice of this reference level is fully justified by the age correlations discussed in the next section. As expected intuitively, the erosion of the terraces on the footwall of the Xylokastro Fault appears to decrease with distance from the fault trace, and to increase with the age and the elevation of the markers. Erosion peaks correspond to incision of 80–90 per cent in the large river valleys near the fault, but the average maxima close to the fault are about 30 per cent for the three terraces (Fig. 10). The mean erosion percentage of the three terraces with increasing age is 11, 17 and 22 per cent, and corresponds approximately to the average value observed at 5–10 km distance from the fault.

Although the above estimates of the degradation of the terraces are precise, they do not take into account some important aspects that are necessary to assess the erosion in other sectors of the Xylokastro Fault footwall, west of the terraced area. For instance, our estimates do not sample areas with elevations greater than 600–700 m, for which the erosion rates are likely to be higher. Similarly, they do not give a measure of the erosion in the more resistant rocks of the basement. These estimates provide, however, definite bounds of 10–30 per cent for the average erosion within most of the $15 \times 15\ km^2$ sector of the footwall capped by the terraces (between 22°35′E and 22°50′E). Moreover, these bounds are representative of the span of time during which the shorelines and the basement rocks beneath them have been deformed.

Another requirement for the mechanical modelling of the deformation of footwall structures is to define precisely the geometry and relative position of the major fault. However, the faults responsible for the deformation of the Corinth shorelines are mainly offshore. The onshore trace of the Xylokastro Fault is clear west of 22°35′, where it is marked both by a distinct scarp and a lithological contrast (Fig. 9).

Footwall slickensides many tens of square metres in area indicate a local, near-surface average fault strike of N100°E and northward fault dip of 45°–55°. The presence of almost dip-parallel grooves and striae on these fault planes suggest dominant normal faulting, with a slight left-lateral slip. The eastward extension of the Xylokastro Fault is obscured by the young alluvium and human settlement along the coast (Figs 3 and 4). We suggest that two subtle slope breaks observed in the field and two slight kinks along the coastline correspond to possible surface traces of the Xylokastro Fault, allowing for a connection, across the slope and along the base of the underwater escarpment at 600–700 m depth, with the distinct, prominent offshore fault seen in the seismic profiles north-east and north of Kiato (Fig. 2) (Brooks & Ferentinos 1984; Higgs 1988). This offshore fault bends progressively north-eastwards to N70°E strike as it marks the base of the scarp north-west of the Perahora peninsula. Another major offshore normal fault discernible in the seismic reflection profiling cuts the base of the underwater escarpment about 3 km north of Xylokastro (Fig. 2). This fault apparently merges with the offshore fault seen in the two profiles farther east. It locally marks the trace of the northernmost, probably youngest, strand of north-dipping faults within the present Rift edge, as discussed in a previous section. Uplift of fan deltas east of Derveni (Fig. 2) and of the terraces near the mouth of the Fonissa river (Fig. 4) are probable effects of recent slip on that offshore fault strand, which duplicates the onshore trace of the Xylokastro Fault (Fig. 2). Fortunately, farther eastwards, the shorelines mapped between the Raizanis and the Trikalitikos rivers lie on the sector of the Rift footwall behind the N–S seismic profile north of Kiato [line 13 in Higgs (1988)] that accurately constrains the geometry and location of the simpler offshore fault seen at the eastward extension of the onshore Xylokastro Fault. Therefore, the slightly curved fault truncating the Gulf of Lechaio in Figs 2 and 4 represents the average trace of the Rift edge in the sector of the footwall where the terraces are mapped. Taking into account its curved geometry, the average strike of the Rift edge here is about E–W. However, this strand may be duplicated on its west part by the northern offshore fault, much like the Pisia Fault is duplicated by the Alepohori Fault in the Perahora peninsula (Figs 2 and 3). The straightforward assumption is that the average trace of the fault passes through the point where the onshore trace of the Xylokastro Fault and the underwater escarpment meet (Fig. 4). We fully discuss the consequences of the uncertainties in fault geometry and position in the modelling section.

4 AGE CONSTRAINTS, CORRECTIONS FOR SEA-LEVEL CHANGE AND FOR REGIONAL UPLIFT

4.1 Correlation in time

Pleistocene sea-level highstands are documented by the oxygen isotopic record derived from foraminifera in deep-sea sediments (e.g. Imbrie *et al.* 1984), and by the altitude of dated coral-reef strandlines in emergent coasts of the world, principally those of Papua New Guinea, which give a detailed palaeo-sea-level curve for the past 340 kyr (Chappell 1974; Bloom *et al.* 1974; Chappell & Shackleton 1986) (Fig. 11). Rapidly rising coastlines such as those of Papua New Guinea have average, constant uplift rates greater than 2 mm yr^{-1} and record

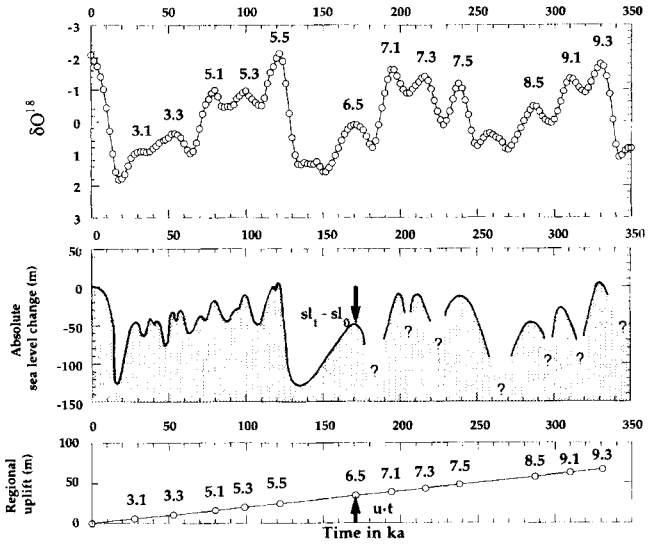

Figure 11. Chronology of global high sea-level stands in the last 350 ka deduced from the SPECMAP $\delta^{18}O$ deep-sea core record (Imbrie *et al.* 1984) (above), correlated with the absolute sea-level fluctuation, mainly derived from coral-reef strandlines on the Huon peninsula of Papua New Guinea (Chappell & Shackleton 1986; Merritts & Bull 1989) (centre), and with a hypothetical component of regional, uniform uplift at the rate of 0.2 mm yr^{-1} (bottom). The black arrows represent the corrections required for one highstand marker (stage 6.5) for sea-level change (sl_t-sl_o) and for regional uplift (u·t).

Pleistocene glacio-eustatic sea-level highstands in detail (Chappell 1983). In coastlines with intermediate uplift rates (between 0.5 and 2 mm yr^{-1}) higher highstands have a tendency to overlap and erase the record of some of the lower interstadials. Because the highstand corresponding to the last interglacial (isotopic stage 5.5) was especially high, about 6 m above present sea level (Chappell & Shackleton 1986), coastlines rising at slow rates (less than 0.5 mm yr^{-1}) record with good accuracy only the most prominent highstands, which correspond to the main interglacials (i.e. stages 5.5, 7.5, 9.3, Fig. 11). In this case the lower highstands, and particularly those corresponding to stages 6 and 8, are completely obliterated during stage 5.5. Thus, in Corinth, the record of a relatively large number of well-preserved Pleistocene highstands immediately suggests (Figs 4 and 6) that the southern coastline of the Gulf of Lechaio has been lifting at rates in the intermediate range. In addition, the converging geometry of the strandlines, apparently associated with progressive footwall deformation and tilt (Fig. 8), reveals that average uplift rates have been two to three times higher south of Xylokastro, near the fault trace, than south of Corinth, 15–20 km away from the fault trace.

The New Corinth and the Old Corinth terraces are among the most prominent and continuous in the Corinth–Xylokastro area (Fig. 4). They are thus good candidates to correspond to very high sea-level stands, similar to the present interglacial. The stratigraphic and palaeontological evidence suggests that the New Corinth terrace corresponds to the Tyrrhenian (Sébrier 1977). This is the stratigraphic level with the typical fauna association with *Strombus bubonius*, generally correlated with the last interglacial, isotopic stage 5.5 [Eutyrrhenian, ≈124 ka (e.g. Vita-Finzi & King 1985; Valensise & Pantosti 1992)]. For the Old Corinth terrace, the U/Th dating of

mollusc shells gives an age of 235 ka (+40, −30) (Sébrier 1977). Two U/Th analyses of the same coral sample (*Acropora sp.*), taken from the Old Corinth terrace 3 km south of the city of Corinth (star in Fig. 4), yield dates of 232 ka (+23.6, −19.7) and of 177 ka (+11.0, −10.1), which differ at the 1σ level (Collier *et al.* 1992). Clearly, these absolute ages are inaccurate and insufficient. Taking them at their face value, however, these ages suggest that the Old Corinth terrace may well correlate with isotope stage 7. With neither absolute dates nor good corals to sample, which is a common obstacle in many places of the world, we use a simple technique which assumes a nearly constant uplift rate at each locality on the coastline (Lajoie 1986; Merritts & Bull 1989). This approach is particularly adapted to assess the ages of the Pleistocene shorelines in the Xylokastro–Corinth area because, as shown below, their 3-D geometry is accurately constrained.

To correlate the strandline record of Corinth it is convenient to project the data onto sections parallel to the fault trace, thus representing uplift observations on coastline localities at the same distance from the fault. This solves the problem of footwall deformation and tilt, which have mainly cylindrical symmetry, and allows for the simplifying assumption of constant local uplift. Four such sections, at 5, 10, 15 and 20 km from the Xylokastro Fault, are obtained by interpolating the data (Fig. 12). Correlation of the inner edges of the two prominent terraces of New Corinth and Old Corinth with the first main sea-level highstands of oxygen isotope stages 5 and 7, in agreement with the stratigraphical evidence and the U/Th dates, gives uplift rates that can be used as guidelines in each section to correlate the rest of the inner edges with the main highstands (Fig. 12). In the three sections where both the Old Corinth and the New Corinth levels are present (at 5, 10 and 15 km from the fault), the correlation with the 7.5 and 5.5 highstands, respectively, yields rates of 1.31 and 1.24 mm yr^{-1} (at 5 km), of 0.96 and 0.73 mm yr^{-1} (at 10 km), and of 0.63 and 0.56 mm yr^{-1} (at 15 km). There are only small differences between rates at the same distance from the fault, consistent with the hypothesis of nearly constant local uplift rates. Correlating the prominent Laliotis shoreline with the first, highest sea-level highstand of stage 9 yields uplift rates of 1.01 and of 0.67 mm yr^{-1}, at 10 and at 15 km from the fault, respectively, which are slightly higher than the corresponding rates deduced from the Old Corinth shoreline. With this correlation, the Laliotis and the Old Corinth shorelines yield almost identical uplift rates of 0.49 and of 0.46 mm yr^{-1}, respectively, at 20 km from the fault. That the uplift rates deduced from the Old Corinth shoreline are systematically higher than those deduced from the New Corinth level, and that the average rates inferred from the older Laliotis level are still higher, might be interpreted as minor rate decrease with time. Finally, the highest prominent shoreline mapped (Nicoletto) would correspond to an interglacial older than the record from New Guinea. Assuming sea level similar to the present interglacial and extrapolating to the past, the uplift rates deduced in the sections at 15 and 20 km from the fault yield ages of about 540 ka and 580 ka for the Nicoletto shoreline. These ages correspond to oxygen isotope stage 15 (Bassinot *et al.* 1994) and imply that the interglacials corresponding to stages 11 and 13 are missing in the Corinth record. We suspect, however, that the complex remnants of platforms and scarps observed in the very eroded, lower part of the Nicoletto terrace (Fig. 4) may correspond to an intermediate terrace. The undefined inner edge of this intermediate level would be at 180–250 m altitude, between the Nicoletto and Laliotis shorelines, and could correspond to stage 11.

The self-consistency of the correlation of the Laliotis, the Old Corinth and the New Corinth levels with the main interglacials (stages 9.3, 7.5 and 5.5) gives support to correlating the intervening shorelines with interstadials, using similar local rates (Fig. 12a): the Temple level correlates with stage 9.1 and the Sataika level with stage 7.1 (plus 7.3?). Below the New Corinth terrace, the Melissi 3, the Passio 2, and the Kariotika 1 levels correlate well with stages 5.3, 5.1 and 3.3, respectively. The variations in the slope of the correlation lines used in each section for a time period of more than 300 kyr (Fig. 12a) may be taken to reflect the uncertainty ($\sigma \lesssim 0.1$ mm yr^{-1}) in the estimates of the average local uplift rates, which range from about 0.5 to 1.3 mm yr^{-1}, at 20 and 5 km from the fault, respectively.

Our correlation differs from that of Keraudren & Sorel (1987). This is mainly because they disregarded the assumption of constant local uplift, neglected sea-level variations, and because their altitude estimates are imprecise. Both correlations are qualitatively coincident, however, in the association of the New Corinth terrace with the highstand of the last interglacial, isotopic stage 5.5, in agreement with the stratigraphical evidence. Similarly, the Old Corinth terrace is related to the older interglacial corresponding to stage 7 in the two correlations. Nevertheless, we prefer to correlate this terrace to highstand 7.5, in better agreement with the constant uplift rate hypothesis, rather than with highstand 7.3, as proposed by Keraudren & Sorel (1987).

In the proposed correlation some relatively low highstands of the global record, in particular stages 6.5 and 8.5, find no clear expression in the Corinth terrace sequence. A possible explanation is that the uplift rates are not high enough to preserve them. South of Xylokastro, where the rates are fastest, however, the lower split level of the Sataika terrace, about 30 m above the New Corinth terrace (Fig. 7), could be an expression of stage 6.5, although this requires that the sea level at that time was somewhat higher than in the model from New Guinea (Fig. 12) (Chappell & Shackleton 1986). The Old Corinth terrace, which correlates with highstand 7.5, higher and younger than stage 8.5, includes two distinct, superimposed marine sequences (conglomeratic layers followed by marls and sands) (Dufaure & Zamanis 1980). Therefore, we interpret the complex structure of the Old Corinth terrace as being the result of the overlapping of stage 7.5 over stage 8.5. This observation may express, provided that the uplift rates are in the intermediate range, the greater tendency to structural complexity due to the overlapping of shorelines of stages immediately preceding main interglacials. Conversely, the simple structure of the Temple terrace with its distinctive 'Poros' facies is consistent with its proposed time of formation (stage 9.1), just after one main interglacial (stage 9.3). The progressive north-westward insertion of terraces is consistent with the higher probability of preservation of relatively low highstands with the increasingly higher uplift rates closer to the Xylokastro Fault. Similarly, the splitting of the main terraces into a large number of well-preserved sublevels immediately south of Xylokastro (Figs 6 and 7) is consistent with the higher uplift rates deduced there.

Closer inspection of the correlation at 5 km from the Xylokastro Fault, where the uplift rate is fastest and the

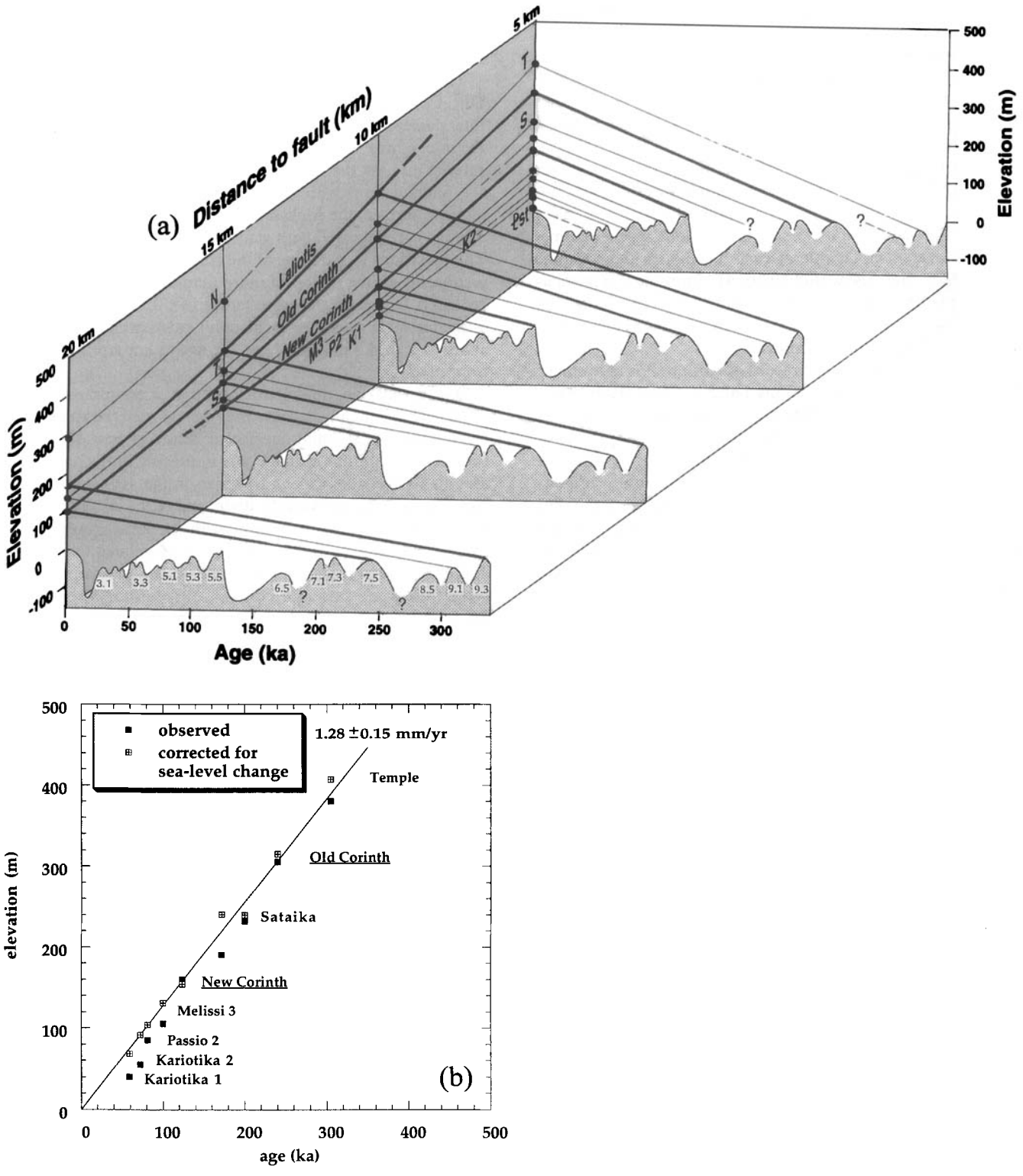

Figure 12. (a) Correlation of Corinth shorelines in space and time. The elevation of shorelines at four sections at different distances from the Xylokastro Fault (5, 10, 15, and 20 km) are correlated with the sea-level highstands of Fig. 11 assuming four constant uplift rates given by the average slopes of the diagonal lines. The sections correspond to vertical planes in Fig. 8, whose mirror image is represented on the left side. The symbols for the terraces are the same as in Figs 6(b) and 7(b). The highest terrace (Nicoletto, N) and the lowest shoreline (lst) are also represented. (b) The detailed time correlation in a section 5 km south of the Xylokastro Fault. The uplift rate averaged for all the shorelines is 1.28 ± 0.15 mm yr^{-1}, and 1.25 ± 0.14 mm yr^{-1} (2σ) if it is averaged only for the last 124 ka. Note that the sea-level correction tends to align the interstadial values (e.g. Kariotika 1, 2, Passio 2, Melissi 3) with those for interglacial highstands (i.e. Old Corinth, New Corinth, Present).

resolution is the best (Fig. 12b), shows in detail the effect of correcting the elevations of the shorelines for sea-level variations deduced from the global record. Without correcting for the sea-level variation, shorelines correlated with interstadials lie at elevations significantly below (20–40 m) those required to fit the uplift rates deduced for the interglacials (New Corinth, Old Corinth). Once the shorelines' elevations are corrected for sea-level variation, the deviation from a uniform rate diminishes. This is particularly clear for the sea-level highstands younger than the last interglacial (stage 5.5), for which, in addition, the resolution of both the isotopic and the coral-reef global records are the best (Shackleton 1987). The present elevation of the inner edges of the Kariotika 1, Passio 2 and Melissi 3 terraces, which we correlate with stages 3.3, 5.1 and 5.3, respectively, would imply significantly lower uplift rates, possibly 50 per cent less, than that required for the New Corinth terrace (last interglacial, stage 5.5). The proposed correlation with the record in Papua New Guinea (Chappell & Shackleton 1986) implies sea-level corrections of 28, 36, 19, 9 and -6 m for the Kariotika 1, Kariotika 2, Passio 2, Melissi 3 and New Corinth shorelines, respectively, which render them consistent with an average constant uplift rate of 1.25 ± 0.14 mm yr^{-1} (2σ) in the last 124 ka (Figs 12a and b). That these shorelines, once corrected for global sea-level variations, accurately define a uniform uplift rate gives strong support to the proposed age correlation. Finally, the ill-defined lowest shoreline located at the base of the cliff seawards of the Kariotika 1 terrace close to the Xylokastro Fault (Fig. 7), and seawards of the Passio 2, the Melissi 3, and the New Corinth terraces elsewhere (Fig. 4), is likely to correspond, near Xylokastro, to the 45 ka or the 40 ka levels of the New Guinea record (Chappell & Shackleton 1986), but overprinted by the Holocene transgression at more than 5 km distance from the fault (Fig. 12).

4.2 Effects of sea-level change and of regional uplift

To model the deformation of several different palaeo-horizontal lines requires the use of a common reference level. To refer ancient shorelines to the present sea level requires corrections. In principle, prominent shorelines that formed during interglacials need small corrections, because they correspond to sea-level highstands that, in the global record, are likely to be within a few metres of the present interglacial (Fig. 11). This is probably the case for the Laliotis, the Old Corinth and the New Corinth terraces, which are the most conspicuous and correlate with main interglacials. For this reason, in the next section we first model the deformation of these three shorelines alone, without corrections. Then, we assume the age correlation of these shorelines with isotopic stages 9.3, 7.5 and 5.5, respectively, and apply the small corrections for sea-level change (≤ 10 m). For shorelines corresponding to relatively low highstands, the required corrections for sea-level change are significant (up to 30–50 m), and strongly sensitive to the accuracy of both the age correlation and the estimated palaeo-sea-level. Therefore, we use the data and corrections concerning interstadials only as a final test for coherence with the models that fit the three interglacial shorelines. Finally, we note that the age correlation of the three main terraces (Laliotis, Old Corinth and New Corinth) with interglacials implies that the erosion estimates with respect to present sea level (Fig. 10) correspond very closely to percentages of the net tectonic uplift, which is the way we use them in the modelling.

An additional difficulty connected with the choice of a reference level to model footwall deformation is the possible existence of a regional component of the uplift. Collier (1990) interpreted the Corinth Isthmus and the terraces south of Corinth as located in hanging-wall positions. Then, Collier *et al.* (1992) argued that the observed uplift in this area results from 'background' uplift of the Peloponnesus, as this regional effect competes with extensional subsidence. These authors conclude that their estimates of 0.3 and 0.44 mm yr^{-1} in the Corinth Isthmus and south of the town of Corinth, respectively, are only minimum values of the background uplift (Collier *et al.* 1992). In contrast with this view, our observations indicate that the basin of Lechaio–Corinth Isthmus, as well as the basin of Alkyonides–Megara (Leeder *et al.* 1991; Collier *et al.* 1992), which trend WNW–ESE, are truncated, uplifted, and tilted by the new normal fault segments, striking E–W to ESE–WNW, that form the present southern edge of the Corinth Rift (i.e. the Xylokastro Fault and its eastward offshore extension, the Pisia and the Alepohori faults, Fig. 2). Unquestionably, the Corinth Isthmus is subject to extensional subsidence due to its position relative to the Loutraki, Kechrie and Agios Vasilios faults, and to the fact that it lies at the north-western extremity of the subsiding Saronic Gulf Basin (Fig. 2). However, that the Corinth Isthmus area undergoes net uplift relative to sea level is likely to result chiefly from a combination of the same tectonic processes as those acting along the terraced southern coast of the Gulf of Lechaio, at a similar distance from the major faults of the Corinth Rift. The strandline record of Corinth implies net tectonic uplift, which varies from a maximum of about 1.3 mm yr^{-1} 5 km south of the Xylokastro Fault, to about 0.5 mm yr^{-1} 20 km south of it (Fig. 12). Moreover, the converging geometry and progressive tilt of the strandlines suggest footwall flexure that reduces southwards from the Xylokastro Fault (Fig. 8). Therefore, the regional component of the uplift can be no more than the lowest observed uplift rate of about 0.5 mm yr^{-1}. Conversely, near Xylokastro, at least 0.8 mm yr^{-1} of the uplift must be due to footwall flexure alone. This implies that the uplift estimates by Collier *et al.* (1992) in the Corinth Isthmus and south of the town of Corinth are to be taken as maximum bounds of a possible regional component of the uplift, rather than as minimum bounds.

A possible way to retrieve the background uplift is to examine the hinterland sedimentary record in the Peloponnesus, away from areas deformed by normal faults. The occurrence of marine Pliocene deposits in many parts of the Peloponnesus and of the Hellenic arc are generally taken as evidence for regional tectonic subsidence, and of subsequent uplift (e.g. Mercier *et al.* 1977). Uplift is usually interpreted to be of regional importance, but the amount appears to be variable from place to place (Kelletat *et al.* 1976). The Neogene deposits on the southern side of the Gulf of Corinth (Keraudren 1970, 1971; Ori 1989; Doutsos & Piper 1990) include a first sedimentary cycle with a maximum probable thickness greater than 1000 m, reflecting a continental to shallow-water, lacustrine environment, and, unconformably overlying these deposits, a second cycle with thicknesses reaching 700–1000 m, consisting of Gilbert-type delta and deep-sea sediments. The first cycle sediments contain a few fauna and palaeoflora, which provide mostly climatic information (Sauvage & Dufaure 1976), and

have inferred middle to late Pliocene age (e.g. Doutsos & Piper 1990). The earliest documented marine marls are those found within the second cycle sediments, at 600 m elevation near Souli. They contain nanoplankton assemblages of the NN20 zone, indicating a middle Pleistocene age (Keraudren & Sorel 1987). The deposits of the second cycle including the marine assemblages and the younger marine terraces are generally less than 20 km from the faults at the present Rift edge and, as shown above, are subject to footwall deformation. The bulk of the first-cycle deposits are about 10–15 km farther south on average, but both the poorly constrained age and the lack of definite evidence for marine layers make it difficult to estimate the net uplift and hence the rates. However, the brackish marls and other shallow-water sediments deposited around Nemea (Fig. 2) close to the threshold between the Corinth and Argos basins, lie now at about 650 m elevation (Kelletat *et al.* 1976). In this threshold area, which seems devoid of large Quaternary faults, the Neogene sediments onlap the drainage divide between the two basins, suggesting that the Quaternary uplift is fairly independent of present or past rift-edge deformation. Furthermore, the Pliocene sedimentary environment in this open area could hardly be isolated from the Corinth and/or the Argos basins, and thus from the Aegean Sea, by major topographic obstacles. We conclude that average uplift here cannot be much less than the difference between present elevation and sea level, which is within a probable range of about 200 to 600 m during the Quaternary (2 Ma). Hence we take 0.1 to 0.3 mm yr^{-1} as likely values of the uplift of the Peloponnesus hinterland, just south of the areas flexed by the present Corinth Rift edge. Modelling of strandline deformation in the next section provides a further constraint on this problem.

5 MECHANICAL MODELLING

In the previous sections we retrieved the current shape of the terraces and their degree of erosion from the morphology. Then we assessed their ages and deduced uplift rates. However, these mostly pertain to the footwall of the Xylokastro Fault, and, as mentioned earlier, information available for the hanging wall is scarce. Thus we cannot directly determine fault slip from this data. A way to overcome this problem is to use the detailed information on footwall uplift, tilt and flexure contained in the deformed palaeo-shorelines to constrain a mechanical model of the deformation which does permit slip and slip rates to be determined. In this section we describe the model and the assumptions that underlie it, as well as our modelling strategy. The modelling procedure is non-linear, so we cannot discuss errors in a general way for all possible models; we can only consider in detail a limited range of parameters close to our final most favoured models. Before concentrating on such a detailed examination, however, we show that gross changes of our chosen values of erosion and deposition of sediment, fault dip or elastic moduli cannot produce viable alternative models in completely different regions of parameter space. For the parameters to which our models are insensitive we do not directly quote possible error contributions, but there is sufficient information in the figures for the reader to be assured that their contribution must be trivial.

5.1 Theory

We follow the modelling procedure outlined by King *et al.* (1988) and Stein *et al.* (1988) (KSR) and since extended and elaborated by a number of other authors (e.g. Kusznir, Marsden & Egan 1991; Ellis & King 1991). They proposed that geological and geomorphic structures result from the sum of processes occurring over many earthquake cycles. In the simplest view, the deformation resulting from N earthquake cycles is simply N times that resulting from one cycle. Each cycle is assumed to be identical, and each event experiences the same rheological and stress conditions. Clearly the method can be extended to more complex situations where all events are not the same, but the congruence of deformation in individual earthquakes with their associated geological and morphological structures provides powerful evidence that earthquakes of similar characteristics commonly repeat over long periods of time.

To model the seismic cycle, KSR adopted the approach of Thatcher & Rundle (1979): a fault modelled as a conservative dislocation surface in an elastic plate overlying a viscoelastic half-space. They showed, however, that successful modelling of geological structures did not require the full viscoelastic treatment. Stresses in the viscous substrate could be regarded as completely relaxed. For this reason, later modelling has ignored time dependence and has treated the lower region as an inviscid fluid. At the same time, KSR pointed out that the gravitational effects of erosion and deposition of sediment previously ignored within the seismic cycle should not be ignored in either the short or the long term. Their most surprising finding, however, was that the apparent long-term elastic modulus of the seismogenic crust was typically reduced by 100 to 1000, presumably by internal anelastic processes. Such reductions have been found by other authors both by similar methods (e.g. Le Pichon & Chamot-Rooke 1991; Masek, Isacks & Fielding 1994) and by using spectral relations between topography and gravity (e.g. Lowry & Smith 1994).

Unlike our dislocation models, a number of authors have modelled fault systems using a broken plate (e.g. Masek *et al.* 1994). However, while such models may be applicable to oceanic hot-spot systems (e.g. Turcotte & Schubert 1982, p. 126), where dykes introduce non-conservative processes, continental faults, by transmitting both normal stresses and normal displacements across their fault plane, transfer torsion, so broken-plate models cannot be appropriate. Many authors have also adopted a 'thin-plate' approximation (e.g. Turcotte & Schubert 1982), which assumes that vertical displacements are the same along any vertical line through the plate. The degree of flexure of such a plate is determined by its flexural rigidity, which is proportional to the cube of its thickness, and its modulus. There is a complete trade-off between thickness and the cube of the modulus. Since neither flexural rigidity nor modulus of rigidity is easy to understand intuitively, it has been common to retain a high modulus and reduce the elastic thickness from that suggested by the seismogenic thickness. This reduced elastic thickness is referred to as the 'effective elastic thickness'. Thus a crust with a seismogenic thickness of 15 km and with a long-term modulus reduced by between 100 and 1000 has been characterized by an effective elastic thickness of between 3.2 and 1.5 km.

In the modelling here, we pursue the same overall technique by using a boundary element method to produce 2-D cross-sections of a finite-thickness plate overlying a fluid half-space

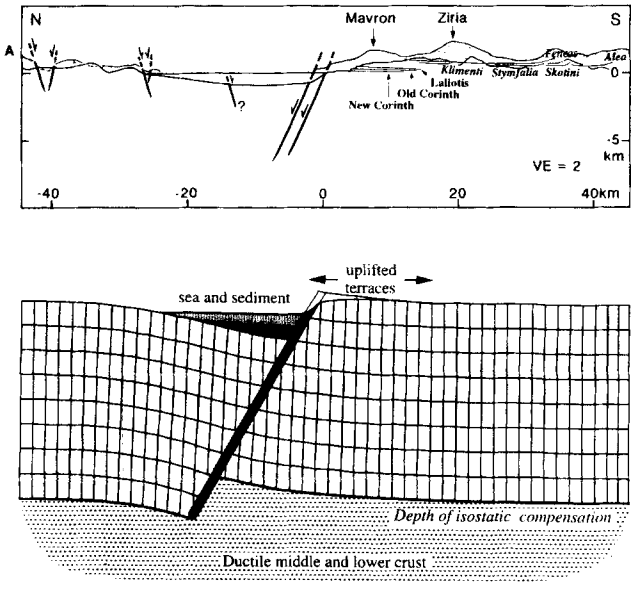

Figure 13. (a) Section of the Gulf of Corinth across the area of Corinth–Xylokastro in the central Gulf (A–B, Fig. 2). The higher topography (shaded) has been projected from a parallel section located 15 km to the west, across Mt Mavron. The projection of the three main deformed shorelines (New Corinth, Old Corinth, Laliotis) and of the longitudinal profiles of the catchments with reversed drainage (Feneos, Klimenti–Stymfalia, Skotini–Alea) are also indicated. (b) Deformation model with the same vertical exaggeration as (a) such that each rectangle is 2 km by 2 km. The model parameters are the same as those used to create Fig. 14(c).

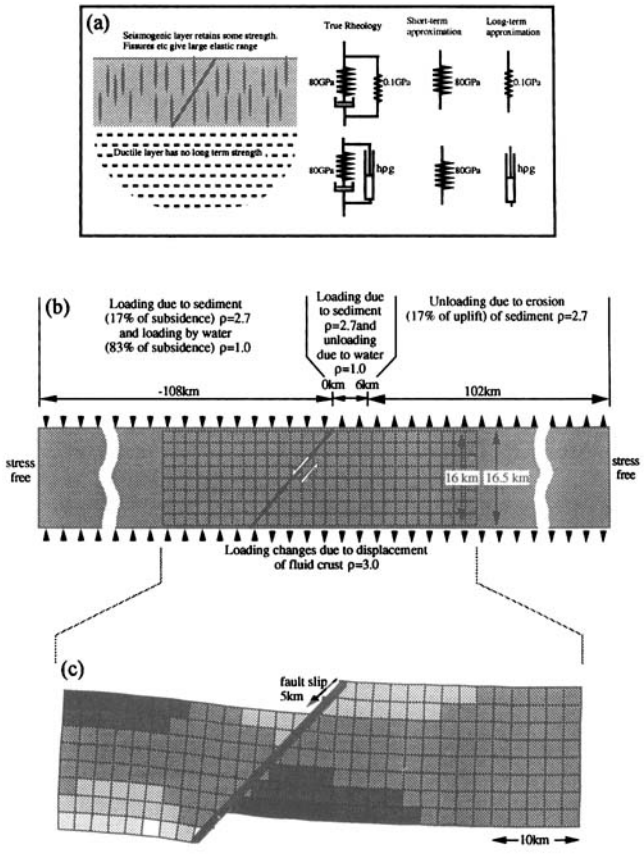

Figure 14. 2-D deformation model. (a) Rheological approximations used in the modelling. The upper part of the crust has long-term strength, but a long-term modulus greatly reduced by fissuring and small creeping faults. Thus the short-term elastic modulus (e.g. 80 MPa) is much higher than the long-term modulus (e.g. 0.1 MPa). For the lower crust the short-term elastic modulus is again about 80 MPa, but the long-term modulus is zero. (b) Boundary conditions applied to the deformed plate. For the convenience of calculations, forces shown at the surface are applied at the base of the plate. This avoids untidy looking effects of discretization at the surface. It also has the effect that changes of modulus only affect the flexural rigidities of the plate and large internal strains do not appear due to the surface loads. The gridded region is that shown in subsequent figures [Fig. 14(c) and Figs 16(b), (c) and (d)]. Fault dip is nominally 50° [actually 49.69°, tan(dip) = 16.5/14.0]. Other features of the model are discussed in the text. (c) Deformation of the region shown in (b) for a fault slip of 5 km. Dark shading indicates areas of areal dilation and light shading areal compression. The mid-grey corresponds to strains within the bounds of ± 1 per cent. Each increment of lighter or darker shading indicates a further strain of 1 per cent. The deformation model in Fig. 13(b) is the same as for this figure, but a greater lateral extent is shown and there is a vertical exaggeration of 2.

(King & Ellis 1990), such as that shown in Fig. 13(b). The effects of isostatic compensation, unloading by erosion of uplifted areas, loading by sediment deposition and loading due to changing marine levels are fully included. We show below, however, that a thin-plate approximation is inadequate for models such as that shown, and the concept of 'effective' elastic thickness is misleading.

The rheological simplifications involved in the modelling are summarized in Fig. 14(a) and are discussed at greater length later. We note that some authors have either adopted or proposed the need for more complex rheologies for the purposes of calculations (e.g. Buck 1993; Le Pichon & Chamot-Rooke 1991; Burov & Diament 1992) and also return to this question.

5.2 Modelling procedure and model sensitivity

The overall form of the model is shown in Fig. 14(b). The fault intersects the surface at 0 km. The base of the plate at 16.5 km is assumed to be the base of the seismogenic zone [in agreement with observations in the region (King *et al.* 1985)], and in turn is assumed to be the depth at which no long-term strength is retained. This is then taken to be the depth at which isostatic compensation occurs. Distances are negative in the hanging wall, and the base of the fault, at a depth of 16.5 km, is at -14 km. This gives a nominal fault dip of 50°, in agreement with the 45°–55° dip observed at the surface on the Xylokastro Fault and the $\approx 45°$ dip of fault-plane solutions of regional earthquakes determined using long-period waves (Taymaz *et al.* 1991). At the surface and at 16.5 km, the boundary conditions are zero tangential stress and a normal stress proportional to displacement. At the base this represents the depth-dependent hydrostatic forces of the mid-crustal 'fluid' assumed to have a density of 3.0. At the surface, loads due to erosion and deposition are also assumed to be proportional to vertical displacement with values differing for different parts of the hanging wall and footwall. All of the hanging wall and part of the footwall (6 km) are taken to be covered with water, and 17 per cent erosion and deposition of sediment is assumed throughout. This is in agreement with the mean erosion percentage determined for the Old Corinth terrace (Fig. 10). In the absence of detailed information in the hanging wall, we

have taken the same value for sediment deposition and added the extra load due to the water. As a result of footwall/hanging wall asymmetry, this requires that the Corinth Basin traps more sediment than that eroded from the footwall block alone. This is not unreasonable since sediment from the northern block also enters the central part of the basin, possibly added to by sediment transported from the shallower parts in the east and west. These boundary conditions are extended for large distances on each side of the fault, where the plate is terminated by vertical stress-free surfaces. The model is similar to, but simpler than, that described by King & Ellis (1990). They sought maximum fault displacements during much longer spans of time under conditions of high erosion and deposition of sediment (80 per cent), whereas here we fix fault displacement, and the erosion and deposition of sediment is modest.

Fig. 14(c) shows the deformation of the region of the plate shown gridded in Fig. 14(b). To avoid the singularities due to junctions between boundary elements, we plot from 0.25 km below the surface to 16.25 km at 2 km intervals. The deformed boxes are shaded in proportion to areal strain, with light shades representing net compression and dark shades dilatation. No irregularities due to discretization of the boundaries can be seen. It can be seen that the regions of high strain have horizontal dimensions comparable to the plate thickness, and it can also be noted that the vertical displacement at the base of the plate is different from that at the surface. Under such circumstances a 'thin-plate' approximation is invalid. The modulus used for the calculation is 0.1 GPa. If a typical unfractured modulus is 80 GPa then the 'effective' elastic thickness calculated in the conventional way is 1.75 km. Fig. 13(b) discussed above is the same as Fig. 14(c), but with geological interpretation added and a vertical exaggeration of a factor of two.

5.2.1 *The effect of changing the erosion and deposition of sediments and changing rock density*

Fig. 15 shows the effects of changing the proportion of loading and unloading of sediments. In Fig. 15(a), three cases are defined and are simplified from the preceding model. Case 1 corresponds to the lightest erosion and deposition that seems reasonable and Case 3 to the heaviest. Case 2 is intermediate between the two and corresponds to the mean erosion determined for the Old Corinth terrace (Fig. 10). It is the one we have used for the later modelling. Fig. 15(b) shows that none of the cases is significantly different for the footwall, the region where the terraces are modelled, although small differences do appear for the hanging wall. The loading in this region is greater because of the combined effect of water and sediment, which taken together produce a load equivalent to about 50 per cent deposition of sediment. The small differences in the hanging wall response, however, have no influence on the modelling of the footwall terraces. When compared to other sources of uncertainty, errors in our estimates of erosion and deposition are a minor source of error in the modelling. They would change the slip estimates by less than about 1 per cent. In later modelling with a component of regional uplift we consider a case with a larger elastic modulus (1–10 GPa) than that used in these tests (0.1 GPa). This is even less sensitive to loading changes than the one shown. The effects of changing the density of the underlying fluid are nearly the same as

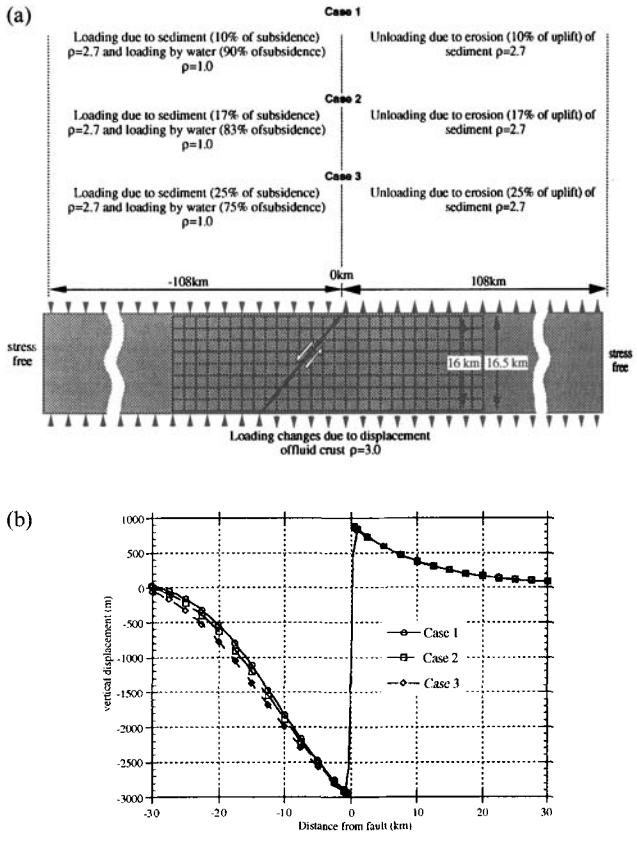

Figure 15. Sensitivity of the model to changes in erosion and deposition of sediment. The tests adopt the lowest elastic modulus used to model the data (0.1 GPa) and consequently indicate the greatest errors that can occur. (a) The three different cases examined vary from minimum likely values (Case 1) to maximum likely values (Case 3). Other aspects of the model are as defined in Fig. 14. (b) Vertical displacements at the surface for the three cases. For the higher levels of sedimentation in the Gulf (70 per cent) used for the long-term modelling, the downward flexure in the hanging wall is exaggerated, but the deformation in the footwall and the uplift to subsidence ratio are scarcely altered.

changing the percentage of erosion and deposition of sediment (and are identical for thin-plate models). Thus the foregoing tests also allow us to state that, even if the density of 3.0 that we have assumed is reduced by 10 per cent or more, the models will scarcely change.

5.2.2 *The effect of changing modulus and elastic thickness*

The effects of changing the elastic modulus of the plate while maintaining the other parameters constant are shown in Fig. 16. Deformation in the footwall is sensitive to modulus when the modulus is greater than 1 GPa for the footwall or 0.1 GPa for the hanging wall (Fig. 16a). Under these conditions, the scaling is that predicted for a thin plate and depends on the cube of plate thickness (approximately); the concept of 'effective' elastic thickness has some meaning (although we will identify some other problems in the next section). For lower moduli, this cubic scaling with thickness breaks down and the form of the surface deformation is nearly independent of modulus. Scaling is now such that the surface deformation depends linearly on the true plate thickness. For comparison,

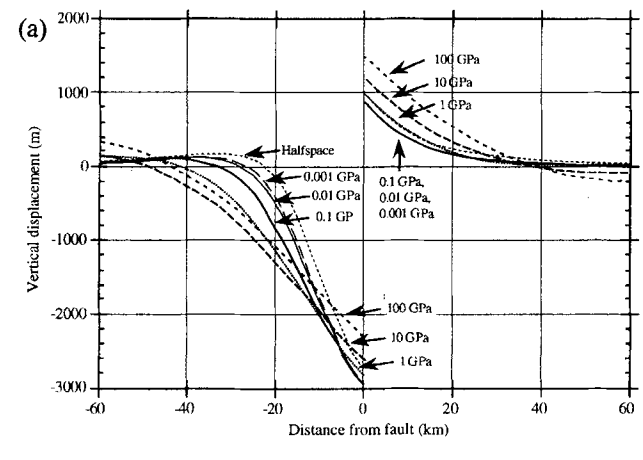

Figure 16. Effect of changing the elastic modulus. (a) Vertical displacements at the surface for values of modulus between 0.001 and 100 GPa. Note that for values of modulus less than 0.1 GPa, uplift-to-subsidence ratios are independent of modulus. For larger moduli the ratio changes. In terms of slip, a change from 0.1 to 1 GPa results in a 10 per cent slip decrease. In later modelling, such a modulus uncertainty arises as a consequence of uncertainty about the degree of regional uplift and is part of the reason why limited knowledge of regional uplift provides one of the greatest sources of error in slip determination. Also shown are the vertical displacements associated with a fault extending to the same depth as the base of the elastic layer in the other models, but in an elastic half-space. This gives surface displacements similar to the very low modulus plate models. (b)–(d) Complete plate deformation for three modulus values. Dark shading indicates areas of areal dilation and light shading areal compression. Mid-grey corresponds to strains within the bounds of ± 1 per cent. Each increment of lighter or darker shading indicates a further strain of 1 per cent. A horizontal line at the base of each figure indicates the base of the plate prior to deformation. The two lower values of the modulus, although differing by a factor of 100, result in almost identical plate deformations.

the rather similar surface deformation for the same fault in an elastic half-space is shown. The processes occurring at depth are shown in Figs 16(b), (c) and (d). The deformation difference between 1 GPa and 0.01 GPa is easily seen, but between 0.01 GPa and 0.0001 GPa the deformation differences are small and can only be discerned at the base of the elastic layer

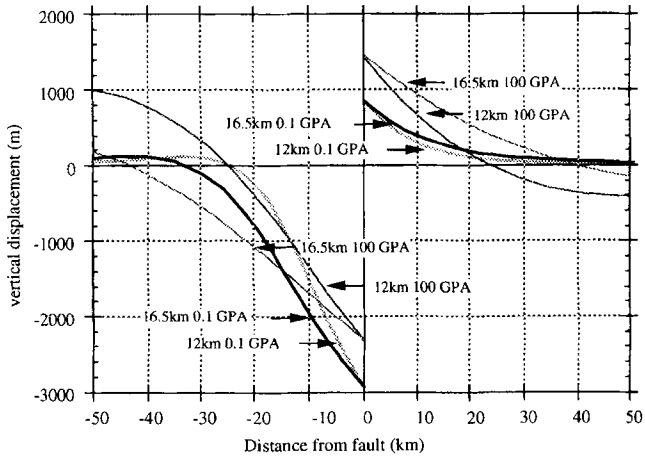

Figure 17. Effect of changing the modulus for two different values of real elastic thickness. A modulus of 0.1 GPa and an elastic thickness of 16.5 km are the values favoured by later modelling. The other values are arbitrarily chosen to illustrate clearly the effects of changing the values (see text).

(particularly below the hanging wall). The Corinth terraces are located in the region of the footwall where the shape of the curves is insensitive to modulus when it is below 0.1 GPa, and where the displacements are similar to those for an elastic half-space.

Fig. 17 shows plots of vertical displacement for true elastic thicknesses of 16.5 and 12 km. The effect of the scaling relations described above can be seen. The difference between the two low-modulus examples where scaling is approximately linear with thickness is much less than that between the high-modulus cases where scaling follows the cubic law. Important features, which will be considered in later discussions of regional uplift, can be seen in this figure. For low moduli, a transition from subsidence to uplift does not occur in the footwall. A 'zero crossing' transition from subsidence to uplift does occur in the hanging wall but the amount of uplift is modest. For the higher moduli, however, substantial reversals from uplift to subsidence occur in both the footwall and hanging wall (Fig. 16) and their location is very sensitive to elastic thickness (Fig. 17).

5.2.3 *The effect of changing fault dip*

The effect of changing the fault dip within reasonable bounds is shown in Fig. 18. Fault displacement is adjusted to give the same vertical throw. For the two examples of modulus shown there are no dramatic differences between the curves. The reasons for the changes can be understood by considering the distribution of buoyancy forces at the base of the plate. These experience a change of sign where the fault cuts the base of the elastic layer, but are displaced differently with respect to the surface location of the fault as the fault dip changes. The location of the point where the sign changes with respect to the surface fault is more sensitive to dip for shallow dips than for steep ones, and it is therefore not surprising that there is less difference between the curves for 60° and 50° than between those for 50° and 40°.

The fact that fault dip and true plate thickness control the distribution of buoyancy forces at the base of the elastic layer is important for thin-plate models. It is incorrect to assume that in the hanging wall above the fault the vertical

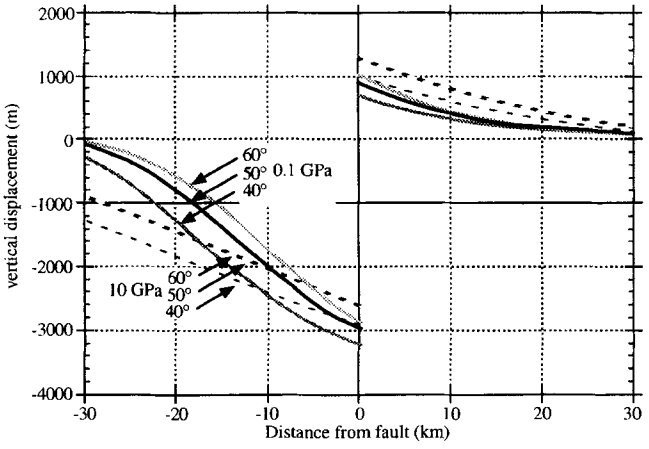

Figure 18. Effect of changing the fault dip for two different values of real elastic thickness. The vertical displacement of 3813 m in each case is the same as that for a 50° (49.7°) dipping fault with a total slip of 5000 m. Fault dips for the Corinth Rift cannot be outside the range of 40°–60°, yielding a total vertical component of slip error less than 10 per cent. The horizontal slip and total slip will additionally include an error associated with calculating the horizontal component trigonometrically from the vertical component for different fault dips.

displacement is the same as below the fault. The sign of the displacement changes as the fault is crossed. The region where this occurs depends on the fault dip and the true plate thickness. Thus two thin-plate models, because they differ in true plate thickness, can have the same effective elastic thickness and the same fault dip, but will have different distributions of buoyancy forces acting on the base of the plate.

5.3 Modelling the observed terrace profiles

Having examined the influence of basic model parameters on the nature of the surface deformation we can now turn to how these can be constrained by the observed terrace profiles. We start by examining the three terraces that are defined best (New Corinth, Old Corinth and Laliotis). The most straightforward modelling procedure is to fit the observed data on the assumption that the average fault strike is E–W and the fault location is at the point where the onshore trace of the Xylokastro Fault and the underwater escarpment meet [$(x, y) = (0, 0)$ in Fig. 4]. For this first-order, direct modelling we use the three palaeo-horizontal lines, ignoring their ages and thus assuming that the sea level for these terraces was the same as at present. Fig. 19(a) shows the best-fitting model under these conditions. Because no transition from uplift to subsidence is observed in the footwall the resulting elastic modulus is low, with a value of 0.1 GPa, placing it in the region where the model is nearly insensitive to modulus. The true elastic thickness or depth at which isostatic compensation occurs is 16.5 km. The fault dip is 50° and the erosion and deposition of sediments is as shown in Figs 14(b) and (c). For each terrace the total fault slip required is indicated in metres. Provided the above assumptions are correct, the model and fault slips are well constrained. However, assumptions about earlier sea levels, regional uplift and errors in the location of the submarine fault responsible for the terrace uplift can significantly modify some parameters.

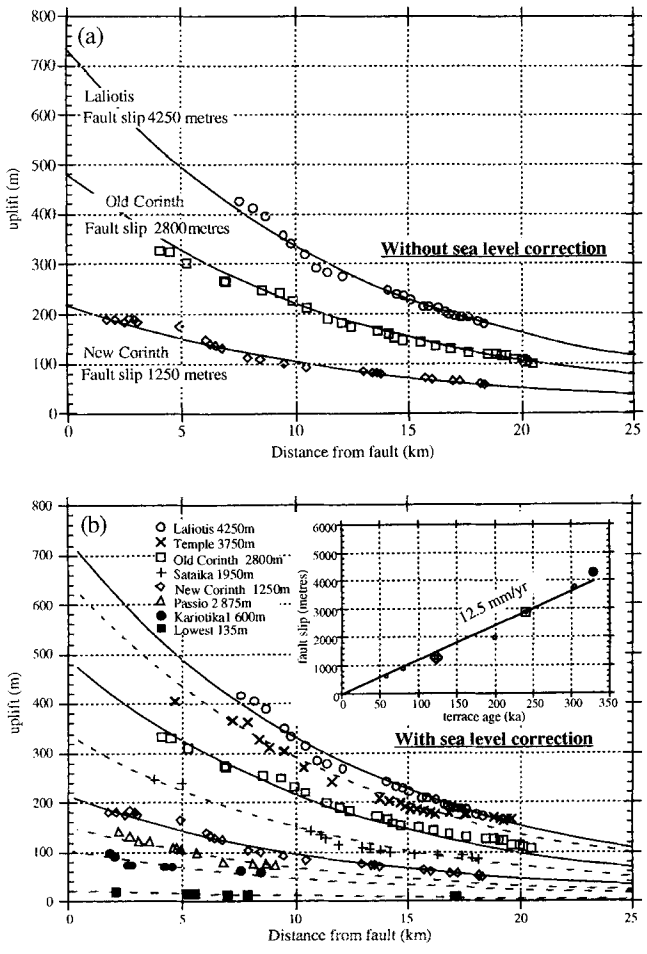

Figure 19. (a) Best-fitting curves for the three best-defined terraces with no sea-level correction applied. The model parameters are discussed in the text in relation to Fig. 14. The values of total fault slip for each terrace required to produce the fits are shown. (b) Best-fitting curves for all the terraces with sea-level correction. The corresponding fault slips are indicated in the inset key for terrace names. The top right inset is a plot of the slip as a function of time, with larger symbols for the three terraces correlated with interglacials.

5.3.1 *Modelling data corrected for sea-level changes*

A second step is to use the terrace ages and the deduced original elevation of the shorelines with respect to the present sea level, as described earlier. Fig. 19(b) shows model fits for the three terraces shown in Fig. 19(a) but corrected for sea-level changes. The maximum data correction is very modest, 10 m for the Old Corinth terrace, and no change is required to retrieve a good fit. The same figure also shows the fit for all the terraces (Fig. 19b). By adjusting only the fault slip, and no other model parameter, close fits can be obtained for all of the data with the exception of that for the lower parts of the Temple terrace. Since some of these terraces are corrected by 50 m or more, the ability to find such a good fit by adjusting fault slip alone strongly suggests that the sea-level adjustments and the terrace ages are correct.

5.3.2 *Modelling data corrected for presumed regional uplift*

There are some grounds, discussed earlier, for supposing that the region has been subject to an overall uplift of between 0

and 0.3 mm yr^{-1}. We have therefore examined such a possibility by adjusting the terrace heights appropriately with age. Fig. 20(a) shows adjusted heights for the three best-determined terraces assuming an uplift rate of 0.2 mm yr^{-1} together with fits to the terrace profiles. These fits are achieved with an elastic modulus increased to 1 GPa and an elastic thickness reduced from 16.5 to 15.1 km. The new model has fault displacements that are reduced by about 25 per cent. Looking back at Figs 16 and 17, it is possible to identify why the regional uplift has changed the model. The addition of regional uplift reduces the amount of uplift that must be accounted for by faulting and thus the predicted fault displacements diminish. The terraces distant from the fault also converge to zero uplift more rapidly with distance from the fault. To accommodate this convergence, both a greater modulus and a lower elastic thickness are required.

Fig. 20(b) shows the terraces corrected for a more extreme uplift rate of 0.4 mm yr^{-1}. The fits now require the following model parameters. The two upper terraces must have an elastic thickness of 10 km with a modulus of 10 GPa, and the lower terrace an elastic thickness of 9 km with the same modulus. The trend to higher modulus and lower elastic thickness occurs for the same reasons as before, but to accommodate the rapid approach of the terraces to zero displacement at distances between 18 and 24 km requires the very high modulus and low thickness. Such values of modulus and thickness seem unlikely. As discussed above, studies elsewhere find much lower long-term moduli for the upper crust, and seismicity in the Gulf of Corinth extends to 15 km or more (King *et al.* 1985), making a real elastic thickness of 9 or 10 km too small. A more subtle problem concerns the reduced elastic-layer thickness for the lowest terrace. If this has come about by a reduction of strength with time, the final values for crustal parameters should affect all of the terraces. Thus, even if greater thicknesses and larger moduli have existed in the past, they should be unobservable at present and all the terraces should be fitted by a 9 km elastic layer. Thus the modelling is not self-consistent.

From the foregoing, it appears that some trade-off occurs between assumed regional uplift rate and a combination of elastic thickness and elastic modulus. Modest regional uplift rates of 0.2 mm yr^{-1} are compatible with plausible values for these parameters. While fits can be made to the data corrected for uplift rates of 0.4 mm yr^{-1}, the elastic thicknesses and moduli become improbable. With the modest values possible, the presence or absence of regional uplift provides both significant uncertainty in the amount of slip on the fault and the largest uncertainty in our ability to determine the long-term effective elastic modulus of the crust.

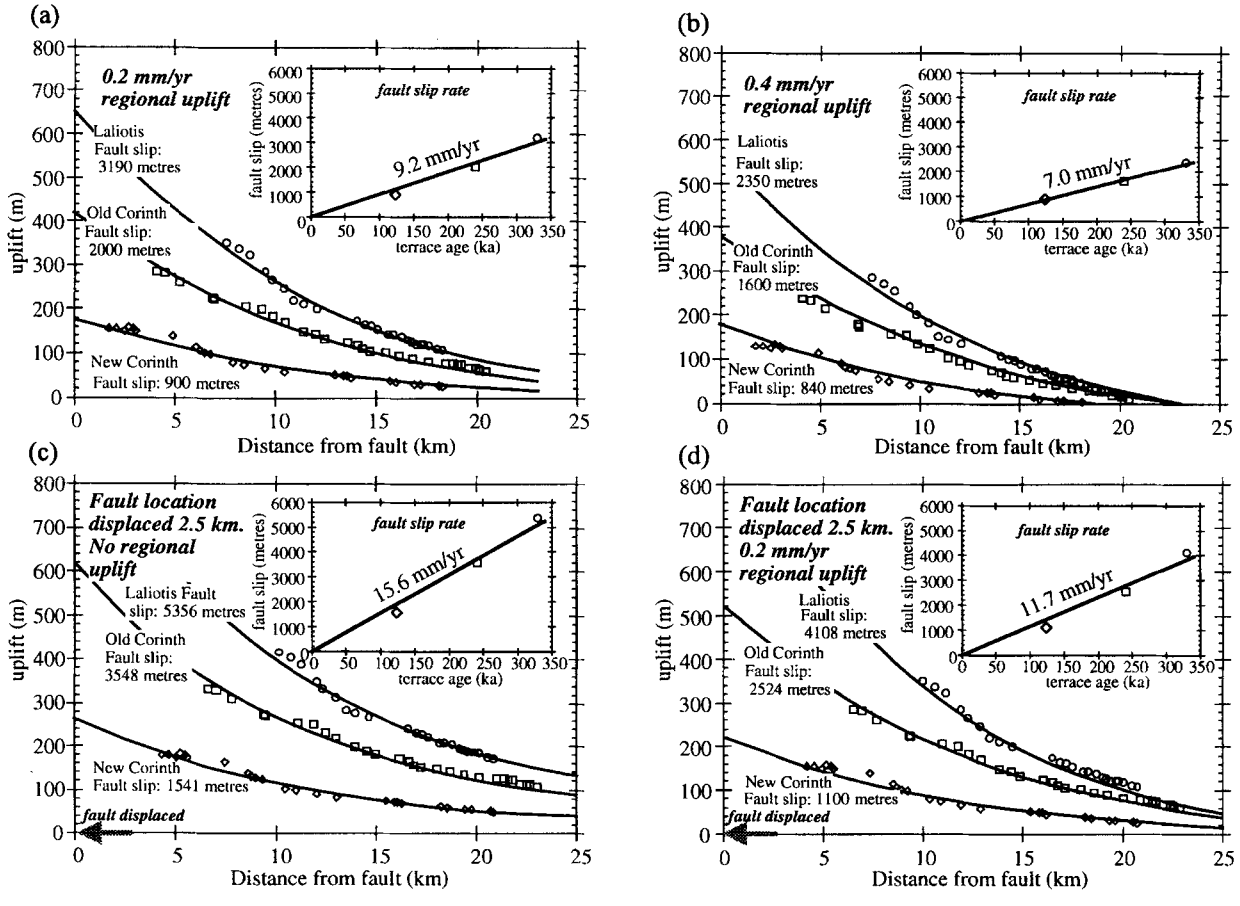

Figure 20. Tests of models with sea-level correction, regional uplift and with the fault shifted further away from the terraces. (a) Model for a regional uplift rate of 0.2 mm yr^{-1}. Fits require a modulus of 1 GPa and a plate thickness of 15.1 km. (b) Model for a regional uplift rate of 0.4 mm yr^{-1}. Fits require a modulus of 10 GPa and a plate thickness of 9–10 km. See the text for a discussion. (c) Fits for terraces with the fault displaced 2.5 km further away from the terraces. (d) Fits for terraces with the same fault shift but corrected for a regional uplift of 0.2 mm yr^{-1}. Insets as in Fig. 19(b).

5.3.3 *The effect of changing fault position*

It has been assumed that a single E–W-striking fault is responsible for the deformation of the Corinth terraces. However, the geometry and exact location of the fault segments truncating the Gulf of Lechaio between Xylokastro and the Perahora peninsula are not accurately defined everywhere, as discussed earlier (Fig. 2). For the terraces closest to the fault near Xylokastro, the error in fault location cannot be large unless a second fault offshore is active. Fig. 20(c) shows the result of assuming that the fault is more distant by 2.5 km, without a regional uplift component, and Fig. 20(d) that of assuming the same offset in the fault location but with a regional uplift rate of 0.2 mm yr^{-1}. In both cases, satisfactory fits can be obtained without changing any parameter other than fault slip, which must be increased by 25–30 per cent. Thus while changing the assumed fault location does not change the elastic modulus required to fit the data, it causes uncertainty for determining fault slip. The second offshore fault seen in the seismic reflection profiling (Fig. 2) is likely to be no more than about 2.5 km distant, and if the two faults share activity equally the mean distance will be 1.25 km. Thus a maximum underestimate of slip of 10–15 per cent rather than 25–30 per cent is the most reasonable.

Finally, while we have not attempted a fully 3-D model, it is possible to estimate the effects of errors that result from our simplified fault geometry. Most terrace deformation results from the parts of the fault that are not much more distant than its closest point. In Fig. 21(a) the fault is divided for convenience into three regions, A, B and C, and in Figs 21(b), (d) and (f) dotted lines indicate the parts of the fault responsible for most of the deformation for given points on the terraces. Deformation of the northernmost region of the terraces is only influenced by the adjacent part of the fault (A) (Figs 21b and c) and an infinite length, E–W-striking fault segment appears to be a satisfactory approximation for the modelling. For intermediate distances to the fault, the deformation of the terraces may be partly influenced by closer faulting (B), with the same strike and less slip (Figs 21d and e) and at greater distances it may be influenced by a similar fault segment located slightly closer but with slip reduced further (C) (Figs 21f and g). In the two foregoing cases, the effect of an infinite length fault with E–W strike, appropriate distance and slip is schematically shown together with a curve representing the terrace deformation with the simplified fault geometry taken for the modelling. The effect must be substantially less than the exaggerated differences represented by these curves. Fig. 21(h) shows an estimate of the likely combined effect, with a slight uplift increase between 5 and 15 km and a slight decrease beyond that. These effects may cause the slight undulations visible in the data (e.g. Fig. 19). Whether or not this interpretation is correct, we can conclude that our simple geometry with a fault infinite in length in the E–W direction is an adequate approximation.

5.3.4 *Estimating fault slip rates*

The foregoing modelling permits estimates of the fault slip rate to be made. These are summarized in Fig. 22 and vary from 7.0 mm yr^{-1} to nearly 16 mm yr^{-1}. The extreme values are, respectively, for an assumed regional uplift of 0.4 mm yr^{-1} and for no regional uplift but for the fault assumed to be 2.5 km farther north of the terraces than our best estimate of its location. This gives a mean slip value for all of these estimates of about 11 mm yr^{-1}, with a range of slightly less than ± 40 per cent. The extreme cases are very improbable, so a more likely range is ± 20 per cent.

5.3.5 *Remarks concerning other modelling strategies*

The modelling we have adopted follows the widely accepted view based on the Brace–Goetze curves (Goetze 1978) that the lower crust behaves in a viscoelastic fashion. However, our best-fitting models occur when the elastic modulus of the upper crust is very low, such that surface displacements for a thick-plate model become similar to those for an elastic half-space. Such half-space models are favoured by Ward (1986) and Valensise & Ward (1991), who put the shear modulus to zero and suggest that this mimics a very weak crust. In fact, for such a calculation the vertical deformation at the surface is independent of both the Young modulus and Poisson ratio or any other combination of elastic parameters, and is only dependent on the fault geometry. We noted, referring to Fig. 16, that a half-space model is similar to our successful models. Thus if our data could be modelled even moderately successfully with either a half-space or a thick plate over a fluid, the ability of the modelling to constrain the mechanical behaviour of the lower crust must be called into question. It would suggest that the upper and lower crust can either have any constant modulus or the upper crust can have a low modulus (sufficient to ensure that the system corresponds to the thick-plate condition, Fig. 16) and the lower crust can act as a fluid. The two models behave in a similar way at the surface because neither permits much vertical motion at the base of the upper crust. For the half-space this is because of elastic forces from below, and for the fluid it is because of gravitational ones.

The two models should, however, differ under conditions of high erosion and deposition of sediment, and it seems unlikely that such cases modelled by KSR and King & Ellis (1990) could be modelled using a half-space. None the less, such potential similarities between conditions where the lower crust retains strength indefinitely or has virtually no long-term strength must cause us to be cautious about our current understanding of crustal rheology.

Figure 21. Effects of changes of fault strike and variations of slip along the Xylokastro Fault. (a) Simplified map showing the fault segments with substantial slip and the region of the terraces, which are modelled with assumed constant strike E–W (bold trace). (b) The terraces close to the fault are only influenced by the short fault segment A. (c) These are modelled on the assumption that the fault is infinite in length and of constant slip. (d) For terraces at an intermediate distance the fault is almost certainly closer and the uplift is influenced by this segment of fault B. (e) Uplift due to a fault closer by 3 km, but of infinite length, with a slip reduced by 10 per cent. The uplift at intermediate distances is partly influenced by segment B. (f) Terraces at greater distances from the fault are influenced both by segment B and segment C. (g) Uplift due to an infinite length fault with a distance and slip corresponding to segment C. (h) The overall uplift is modified because of the foregoing effects. At intermediate distances, uplift will be slightly greater than predicted (though less than an infinite-length fault corresponding to B), and at greater distances uplift will be slightly reduced or unchanged by the influence of B and C.

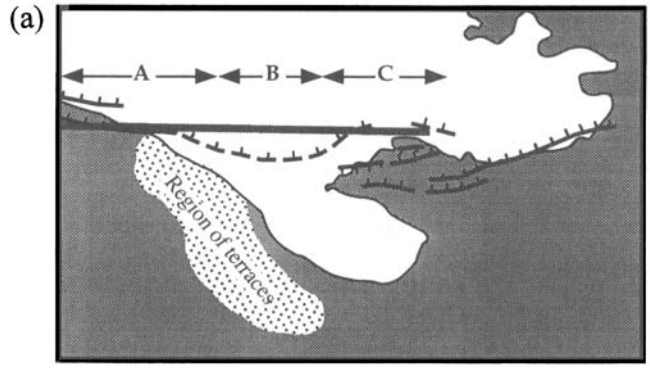

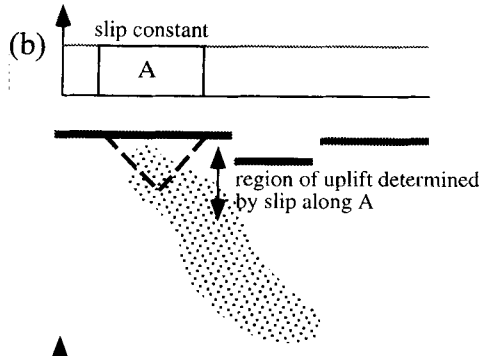

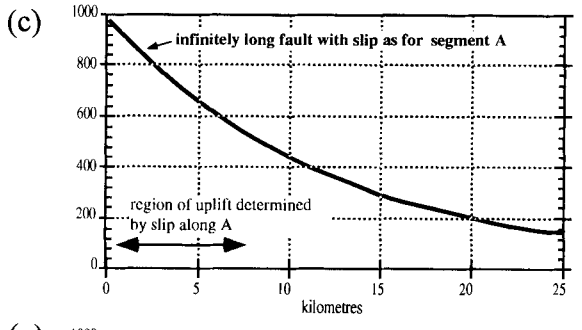

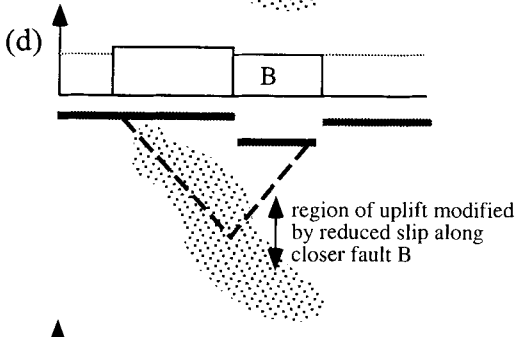

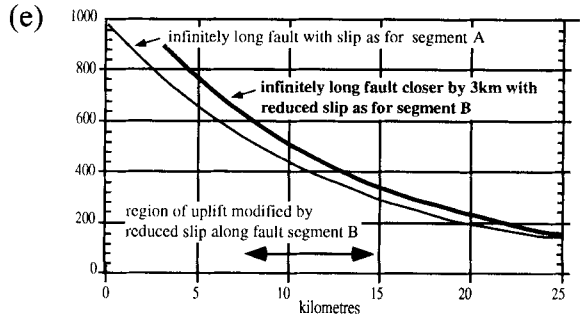

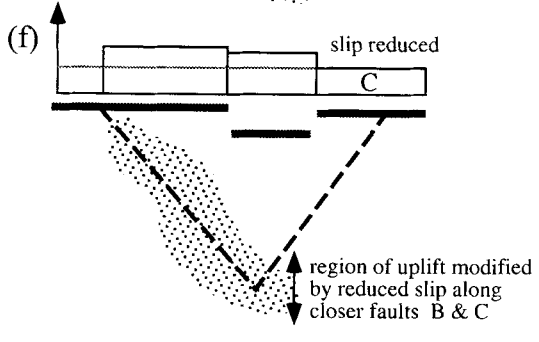

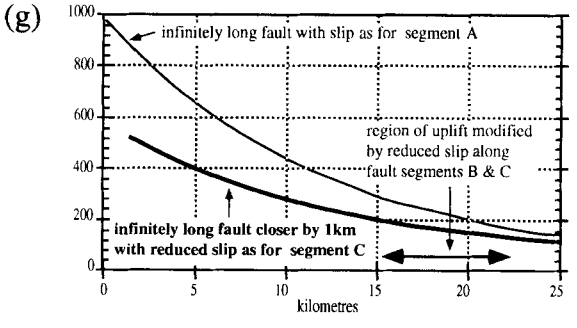

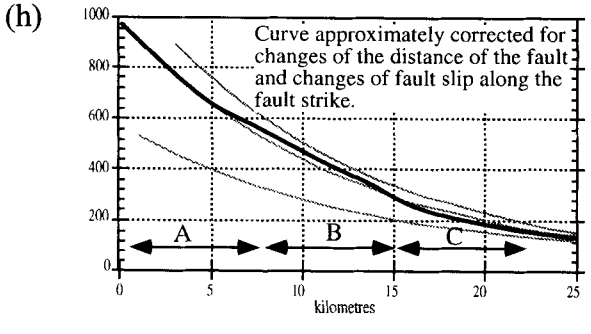

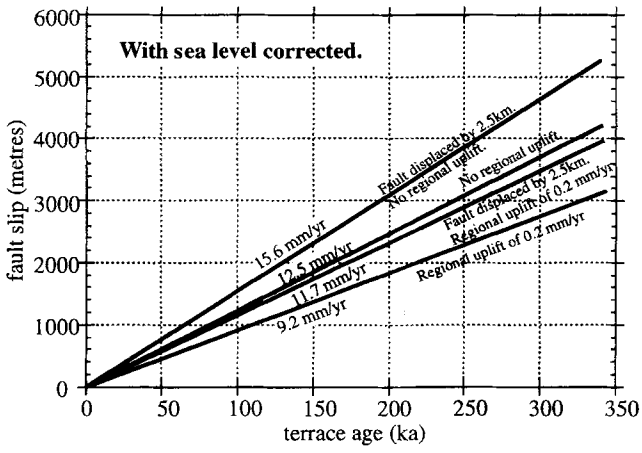

Figure 22. Fault slip rates predicted by the previous models. The lines are taken from the inset plots in Figs 19(b) and 20.

6 MECHANICS OF THE CORINTH RIFT SYSTEM

6.1 Errors in fault slip rates from the terrace modelling

We have discussed some of the sources of error in both the collection of the data and the modelling. We now assemble these in five categories, together with other uncertainties to establish an overall reliability for our slip estimate.

(1) We considered errors in the measurements of the position and elevation of the shorelines. These are small, less than the size of the symbols which represent their position in Fig. 8.

(2) The errors in the age correlation and in the estimates of past sea-level highstands have been discussed. They rely on correlating the terraces with the worldwide chronology based on oxygen isotopes, dated uplifted coral-reefs, and the Milankovitch cycle (Figs 11 and 12), but are supported by local stratigraphical evidence and U/Th dates. Our correlations are so well constrained that it is hard to believe that they could be seriously in error. Rates of tectonic uplift as a function of distance from the fault vary from 0.5 to 1.3 mm yr^{-1}.

(3) We have estimated the model sensitivity to variation of the most significant mechanical parameters (loads due to erosion and deposition, density, elastic modulus and thickness, and fault dip, Figs 15, 16, 17 and 18). For reasonable models with an elastic modulus of the order of 0.1 GPa and a plate thickness of about 16.5 km there is little sensitivity to variations of modulus, changes of erosion or deposition, or fault dip. We have not attempted to define exactly the small potential errors in each case, but suggest an overall error of less than 10 per cent in our final slip estimate.

(4) Much more important sources of error appear to be associated with uncertainty in fault position and the possible presence of regional uplift (Fig. 20), and for these we have directly examined sensitivity. We find a trade-off both between flexural rigidity and true elastic thickness and between fault position and reference level (which depends on the amount of regional uplift). Errors are not random. The fault might be more distant from the terraces than we have assumed but not closer. Similarly, regional uplift is possible, but regional subsidence is not. The sense of these errors is opposite and thus tends to cancel; although a slightly more distant fault or the effects of regional uplift can change slip estimates, the two acting together would not. We have also explored the influence of the 3-D geometry of the fault, which changes strike and varies in slip from east to west (Fig. 21), and showed that, although this might explain minor features of the terraces, it has little effect on our slip estimates. Taken together, we consider the total error in the estimated slip to be less than 20 per cent (Fig. 22).

(5) The estimated slip and slip rates are well constrained by the terrace observations, which also constrain the model parameters. Although this modelling is robust, there remains the possibility that the strategy is wrong. A model-independent way to test the validity of the deduced slip values is to compare footwall uplift to hanging-wall downdrop ratios (u/d) obtained in Corinth with those observed for similar faults elsewhere in the world. In the models the u/d ratio is about 1/3.5 for the no-regional-uplift hypothesis (Fig. 19b), and 1/2.7 considering 0.2 mm yr^{-1} of regional uplift (Fig. 20a). The former is very similar to the u/d ratio for normal faulting in the Basin and Range [e.g. Cricket Mountain (Stein *et al.* 1988)]. However, uplift to subsidence ratios approaching 1:2 have also been observed [Borah Peak (Stein *et al.* 1988) and the Teton range (Byrd, Smith & Geissman 1994)]. In both places erosion is high. This can result in uncertainties in determining a pre-deformation reference level (hence uplift u/d ratios are poorly determined) or, if real, the uplift may be explained by an isostatic response to high footwall erosion (King & Ellis 1990).

Thus, when compared with analogous features in regions of low erosion comparable to the Gulf of Corinth, the uplift to subsidence ratio and hence the slip predicted by the modelling is reasonable. We note later that the long-term deformation predicts a sediment infill of the Gulf of 5 km, wheras reflection profiles have so far only reached a depth of 1 km (Brooks & Ferentinos 1984). Should future work demonstrate that the depth to basement is not substantially greater than this, then, in the absence of high footwall erosion, profound changes will be needed in the modelling strategy to provide an explanation.

6.2 Long-term deformation across the central Gulf

The Xylokastro terraces allow modelling for the last 350 ka. However, the present edge of the Corinth Rift has been evolving for about 1 million years, cutting an earlier landscape. Tilted Plio–Pleistocene sediments and the middle–late Pleistocene drainage reversals can also be identified (Fig. 2) and used to provide information about the longer-term evolution of the Gulf. Fig. 23(a) shows the fit to the section through this landscape using similar average model parameters to those used for the terraces (50° dip; modulus between 1–0.1 GPa; true elastic thickness of 15–16.5 km) and under the hypothesis of 0.1 mm yr^{-1} of regional uplift. In a similar way to that employed for the terraces (see Fig. 10), the erosion of the footwall for this longer time period can be estimated from the degree of incision of the mountains composed of uplifted Plio–Pleistocene fan-delta conglomerates (for instance Mt Mavron, Fig. 2). Although estimated less precisely, the erosion is less than 50 per cent, and is more likely to be about 30 per cent of the total uplift. It is evident that the sedimentation in the Gulf must be greater than this, and we concluded that a value of 70 per cent is reasonable. This value also provides an approximate balance between likely long-term erosion around the Gulf and a reasonable total contemporary sediment fill.

The new deformation curves have forms little different from those with lower deposition; in particular the uplift to subsidence ratio at the fault is scarcely changed. Downward flexure on the northern side of the Gulf is increased in the manner shown for lower sedimentation values (Fig. 15). Part of this flexure could be accommodated by antithetic faulting (Figs 2, 13a). However, for this first-order modelling the contribution of such faulting is not specifically assessed. Although the model is more sensitive to error than the terrace models, its contribution to slip errors is still less than perhaps 15 per cent, much less than the uncertainty in the factors we fit in Fig. 23.

The dashed curves in Fig. 23(a) (inset) represent two flexed horizons constrained in the footwall by the elevation of the catchments with reversed drainage, and by the elevation of the top layers in the fan-delta conglomerates of Mavron Oros, also fed by northward directed drainage. These may be considered as minimum and maximum bounds for the total footwall flexure. The smaller slip of 10 km corresponds to a hypothetical base level to which the original northward-flowing drainage of the catchments of Feneos and Klimenti may have graded. The larger slip of 13 km corresponds to the earliest stage of fault development we can deduce from sedimentological and morphological remnants seen in the present topography (i.e. the highest marine base level compatible with deposition of continental sediments in the fan delta). Another estimate can be made using the maximum elevation of the marine sediment outcrops near Souli. Taking the constant slip rate of 11 mm yr^{-1} deduced from the terrace's deformation to account for the slip of 5 km, we obtain 455 ka, which corresponds fairly well to the age of the fossils found at Souli (Keraudren & Sorel 1987). Similarly, taking the average total slip of 11.5 ± 1.5 km to result from faulting at the same constant slip rate as above gives a first-order estimate of the fault inception at about 1.05 ± 0.15 Ma, in close agreement with the stratigraphic age of the fault. Although this long-term model confirms the modelling of the terrace data in a general way, it does not constrain the mechanical parameters further.

The long-term model predicts a large amount of hanging-wall sediment, giving a total sediment infill for the 11.5 km slip model in Fig. 23(a) of about 5 km, of which only the uppermost 1 km, composed of a turbidite sequence, has been described with seismic profiling beneath the floor in the centre of the Gulf Basin (Brooks & Ferentinos 1984). A minimum long-term slip of about 7 km (giving a u/d ratio approaching 1/1.3) could thus be obtained taking the base of the observed sediments as representing the total hanging-wall flexure for the same total average flexure in the footwall. These improbable values provide a model-independent, extreme lower bound for the long-term slip estimate (40 per cent less than our favoured estimate). However, using a lower u/d ratio for both long- and short-term estimates would change proportionally the slip rates without changing the age of the fault.

Even allowing for such a possibility, we find that the overall geometry of the Corinth Rift is similar to that of large, mature half-graben systems in the Basin and Range. The main difference is that the Corinth Rift appears to have evolved about 10 times faster.

6.3 Slip rate and seismicity

The very high rates of normal slip (11 mm yr^{-1} and at least 6–7 mm yr^{-1}) and of extension absorbed by the Xylokastro Fault (7 mm yr^{-1} and at least 5 mm yr^{-1}), which is the largest fault in the region, are comparable to the overall extension rates across central Greece averaged over the last 70 years from the seismicity (about 7 mm yr^{-1}) (Taymaz, Jackson & McKenzie 1991) and over the last 90–100 years from the geodesy (about 12 mm yr^{-1}) (Billiris *et al.* 1991).

When trying to understand slip rates and seismicity for the Gulf in more detail, problems arise. This is due partly to the uncertainty in relating seismicity to particular faults, and partly to the apparent lack of events to account for deformation rates. The exact location of the rupture in the main shock of the 1981 earthquake sequence (Ms 6.7) has been questioned. However, recent work argues that it did not rupture the offshore extension of the Xylokastro Fault but the Pisia Fault, on the Perahora peninsula (Taymaz, Jackson & McKenzie 1991; Hubert *et al.* 1996). In contrast, the 1928, Ms 6.3 event in Corinth could have ruptured the Xylokastro Fault offshore north-west of the Perahora peninsula (Ambraseys & Jackson 1990), which is the easternmost of the segments truncating the Gulf of Lechaio, in continuity with the Xylokastro Fault (Fig. 2). As mentioned earlier, other historical earthquakes with magnitudes probably exceeding 6.5 caused heavy destruction in the city of Corinth in 77, 543, 580 and 1858 (Papazachos & Papazachos 1989; Ambraseys & Jackson 1990). Given the uncertainty in the location of the events and the number of active fault segments near Corinth, it is difficult to establish whether these earthquakes ruptured the Xylokastro Fault. Taking a slip rate of 11 mm yr^{-1}, an event of magnitude 7–7.5 with 2–4 m of slip should occur every 200–400 years on the Xylokastro Fault, and thus the number of known events appears to be too small.

This may be because the historical catalogue is incomplete, or a significant proportion of the slip is aseismic (perhaps 50 per cent). In a study of the well-constrained deformation in the western USA, King, Oppenheimer & Amelung (1994a) have shown that, if the seismogenic zone is taken to be the depth from the surface to the deepest events, only about 50 per cent of the deformation is taken up by seismic slip. This is because near the surface and at depth, deformation occurs by creep. The motion, none the less, is localized on or close to faults and is not widely distributed. Our observations of terrace deformation, from which we estimated the fault rate directly, are not incompatible with this view. In any case, further investigation is needed to assess directly the proportion of seismic slip on the Xylokastro Fault.

6.4 Segmentation, short-term slip and long-term slip elsewhere in the Gulf

Faults along the southern side of the Gulf divide into the distinct segments identified in Fig. 2. Their lengths are hard to determine accurately because the extremities of the individual échelons are partly underwater, but are similar to those observed in, for example, the Basin and Range and elsewhere in the world (Machette *et al.* 1991; Jackson & White 1989). There is some indication that the central segments are somewhat longer (Xylokastro, Heliki, 25–30 km) than the more distal ones (Psathopyrgos, Pisia, Alepohori, 15–20 km).

Besides its typical half-graben asymmetry in cross-section, the Corinth Rift is also asymmetric along strike, with very different deformations towards the two ends (Fig. 2). There is a gradual westward decline in the total amount of extension

from the Xylokastro segment west towards the Psathopyrgos segment, suggesting dominant westward propagation of the rifting process. Slip rates on faults other than the Xylokastro Fault are more difficult to constrain, but for the Heliki Fault segment a rate of uplift of the order of 0.5–1.3 mm yr^{-1} has been deduced from the ill-defined Pleistocene terraces north-west of Derveni, less than 2 km from the fault (Fig. 2) (Dufaure & Zamanis 1980; Rigo 1994), and from raised *lithophaga* borings of dated Holocene age (Mouyaris *et al.* 1992). If the fault behaves in a similar fashion to that at Xylokastro then the slip rate should be between 3 and 8 mm yr^{-1}.

East of the Xylokastro Fault there is a more abrupt decrease in the total extension as the Rift veers to the north-east, truncating obliquely first the Lechaio Basin which contains the terraces we have examined and then the Megara Basin (Fig. 2). Although the terraces and associated Pleistocene sediments in the Lechaio Basin are the best preserved, evidence to determine fault slip can also be found in the Megara Basin. There is also some evidence for drainage reversal similar to that used to gain longer-term information about motion on the Xylokastro Fault.

Palaeo-sea-levels where the Alepohori Fault passes north of the Megara Basin are hard to determine, although one clear terrace with U/Th dated corals at 127 ± 6 ka (Collier *et al.* 1992) and with an inner edge at about 40 m (above sea level) can be identified (R. Collier, personal communication). This corresponds to oxygen isotope stage 5.5 (124 ka) and thus correlates with the New Corinth terrace. The observation is shown in Fig. 23(b) by a single point at 1 km distance from the Alepohori Fault trace. Assuming that the mechanics of the fault here are similar to that at Xylokastro, and that there is no significant regional uplift [which seems appropriate here (Collier *et al.* 1992)], this gives a total slip of 220 m and hence an average slip rate of about 1.8 mm yr^{-1}. To assume a simple mechanical equivalence with the fault farther west may be slightly in error, however. On theoretical grounds the u/d ratio at the extremity of a fault is less than near its centre (King, unpublished) but at the most the total slip and slip rates are overestimated by 50 per cent. Thus, we must conclude that during the last 124 ka the averaged slip rate at Alepohori (we have not shown it to be constant) has been 6–12 times less than at Xylokastro (which numerous terraces show has been constant). None the less, both rates are high, greater than those determined for normal faults in the Basin and Range province in the western USA. For instance, the slip rate deduced from trenching on the Wasatch Fault system varies from about 1 mm yr^{-1} at its central segments to about 0.1 mm yr^{-1} at the distal segments (Machette *et al.* 1991).

Although the information is poorer than for the Xylokastro segments, we can also use similar techniques on more ancient markers to assess longer-term slip for the Alepohori segment. The maximum uplift for the footwall is constrained by the maximum elevation of the reversed drainage catchment in the Megara Basin (300 m at 5 km distance from the fault), and the minimum by the height of the morphological scarp (about 200 m from the fault trace). Again assuming the same model parameters as for Xylokastro, these give a mean total slip at Alepohori of 1.5 ± 0.5 km (or about 1 ± 0.5 km if u/d is somewhat higher) (Fig. 23b). The general morphology of the fault in this region suggests that the total displacement changes rapidly along the strike. Less than 5 km to the north-east the fault disappears and total slip is consequently zero, while farther to the south-west a larger scarp along the fault suggests slip of about 3.5 km (Figs 23b, 2).

While these observations must be taken with caution because fault slip is changing rapidly along strike, simple extrapolation of the relatively short-term rate of 1.8 mm/yr indicates inception of the fault at Alepohori at about 1 Ma. Taken at face value this is an improbable result since it suggests that the easternmost segment of the Rift is about the same age as its central segment. Such an observation is incompatible with observations worldwide upon which simple scaling laws for the growth of fault systems are based, since it implies that the Gulf system started with its present length and grew in total displacement without fault propagation. However, such unusual characteristics appear to be specifically associated with the abrupt eastern end of the Corinth Rift, not with its western end. The data, however, do not prove that the slip rate for the Alepohori Fault has been constant over the long term. For example, it is possible that the slip rate was faster in Alepohori before 124 ka, perhaps the same as in Xylokastro, and that the fault inception is only at 0.25 Ma. Although our observations do not allow us to demonstrate directly that this has occurred, we marshall further arguments in the next section that suggest that the evolution of the Gulf by fault propagation episodes is inescapable.

6.5 Scaling

The maximum displacement-to-length ratio (d/L) of the Corinth Rift, taking 11.5 km of total maximum slip and a total length of 130 km, from the western tip of the Psathopyrgos Fault to the eastern tip of the Alepohori (Psatha) Fault, is about 9×10^{-2}. This is in agreement with the value for this ratio found worldwide for large normal faults (Walsh & Watterson 1988; Schlische 1991). For smaller faults, the d/L ratio has been observed to be less by a factor of 10 or more (Scholz *et al.* 1993; Dawers, Anders & Scholz 1993; Walsh & Watterson 1988). Cowie & Scholz (1992a,b,c) and Scholz *et al.* (1993) use these observations to suggest self-similar behaviour, attributing differences between small and large faults to systematic material property variations between the data sets, while Walsh & Watterson (1988) suggest a square-root scaling of fault length with displacement as a general law. Either view contrasts strongly with the predictions of conventional fracture mechanics (Lawn & Wilshaw 1975), which for a scale range of 10 000 suggests that d/L ratios should decrease by 100 rather than increase by 10.

Our simplest deduction, that constant slip rate persisted throughout the evolution of the eastern Gulf, suggests a fault of constant length increasing steadily in displacement. Such an interpretation appears to be incompatible with the body of data from other fault systems and any current model of fault evolution. Alternative interpretations of the data which allow the Alepohori faulting to be younger require that the fault rate near the end of the fault has in the past been substantially greater than it is at present. This is incompatible with a steady self-similar evolution by propagation which would predict an increase of slip rate as the process zone passes by and not a decrease.

A possible explanation that retains the essentials of self-similar growth over the long term but is compatible with our observations is to assume that systems such as the Corinth Rift have evolved by the addition of discrete segments. Before

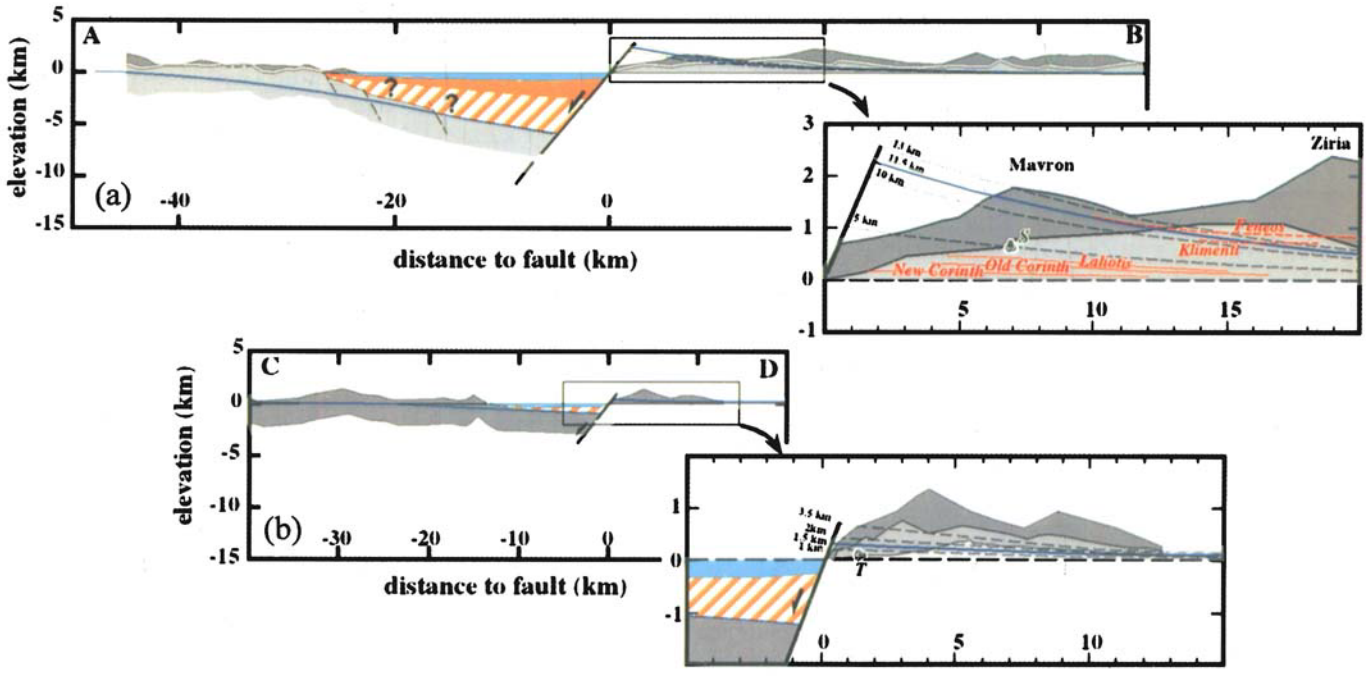

Figure 23. Long-term deformation models across two different segments of the Corinth Rift (A–B, C–D, Fig. 2). Insets, with a vertical exaggeration of 2, show details of the fits to morphological constraints discussed in the text. (a) Section at the centre of the Rift (Xylokastro segment) with 11.5 km slip on the fault. The darker background topography across the Mavron Oros and the peninsula south of Delfi (Fig. 2) is as in Fig. 13(a). Initial conditions are defined on the footwall by a horizon, now deformed (solid blue flexed line). This horizon represents a former base level (palaeohorizontal) compatible with the geometry of the basins with reversed drainage, and with the occurrence of tilted continental conglomerates in Mavron Oros. The flexure is modelled with the same parameters as the terraces under the hypothesis of 0.1 mm yr^{-1} of regional uplift, but with erosion and sediment deposition fixed at 30 per cent and 70 per cent of vertical displacement. The base of sediments is consistent with the flexure of the hanging wall, but some antithetic faulting is required, especially to fit the background topography of the Delfi peninsula. Sediments seen with seismic profiles (orange) plus inferred sediments (striped orange) have a total thickness of about 5 km. The inset shows the fit with 11.5 ± 1.5 km average slip (solid) within dashed minimum and maximum slips: 10 km at maximum elevation below the tilted basins of Feneos and Klimenti; and 13 km constrained by elevation of conglomerates in Mavron mountain. The lower fit at 5 km slip corresponds to the highest occurrence of marine fossils at Souli (point S with shell). Projections of the main terraces are presented for comparison. (b) Section at the eastern end of the Rift (Alepohori segment) with 1.5 km slip. Flexure parameters are as for the Corinth terraces, but with no regional uplift. Likely initial conditions are given by the geometry of the tilted Megara Basin and by the morphology of the Alepohori Fault scarp. The hanging-wall sediment thickness allowance is about 700 m (striped orange). The inset shows the footwall profile with the topography of Megara Basin (light shade) stacked together with that of flanking mountains immediately south-west (dark shade) and north-east of it (medium shade). The average fit at 1.5 ± 0.5 km slip is constrained by the higher fit near the maximum elevation of sediments in the basin and by the lower fit to the 200 m high fault scarp to the north-east. The highest slip of 3.5 km fits the larger fault scarp to the south-west, toward the Pisia Fault. A slip of 220 m fits the inner edge of the dated terrace (point T with shell), yielding a rate of 1.8 mm yr^{-1}.

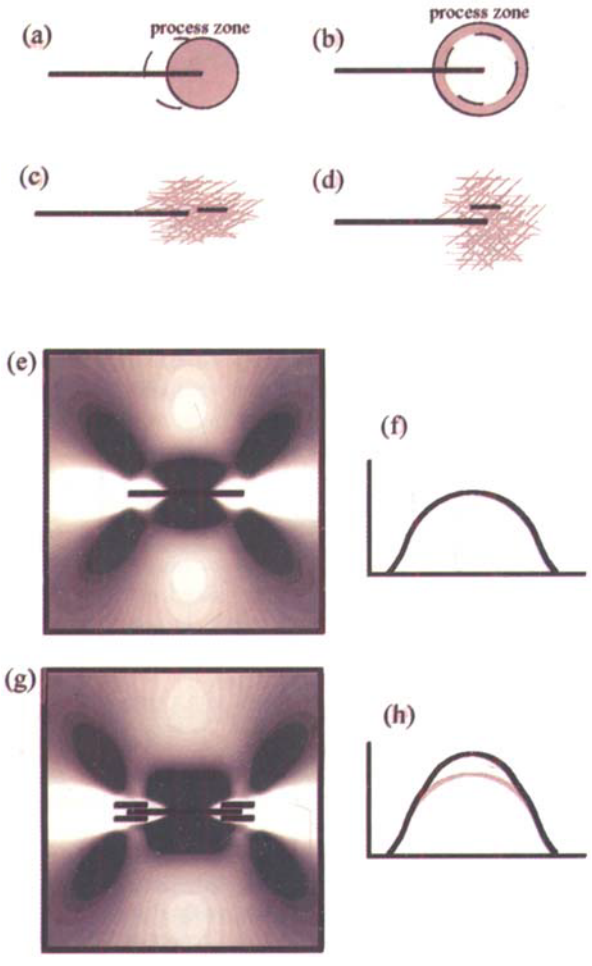

Figure 24. Mechanical interpretation of process zones. The process zones for propagating faults are shown schematically as circular regions. These could either (a) propagate retaining the same dimensions as the fault slip increases and the fault extends, or (b) grow in dimensions, allowing increased fault slip without fault extension. These process zones normally result from slip or opening on numerous fractures, some of which are large (c and d). (c) If such a fracture lies ahead of the fault rupture, the propagation rate of the fault will increase. (d) If to the side, the process zone will increase in width without further propagation. (e) The total shear stress due to slip on a fault subject to uniform distant shear stress is shown. Light areas correspond to increased shear stress and dark areas to reduced shear stress. (f) The corresponding fault displacement. (g) Small faults are added parallel to the end of the main fault. (h) This allows increased slip on the main fault without changing the form of the slip function and hence the stress concentration at the ends of the main fault. The distance between the main fault and satellite faults is similar to that between the Alepohori main fault and the Kaparelli antithetic faults at mid-depths in the seismogenic zone. The calculations are the same as those carried out for Coulomb stresses by Stein, King & Lin (1992, 1994b), and King *et al.* (1994a), but friction is taken to be zero. The aftershocks that they model can be considered to be one form of process-zone deformation.

a segment is added the fault stays the same length and increases in slip until d/L becomes too large. Another segment is then added in a phase of rapid propagation, so that the mean d/L drops. This is then followed by another period when slip increases without an increase in fault length. Such a hypothesis would require that the Corinth system is now in a stage of evolution when its length is not increasing.

The idea that a fault system evolves by the rapid addition of segments has been proposed for the El Asnam reverse fault by King & Yielding (1984). They suggested that the process zone of a fault, instead of retaining the same dimensions and propagating steadily as shown in Fig. 24(a), can stay in the same place and for periods of time simply increase in size (Fig. 24b). In the models proposed by Cowie & Scholz (1992a,b,c), this cannot occur. The yield strength of the material is assumed to be constant and thus the process-zone dimensions and hence also the fracture toughness increase smoothly in proportion to the fault length (the condition for strict self-similarity). For fault slip to increase without the fault length increasing, the process zone must be capable of changing size independently of the fault length.

Dawers *et al.* (1993) and Scholz *et al.* (1993) tested their model against faults in the homogeneous Bishop Tuff of Volcanic Tableland in California, where uniform yield strength is likely. In general, however, crustal rocks are much less homogeneous and pre-existing weaknesses mean that an advancing process zone enters material of variable character. This can give rise to the effects shown in Figs 24(c) and (d). In Fig. 24(c) a weakness (or secondary fault) is shown to lie approximately ahead of the propagating rupture front. Under these conditions the rupture front can be expected to advance more rapidly than normal with the overall width of the process zone becoming narrower (Fig. 24a). In Fig. 24(d), the weakness is shown to lie to one side of the rupture front. In this case slip on the secondary fault reduces stress at the end of the main rupture, causing its propagation rate to decrease in association with a widening of the process zone (Fig. 24b). In both cases slip on the main fault increases. The situation shown in Fig. 24(d) can be modelled numerically. Fig. 24(e) shows the total shear-stress surrounding a free-slipping fault subject to uniform shear at a distance and the corresponding fault slip (Fig. 24f). White areas correspond to an increase of shear-stress and dark areas to shear-stress reduction. The applied distant stress corresponds to a uniform mid-grey. If stress is relaxed in any of the elevated stress regions, slip on the main fault will increase, and thus failure in any of the light regions has the same effect as failure in a more conventional process zone considered to be localized near to the fault tip. The observation that aftershocks in California occur in all of the zones of increased stress (see King, Stein & Lin 1994b) suggests that, for crustal faults, process zones are not highly localized. Fig. 24(g) shows the effect of introducing small free-slipping faults parallel to the main fault, but on each side of the end of the main fault. With these in place the distant stress can be increased such that the stress and the slip profile at the end of the main fault are unchanged from before, but the slip at the centre is substantially increased (Fig. 24h).

It is interesting to note that, as the process zone becomes larger, it is statistically more likely to encounter substantial weaknesses. Thus, in a medium with a fractal or quasi-fractal distribution of defects, process zones will grow more than predicted by a purely self-similar process. This is equivalent to suggesting that the mean yield strength of a sample of rock decreases with size and provides a mechanism for the change in scaling from the small faults in layered, rather homogeneous rocks (coal mines, volcanic ashes, etc.) to the large faults (such as the Wasatch Fault or the Corinth Rift) that cut completely the more heterogeneous seismogenic crust. It also supports, if not strict square-root scaling, a trend in the direction suggested by Walsh & Watterson (1988).

The possibility that the process outlined above operates in the Gulf of Corinth is supported by the distribution of active faults at its eastern end, with an antithetic fault playing the role of the secondary process-zone faulting shown in Fig. 24. In the 1981 earthquake sequence, the most easterly event occurred on the antithetic Kaparelli Fault which had the effect of reducing stress on the eastern extremity of the main north-dipping fault (Hubert *et al.* 1996). King *et al.* (1985) pointed out that motion on this antithetic fault can only continue for a limited number of earthquakes because eventually there are kinematic requirements that further deformation should be accommodated by motion of the main fault. While the main fault is not at present extending, in due course it must extend north-eastward, presumably creating a new segment. The northern side of the Gulf has a series of antithetic faults which are smaller than the north-dipping ones and appear to be older than the more distal Kaparelli Fault (Fig. 2). They may represent earlier phases in the process of evolution by jumps.

7 DISCUSSION

7.1 Mechanical implications

The program that we use to model the terrace deformation is based on the equations of linear elasticity for the plate, but the use of such a formalism can be criticized. The deformation greatly exceeds the elastic limit of engineering samples which fracture when strained by 0.01 per cent or less (Lawn & Wilshaw 1975), and since geological structures are subject to much greater strain, elastic models seem inappropriate. The brittle crust, however, contains numerous fractures and small faults and it can be argued that an elastic model is an adequate approximation to the overall behaviour. The deformation may be expected to include a truly elastic part and a fully recoverable part accommodated by opening or closing pre-existing fissures. A further part results from slip on pre-existing small faults and from new fracture. Some of the deformation due to the latter can be largely recoverable although subject to hysteresis (Holcomb 1981). Under conditions where the deformation is recoverable and roughly proportional to applied stress, the deformation is correctly described as elastic although dissipative. However, even irrecoverable or dissipative deformation can be nearly linearly proportional to monotonically increasing stress (the situation modelled), and in so far as this is correct, such deformation is also well enough approximated by a linear elastic model. In many cases, rock samples in laboratory tests can accommodate strains of a few per cent before failure (Jaeger & Cook 1969) and the models that we propose do not require strains far in excess of this.

Serious departures from linearity only occur if new damage is not distributed through the medium, but accumulates locally to create a new fault, dyke or other major structure. Such features, like the antithetic faulting in the Gulf, can be readily identified in the field if they are associated with signifi-

cant deformation, and can be specifically incorporated in calculations.

The use of low elastic moduli and large strains for modelling flexure raises similar problems to those raised by the large displacement-to-length ratios observed for the crustal faults discussed above. The mechanical descriptions proposed by all authors are based on modifications of crack models and require that substantial strains occur over large regions; that is, strains of the same order as the d/L ratio (10^{-1}) over regions within about one fault length from the fault. Since these cannot be associated with stresses of the order of the many tens of kilobars required by the conventionally assumed (or short-term) crustal modulus, we must assume that the crust has a much lower long-term modulus.

To bring stresses down to plausible values requires the effective modulus of the crust to be reduced by a factor of between 100 and 1000, the same as that required to model flexure. This is often described by a reduced flexural rigidity or a reduced effective elastic thickness (equivalent descriptions for thin-plate models). When the modulus is reduced by much more than 100, a thin-plate approximation becomes invalid. Flexure at the surface no longer scales with flexural rigidity, and hence both it and the effective elastic thickness lose meaning. We also noted earlier that thin-plate models fail to allow correctly for fault dips, and that thick-plate models can become similar to half-space models.

7.2 Regional uplift

An impetus to this study of the Corinth terraces was to address the long-debated problem of fast regional uplift of the Peloponnesus and of the Hellenic arc (e.g. Le Pichon & Angelier 1981; Collier *et al.* 1992). Our observations imply that uplift of the Corinth terraces may be explained by flexural processes alone, and that a regional component is not essential. However, a modest regional uplift (0.1–0.2 mm a^{-1}) is possible and compatible with the evidence for uplift in the Peloponnesus hinterland. Most of the Aegean is subject to stretching and crustal thinning and is associated with cooling from enhanced heat flow, both of these processes predicting regional subsidence. Nevertheless, the Hellenic backbone of the Peloponessus and of central Greece appears to have experienced little extension and retains considerable crustal thickness ($\approx$40 km) (Makris 1978). Subsidence in mainland Greece is thus not regional, but, as discussed further below, is localized only within the main graben systems that widen and deepen southeastwards into the Aegean (Fig. 1). Therefore, background uplift and uplift rates must decrease gradually from the central Peloponessus towards the Aegean, and a zone of transition from net uplift to net subsidence must exist, most likely along the eastern margin of the Peloponessus.

Two processes seem plausible to produce the regional uplift. The first invokes underplating associated with light sediments left behind by the descending slab in the Hellenic subduction zone (Le Pichon & Angelier 1981; Roberts & Jackson 1991). The sediments added to the base of the crust cannot be greatly reduced in density (perhaps 5 per cent of 2.9), and thus a substantial amount must be added to create significant uplift. Roughly, the rate of accretion must be 10 times the uplift rate, or 1–2 mm yr^{-1} or greater. Over a period of 1 Ma this would add 2–4 km to the base of the crust. It is not impossible that such crustal thickening has occurred.

A second mechanism suggests regional uplift resulting from regional erosion (e.g. Westaway 1994). Erosion of the Corinth Rift shoulders is likely to be of the order of 30 per cent of the uplift over the last 1 Ma, and balances with sediment accumulation in the Gulf representing about 70 per cent of the subsidence, as discussed earlier. This process allows for, but does not require, about 0.1 mm yr^{-1} of regional erosion which is probably balanced by an equivalent amount of regional uplift. However, this uplift could be isostatically compensated either by lateral viscous flow in the lower crust or by underplating of light material, or by a combination of both processes.

Whatever the mechanism, it is clear that it has not operated everywhere in the Hellenic arc at the same rate and during the same time as the extensional processes in the Aegean, otherwise all the arc would now lie above sea level. For now, one can only speculate on how such changes might have occurred. For instance, the rate of underplating may have increased with time since the subducted crust became progressively lighter and more buoyant on average, as the continental margin of Africa approached, carrying a larger and larger sediment load. Such a change may have also triggered E–W extension and formation of the new, N–S-striking normal faults responsible for the segmentation of the Hellenic arc and for the subsidence below sea level of parts of it (Fig. 1) (Lyon-Caen *et al.* 1988; Armijo *et al.* 1992).

7.3 Localization and asymmetry of extensional strain

The Corinth Rift exhibits many features that are shared by normal faulting structures elsewhere in the world. It is an asymmetric graben with a main fault dipping relatively steeply, and with antithetic faults that do not seem to have total displacements of more than 10 per cent of that of the main fault. Both the main faulting and the antithetic faulting are segmented with segment lengths that scale roughly with brittle crustal thickness (e.g. Jackson & White 1989), and their evolution appears to be related to repeating earthquakes. More than one episode of faulting has been involved in the creation of the Corinth Rift, with later deformation displaced northwards into the hanging wall of the earlier phase. This has been observed in other continental rifts, for instance in the Gulf of Suez (e.g. Garfunkel & Bartov 1977; Courtillot, Armijo & Tapponnier 1987). The most recent phase of deformation has lasted about 1 Ma, with a likely rate of fault slip of about 1 cm yr^{-1} and opening of 7 mm yr^{-1}. Unlike other features of the Gulf, this is unusual. Typical normal faults have slip rates of the order of one-tenth of this value, and high extension rates are normally associated with major plate boundaries rather than with the internal deformation of continents. The Quaternary slip rates of all of the other major normal faults in the Aegean are poorly known, but many, including those associated with the large graben systems of western Anatolia, are likely to have much slower rates, of the order of 1 mm yr^{-1} (e.g. Westaway 1994).

Although some rift systems form quasi-linear features extending for hundreds or thousands of kilometres through otherwise undeformed terrain (e.g. the Baykal and the East African rifts), others do not. In the case of localized, single rifts, normal faulting crosses or follows the boundaries of older cratonic blocks, while in other cases the extension appears to be associated with the gravitational collapse of wide, thick, hot mountain belts (Gaudemer, Jaupart & Tapponnier 1988).

The high plateau of Tibet is the best example. Several subparallel fault systems occur in Tibet, and they correspond to the early stages of widespread continental extension (Armijo *et al.* 1986). Similarly, the Basin and Range province, located where high mountains formed in the Laramide orogeny, is associated with many extensional fault systems, and it is generally admitted that they are the late stages of a similar process. In the Aegean the extension appears to be diffuse over the largest scale, but at a more detailed level it appears to be mostly localized within a few rift systems spaced regularly by about 60–75 km (Fig. 1). North of the Gulf of Corinth there are three major grabens, namely the Evvia graben, the North Evvia Basin and the North Aegean trough, all of which have, to some degree, the same asymmetry as the Corinth Rift. The earlier structure of the Corinth Gulf itself extends south-eastwards into the Saronic Gulf, and an additional southern extensional zone can be identified in the Argos Basin (Fig. 1). These five main rift systems on the Greek side of the Aegean Sea appear to widen and to deepen south-eastwards into that Sea. Fig. 1 also shows a pattern of mostly asymmetric grabens which have similar length and spacing on the Turkish side of the Aegean, including the Kerme-Kos, the Büyük and Küçük Menderes, the Alasehir, the Simav-Bakirçay, and the Edremit Gulf rift zones. These mostly onland grabens of the Anatolian side have experienced less cumulative extension than the Corinth Rift, and apparently much slower Quaternary slip and average extension rates (of the order of 3×10^{-16} s^{-1}) (Westaway 1994).

In contrast to the case for fault segment lengths ($\approx$20 km), the spacing between long, major rift systems (60–75 km) is unlikely to be associated with brittle crust thickness. For example, the seven major, 300–500 km long Tibetan Rift systems are separated by distances of 150–200 km, while crustal seismicity appears to be limited to a depth of 15 km and the flexural flank uplift zone is too narrow to be consistent with a thick brittle crust (Armijo *et al.* 1986; Masek *et al.* 1994). That this is easily seen in Tibet is due to the incipient character of extension, of only about 2 per cent (Armijo *et al.* 1986). Conversely, large amounts of cumulative extension (of 50–100 per cent) in regions like the Basin and Range appear to be associated with short-wavelength faulting, whose average spacing of 30 km scales approximately with the thickness of the crust (Fletcher & Hallet 1983). Observations of this type of faulting in the Basin and Range and elsewhere have given rise to rotating rigid block or domino faulting models. Such closely spaced faulting is likely to occur in some parts of the deep, central Aegean Sea which has been substantially stretched ($\approx$80 per cent: Le Pichon & Angelier 1981; Jackson & White 1989) and where 5–20 km wide, tilted blocks are often seen on seismic profiles (Mascle & Martin 1990). For the rift systems visible onland on both sides of the Aegean, however, the intervening blocks appear to be too wide (60–75 km) to rotate about horizontal axes (Jackson & White 1989). This is consistent with the relatively small amount of cumulative extension, which increases from less than 5 per cent in the mountains surrounding the Aegean Sea (a value of the same order as in Tibet) to no more than 10–30 per cent near to the coast (Fig. 1) (e.g. Roberts & Jackson 1991; Westaway 1994). Greater amounts of extension in the central Aegean, on the other hand, have apparently generated shorter-wavelength faulting, which may have concealed an initial longer-wavelength rift spacing, now well preserved only on the Aegean margins.

Mantle processes have been invoked to explain long-wavelength periodicities in extending continental regions. In the Basin and Range, for instance, a 200 km pinch-and-swell structure seen in the Bouguer gravity anomaly maps has been correlated with the topography (Froidevaux 1986) and with tilting domains (Zuber, Parmentier & Fletcher 1986). Such a wavelength is similar to the separation of structures in Tibet (150–200 km), where subcrustal normal faulting earthquakes (90 km deep) occur (Molnar & Chen 1983), suggesting that the mantle lithosphere there still has significant strength, in spite of the young 'thermal' age of the crust, and of the high values of observed heat flow [$\approx$91–146 mW m^{-2} (Francheteau *et al.* 1984)]. Therefore, development of periodic necking instabilities in a strong upper mantle, as proposed by Ricard & Froidevaux (1986), gives a plausible explanation for primary graben localization whether in Tibet or in the Aegean.

Wallace (1981) argues that, in the Basin and Range, upper-crustal deformation is localized at any given time (over the last hundred thousand years), but that the locus of deformation in the crust migrates over the course of time, resulting in more distributed surface deformation. If localization remains fixed in the mantle for longer periods than in the crust, then detachment surfaces must exist in the lower crust. Such detachments, which are well established in fold and thrust belts, are efficient sources of asymmetry at a wide range of scales (Boyer & Elliot 1982). In convergent mountain belts, shallow thrust faulting apparently starts close to main mantle overthrusts and, due to increased amounts of potential energy stored in the ranges, migrates away from them (e.g. Molnar & Lyon-Caen 1988). Hence, mountain ranges tend to increase their width as it becomes more difficult to thicken the crust further. In rift zones a reverse situation takes place, necking being a self-sustained process. Extensional faults keep moving towards the necking axis, causing progressive migration of deformation into fault hanging walls. This implies the existence of aseismic, extensional detachment zones below the brittle crust [for example as proposed for the Aegean by Gautier & Brun (1994)], with low-angle normal faulting in the 10–15 km depth range (King *et al.* 1985; Eyidogan & Jackson 1985; Rigo *et al.* 1996).

7.4 Large-scale mechanics and evolution of the Aegean

Three prominent features of the Corinth Rift need to be explained within the broader boundary conditions imposed by the regional tectonic setting. (1) The unusually fast extension rate in the Corinth Rift, which contrasts with the one-order-of-magnitude slower rates in other parts of the Aegean. (2) That this rapid extension is associated with a very young (1 Ma) phase of faulting cutting an older extensional basin. (3) That cumulative extension during the younger phase diminishes progressively toward the western tip, suggesting dominant westward propagation of the rifting.

Various models have been proposed for the kinematics of the region. Early 'rigid-block' views (McKenzie 1972) had the Anatolian block and the Aegean extruding to the west and south-west, their boundary with the 'stable' European block extending south and west as an extension of the North Anatolian Fault and the North Aegean trough. This implied a boundary with predominant strike-slip motion roughly perpendicular to the strike of the Corinth Rift. Such a feature does not exist. An escape from this problem was provided by continuum models of extension (Jackson, Haines & Holt 1992;

Jolivet *et al.* 1994), which downplay the significance of plate-scale features in favour of distributed deformation. Our observations of the Corinth Rift, however, suggest very localized deformation, in keeping with mounting evidence suggesting that major fault zones and associated mantle features persist for too long and accommodate too much deformation for continuous deformation approximations to be valid (Tapponnier, Peltzer & Armijo 1986; Peltzer & Tapponnier 1988; King *et al.* 1994a).

By modifying an earlier 'bookshelf' faulting model (Jackson & McKenzie 1988), the simple 'broken-slat' kinematic model proposed by Taymaz, Jackson & McKenzie(1991) has gone some way to producing a compromise. It partly overcomes the problems of earlier models by proposing that rifts in central Greece accommodate shear and extension, although by distributing significant dextral shear in western Anatolia. At a smaller scale this model is consistent with the apparent east-to-west decrease in the amount of extension in the Corinth Rift, and with the observation that, because of the overall clockwise rotation, the eastern tip of the Corinth Fault system at the Pisia and Alepohori segments cross-cuts the older south-east trend towards the Saronic Gulf. At a larger scale, and, more importantly, in quantitative terms, however, the model of Taymaz *et al.* (1991) fails to explain the difference in the slip rates between the Greek and Anatolian sides of the Aegean, particularly the fast slip rate in the Corinth Rift. A further defect of the model is that it requires distributed shear along the E–W-oriented grabens of western Anatolia and does not allow for the observed N–S extension.

Other observations are not explained by this or other previous models. First, there is now convincing evidence that crustal extension around and inside the Aegean probably precedes by 7–10 Myr (e.g. Angelier *et al.* 1982; Mercier, Sorel & Vergely 1989; Seyitoglu, Scott & Rundle 1992) and perhaps by 17–20 Myr (e.g. Jolivet *et al.* 1994), the inception (at about 5 Ma) of strike-slip faulting related to the westward motion of Anatolia along the North Anatolian Fault (NAF) (Barka 1992). The eastern part of the NAF may have started to move earlier, at about 10 Ma (Sengör 1979) before propagating west from the Arabia–Europe collisional front. Thus an important part of the finite extension in the Aegean should not be explainable by a model based only on contemporary tectonics. The NAF must have propagated into already stretched lithosphere, reactivating or increasing the activity of parts of the pre-existing zones of extensional weakening (e.g. Dinter & Royden 1993). Such a sequence in the timing of the deformation in the Aegean is in keeping with the view that the curvature of the Hellenic arc was acquired during two phases, with the first in the middle Miocene ($\approx$15 Ma) or perhaps earlier (Kissel & Laj 1988).

Second, right-lateral strike-slip faulting is not diffuse in the northern Aegean and in western Turkey as proposed by Taymaz *et al.* (1991) and Jackson *et al.* (1992). There is no evidence for right-lateral strike-slip faulting in western Turkey south of the area of the 1953 Yenice-Gonen earthquake, which may be considered to have ruptured part of the southern, discontinuous branch of the NAF (Barka 1992) (Fig. 1). South of that branch the large-scale, recent tectonics of western Turkey are clearly dominated by major E–W-trending rifts with clear N–S extension, a tectonic style that appears to extend westwards into the north-central Aegean. Similarly, it is probable that the southern branch of the NAF is connected, across the northern Aegean, with the Skyros Basin (e.g. Taymaz *et al.* 1991) and further south-westwards, with the North Evvia Basin. Most of the finite strike-slip displacement between the central Aegean and 'stable' Europe is probably concentrated along the most prominent, narrow northern branch of the NAF going from the Sea of Marmara to the North Aegean Trough (NAT) (Barka & Kadinsky-Cade 1988; Barka 1992). Although poorly constrained, the extension across the Sea of Marmara, the NAT and other related basins in the north Aegean suggests that slip on the northern branch of the NAF may represent 50–75 per cent of the total displacement. That there is no detectable palaeomagnetic rotation of the Biga peninsula, within a block situated between the northern and the southern branches of the NAF (Fig. 1) (Kissel *et al.* 1987) is consistent with the view that much less total displacement has been taken up by the southern branch. Nevertheless, the 1953 Yenice-Gonen earthquake ($M = 7.4$) ruptured a 60 km long segment of that branch during a faulting sequence along most of the NAF during 1939 to 1967, suggesting more current slip than suggested by the longer-term topography and bathymetry. In summary, strike-slip motion does not seem to be distributed, but is accommodated on no more than two branches of the NAF about 100 km apart, as previously proposed (e.g. Sengör 1979).

If shear on the North Anatolian Fault is not distributed throughout western Anatolia and the north-central Aegean then it must continue into the northern Aegean and be absorbed by structures to the south-west. With the hypothesis that the NAF post-dates much of the Aegean extension, a model of the kinematic evolution must allow for a pre-North Anatolian Fault phase of deformation followed by progressive strain-style change as strike-slip motion propagates into the northern Aegean. An outline of such an evolution is shown in Fig. 25.

During a first stage which started at 15 Ma or earlier, extensional collapse of the thick crust in the Hellenic belt and adjacent regions toward the Hellenic subduction zone may have been the dominant process (Fig 25a). As a result, necking instabilities may have developed in the lithospheric mantle across all of the Miocene Aegean 'plateau', with roughly an E–W or ENE–WSW strike, parallel to the subduction zone. As roughly N–S extension proceeded, with maximum stretching in the central Aegean, the curvature of the Hellenic arc increased, with associated clockwise and counterclockwise rotation of the western and eastern sides of the Aegean, respectively (Fig 25b). Such rotation is consistent with the palaeomagnetic observations and corresponds roughly to the middle Miocene phase proposed by Kissel & Laj (1988). During this first stage the tectonic loading and the regional deformation were roughly symmetrical.

During the second stage of this evolution, the collision of Arabia with Eurasia caused westward motion of Anatolia with the rapid westward propagation of the North Anatolian Fault, which possibly started about 10 Ma or earlier in eastern Turkey. The fault may have reached the Aegean later, thus introducing, by about 5 Ma, the asymmetrical loading existing today (Fig. 25b). Hence, the NAF propagated into the already extending North Aegean region. As it entered the region it appears to have splayed into branches cutting and interconnecting pre-existing rifts, thus forming pull-aparts such as the Sea of Marmara. The most prominent branch propagated along a localized and continuous strand that comes out from

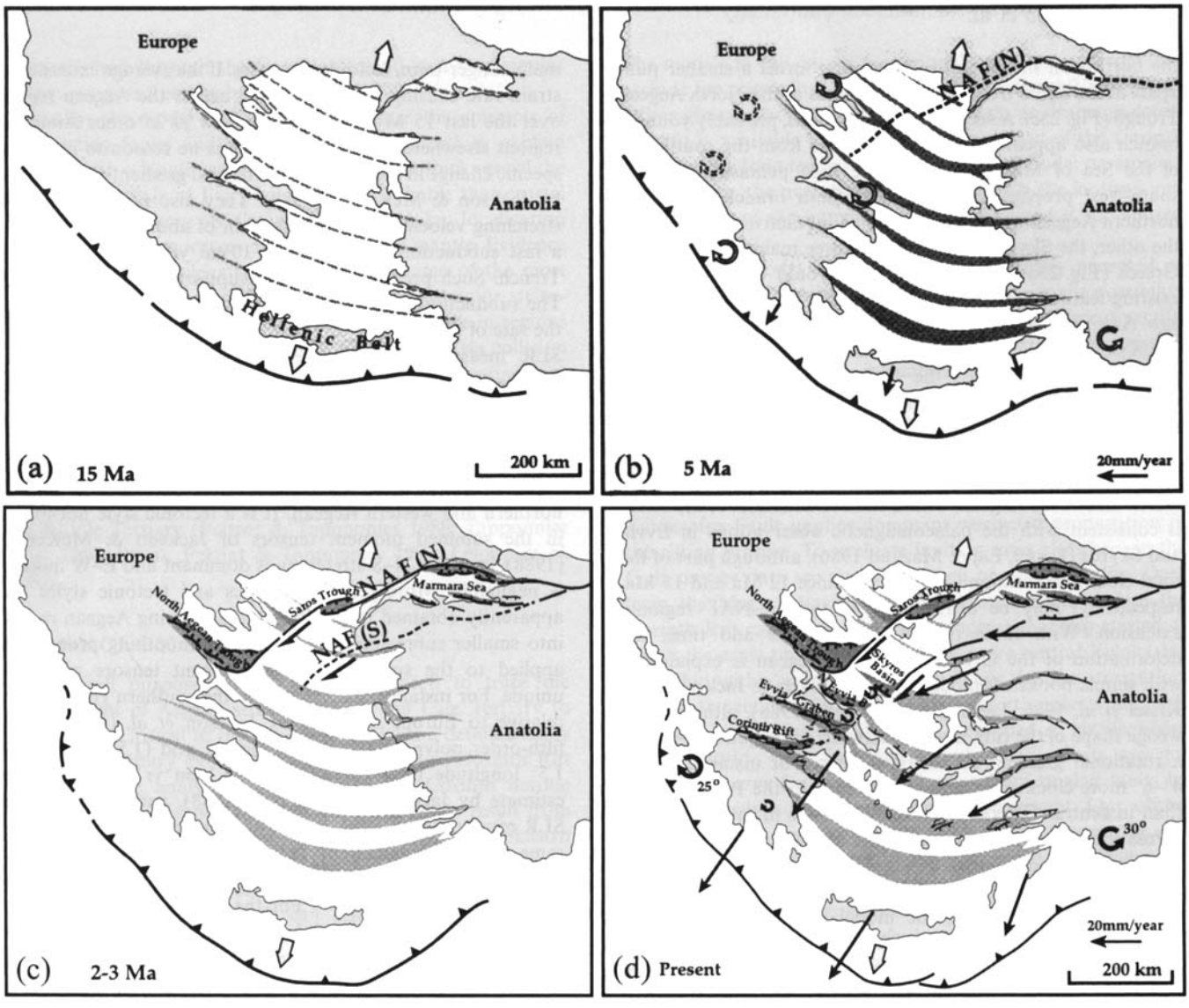

Figure 25. Tectonic evolution of the Aegean region. (a) Onset of regional extension probably at about 15 Ma, or possibly earlier in some places. The stretching direction is roughly N–S, across a plateau with thick crust behind the Hellenic belt (open arrows). Subduction with uncertain location was already active prior to this time, providing weak resistance across the southern boundary. Dashed lines indicate the initial locations of regularly spaced rift zones, which represent sites of localized lithospheric failure. (b) By 5 Ma ago, the main rift zones (light grey) have opened substantially, with maximum extension in the centre of the Aegean. Structures at this time are roughly symmetrical about a N–S axis. The amount of extension decreases toward the western and eastern margins, producing respectively clockwise and counterclockwise rotation and creating the curvature of the arc. The open circular arrows indicate places where such rotations are observed (Kissel & Laj 1988). Rotation in northern Greece and in Epirus (stippled arrows) could be partly older than 15 Ma and/or associated with nappe enplacement (Kissel, Laj & Müller 1985). Bold arrows on the Hellenic arc indicate displacement (≈ 1 cm yr^{-1}) with respect to both Europe and Anatolia due to slow average extension (about 5×10^{-16} s^{-1} in the centre of the Aegean). Dashed lines outline where the North Anatolian Fault (NAF) will propagate into the Aegean, after having propagated from eastern Turkey since about 10 Ma (Sengör 1979). (c) Symmetrical extension proceeds as before in most of the Aegean (light grey), but as the NAF propagated south-westwards it reactivated some segments of the former rift zones causing faster extension (dark grey). Growing by steps and forming high angles with the former rift zones, the northern branch (N) of the NAF may have reactivated first the Sea of Marmara, with pull-apart geometry, then the Saros trough, and terminated by reactivating the North Aegean trough, which is the most prominent basin in the north Aegean. It was this motion of Anatolia that started to produce the contemporary mechanical asymmetry of the Aegean. The incipient location of the southern branch (S) of the NAF is shown by a dashed line. This later branch bypasses the southern side of the Sea of Marmara pull-apart. (d) Present situation. Right-lateral motion is now partitioned between the northern and southern branches of the NAF, with 60 km and 20 km total slip, respectively. This is in reasonable agreement with the geology (e.g. Sengör 1979; Barka 1992) and with the current Anatolia/Europe motion according to SLR and GPS measurements (Oral *et al.* 1995). Bold arrows represent such current motion with respect to the European plate. Motion depicted for the end of previous extensional stage (b, bold arrows) is consistent with current residual displacement once the movement on the NAF (Anatolia/Europe) is removed. Most of the Aegean, the Hellenic arc and the Peloponessus are extruded south-westwards with Anatolia. Propagation of the southern branch of the NAF across the Aegean may have progressively reactivated the Skyros Basin, the North Evvia Basin, the Evvia Graben, and finally the Corinth Rift. The region where the two strike-slip faults lose identity can be regarded as a large process zone. Accelerated clockwise rotation may occur within the process zone in Greece. The small bold circular arrows correspond to places where such a rotation is observed (Kissel *et al.* 1986), although part of it could be older in Evvia and Skyros. Rifting associated with strike-slip faulting is maximum adjacent to the two branches of the NAF and dies out westwards, giving a wedge shape to each reactivated system (dark grey). The Corinth Rift at Xylokastro absorbs N–S extension at 7–8 mm yr^{-1} representing 20–30 per cent of the total right-lateral motion on the NAF. Slow extension persists in the rest of the Aegean and western Turkey (light grey). The two large circular arrows represent total bending at the two ends of the Hellenic arc since 15 Ma (from a to d); 25° clockwise (at Zakinthos) and 30° counterclockwise (at Bey Daglari), consistent with palaeomagnetic observations (Kissel & Laj 1988).

the north-west of the Sea of Marmara, forms a smaller pull-apart at the Saros trough, and terminates at the North Aegean Trough (Fig. 25c). A second, less continuous, probably younger branch also appears to have propagated from the south-west of the Sea of Marmara across the Biga peninsula. Further south-west propagation of that southern branch across the northern Aegean may be responsible for reactivating, one after the other, the Skyros Basin and the three main rifts of central Greece (Fig. 25d). The Corinth Rift would be the last pre-existing feature to be reactivated in such a way, about 1 Myr ago. As a result of this process, the new fault system including the Xylokastro Fault propagated along the southern edge of the Corinth Rift, across the Neogene sediments associated with the previous, slow extension. Rapid uplift and flexure of the Corinth terraces became one of the most spectacular contemporary effects of this final development. Rapid extension restricted to the Corinth Rift and to the other main rifts of the Greek side of the Aegean, within the two branches of the NAF, is consistent with the palaeomagnetic observations in Evvia and Skyros (Kissel, Laj & Mazaud 1986), although part of the total clockwise rotation (48° and 16° since 12 Ma and 15 Ma, respectively) may be attributable to the pre-NAF regional extension. With these restrictions in space and time, the deformation of the Greek side of the Aegean is explainable with simple bookshelf models (e.g. McKenzie & Jackson 1983; Kissel *et al.* 1986; Jackson & McKenzie 1988), although the wedge shape of the rifts, due to westward propagation, requires a rotational gradient across the blocks. For instance, about 4°–6° more clockwise rotation is needed in the Peloponnesus than in central Greece, given the difference in total extension across the eastern and western parts of the Corinth Rift.

While the model shown in Fig. 25 is schematic, it incorporates the following significant features of earlier models without their shortcomings. First, the model is consistent with the current displacement field. The suggestion that the Peloponnesus and most of the deforming Aegean region are being extruded south-westwards, together with the Anatolian block, is consistent with recent measurements of displacements with GPS and SLR for periods of 2–6 years (Fig. 25d) (Oral *et al.* 1995). Removing from this displacement field the current slip along the North Anatolian Fault (≈ 25 mm yr^{-1}) yields an estimate of the motion of the Hellenic arc with respect to Europe (≈ 1 cm yr^{-1}) which is consistent with the displacement field required for the increasing symmetrical extension in the model from 15 Ma to the present (light grey, Fig. 25).

Second, the model incorporates more plausible strain rates than hitherto inferred from directly summed seismic moment tensors. Only 1 cm yr^{-1} of extension causing crustal thinning occurs between the Hellenic arc and Europe, and corresponds to a maximum strain rate of about 5×10^{-16} s^{-1} across the Aegean, similar to rates in Tibet (Armijo *et al.* 1986) and in the Basin and Range (Eddington, Smith & Renggli 1987). Further N–S extension occurs as a result of shear across the NAF to give a further average rate of about 1×10^{-15} s^{-1} but this is compensated by an E–W shortening of the same amount. This contrasts with the much faster N–S extension rate (4×10^{-15} s^{-1}) with no compensating E–W contraction averaged from the seismicity across the entire Aegean region by Jackson & McKenzie (1988). This result comes from integrating seismicity over a short time (70 years) compared to typical recurrence times of large earthquakes (100–1000 years), and there is no reason why this should be representative of the main, longer-term, tectonic processes. If the average extensional strain rate causing crustal thinning across the Aegean region over the last 15 Myr has been as slow as in other stretched regions elsewhere in the world, there is no reason to infer any specific change in the regional geothermal gradient as suggested by Jackson & McKenzie (1988). They also predicted a N–S stretching velocity across the Aegean of about 6 cm yr^{-1} and a fast subduction rate of about 10 cm yr^{-1} in the Hellenic Trench. Such predictions are not supported by observations. The subduction rate they inferred is substantially higher than the rate of about 4 cm yr^{-1} that one can now deduce from the SLR measuremets [≈ 3 cm yr^{-1} of SSW-directed Crete–Europe displacement (Smith *et al.* 1994; Noomen, Ambrosius & Wakker 1993), plus ≈ 1 cm yr^{-1} of N–S Africa–Europe convergence (DeMets *et al.* 1990)]. This rapid subduction rate is basically due to the fast south-westward extrusion of Anatolia together with Aegea, with fast motion localized across the northern and western Aegean. It is a tectonic style not found in the summed moment tensors of Jackson & McKenzie (1988), in which N–S stretching is dominant and E–W motion is negligible. More reasonable rates and tectonic styles are apparently obtained by splitting the deforming Aegean region into smaller subregions. However, the smoothing procedures applied to the summed seismic moment tensors are non-unique. For instance, the velocity of the southern Hellenic arc relative to Europe obtained by Jackson *et al.* (1992) using fifth-order polynomials to fit a regular grid (1.5° latitude by 1.5° longitude boxes) reduces to 3 ± 1 cm yr^{-1} [half of the estimate by Jackson & McKenzie (1988), and similar to the SLR results (Smith *et al.* 1994; Noomen *et al.* 1993)], but the same velocity obtained by Jackson, Haines & Holt (1994) using bi-cubic splines fitted to an irregular-shaped grid reduces further to 1.3 ± 0.5 cm yr^{-1}. For the moment, it is difficult to establish the significance of the different results from summed seismic moment tensors. However, strain rates pertaining to rapid extension on the Greek side of the Aegean can be directly deduced from our observations at Corinth. If stretching at 7–8 mm yr^{-1} across the centre of the Gulf at the Xylokastro Fault is related to 70 km wide blocks, in keeping with the spacing of the main rifts, the time-averaged strain rate is 3.2×10^{-15} s^{-1}. This is compatible with the extensional velocity of 10–14 mm yr^{-1} averaged over 100 years across the main rift systems of central Greece with geodetic measurements by Billiris *et al.* (1991).

Third, the large shear expected within the Greek mainland from earlier models and incorrectly transferred by the broken-slat model to Anatolia and the central Aegean is dealt with in two ways. On the one hand, since the shear appears only with the arrival of the propagating NAF, its total amount is less than predicted by a model that remains unchanged throughout the evolution of the Aegean. On the other hand, the rather complex termination of the NAF in the Aegean can be viewed as a large-scale process zone. Deformation within a process zone during its passage can produce strains reaching 10 per cent. As the process zone increases in size, including large parts of the densely faulted north Aegean, the average velocity of propagation of the NAF must drop. As with the smaller-scale propagation of the eastern tip of the Corinth Rift this can occur without creation of major localized features, although after passage of the process zone a major feature will appear. In other words, a strike-slip fault zone should

ultimately cut through the Greek mainland in a way similar to that proposed earlier by McKenzie (1972).

Finally, the model of Fig. 25 incorporates the concepts of propagating faults and process zones, developed to explain features with a length-scale comparable to the thickness of the crust. At the scale of Fig. 25 it seems improbable that crustal rheology alone governs the mechanics. Similar localization and propagation processes must occur in the mantle. Evidence that this occurs is clear in other regions. Some of the most outstanding examples are found in Asia, where major strike-slip faults appear to have transformed convergence in regions surrounding the mountainous core of the India–Asia collision zone into extension in regions near their propagating tips (Tapponnier *et al.* 1986). One such major fault is the left-lateral Ailao Shan–Red River shear zone, which over a longer time-scale than that of the North Anatolian Fault appears to have propagated south-eastwards from Tibet, causing rapid opening of splay extensional basins in the South China Sea in the middle Tertiary (Peltzer & Tapponnier 1988; Tapponnier *et al.* 1990; Briais, Patriat & Tapponnier 1993; Leloup *et al.* 1995).

8 CONCLUSIONS

The overall purpose of this paper has been to trace the development of Aegean structures from the Late Tertiary to the Present. Critical to this objective has been a detailed study of the Quaternary evolution of the asymmetric Corinth Rift centred on an analysis of the well-known Corinth marine terraces. When mapped in detail these appear to result from uplift and flexure of the footwall of the major Xylokastro normal fault bounding the south side of the Rift. From simple geological arguments it can be shown that, contrary to certain earlier views, regional uplift can only contribute modestly to the overall terrace uplift. A precise correlation of the terraces with the worldwide chronology of glacio-eustatic sea-level highstands in the last 350 kyr is supported by local stratigraphical evidence and U/Th dates. This provides us with a unique set of well-defined, well-dated markers (palaeo-horizontal lines originally at sea level) to constrain the deformation of the Rift shoulder and its evolution.

Direct observations of the displacement on the major normal fault are not possible since the hanging wall lies beneath the waters of the Gulf and thick sediment. However, the uplift and flexure of the footwall documented by the terraces permits a simple mechanical model to be created. The model assumes that the seismogenic crust forms an elastic plate overlying a viscoelastic lower crust—a model consistent with our current understanding of the earthquake cycle. While retaining strength in the long term, the seismogenic layer behaves as if its modulus is reduced by a factor of about 1000. Such a reduction, found elsewhere in the world for similar structures, is commonly expressed as a reduced 'effective elastic thickness' rather than a reduced modulus, the two being related through the concept of the flexural rigidity of a thin plate. Our 'thick-plate' models suggest that this relation is misleading. Furthermore, the common assumption that the lower crust is without long-term strength may have to be challenged.

Using such modelling, all the terraces can be fitted for fault slip increasing with terrace age. Our time correlation suggests maximum uplift rate of 1.3 mm yr^{-1} and our modelling yields a constant slip rate of 11 $\pm$ 3 mm yr^{-1} for the last 350 kyr. The models fit the data if no regional uplift has occurred and exclude the possibility of rates greater than about 0.2 mm yr^{-1}. Other geomorphological information such as drainage development is available to constrain the evolution of the Corinth Rift over the long term. Assuming the same model parameters and slip rate, the overall morphology of both the footwall and visible parts of the hanging wall are explained if slip started 1 Myr ago.

While the model we adopt is simple, widely accepted as appropriate, and fits the data, we cannot exclude the possibility that some other modelling strategy might give different results. An upper limit to possible error is provided by existing reflection profiling data indicating the minimum sediment thickness in the Gulf. This would allow at most a 40 per cent reduction of total slip, giving an extreme minimum slip rate of about 6–7 mm yr^{-1}.

In contrast with the abruptness of the Corinth Rift's eastern end, gradual tapering of cumulative extension west of the Xylokastro Fault implies dominant westward propagation of the rifting process. To evaluate faulting rates elsewhere in the Gulf, terrace data are available, albeit of poorer quality. Data from the Megara Basin near the abrupt eastern end of the Corinth Rift can be interpreted to suggest that slip started at about the same time (1 Ma) as at the more central Xylokastro Fault but with a more modest rate. While this is a straightforward interpretation of the observations it suggests an evolutionary history for the rifting not described so far elsewhere in the world. Very long faults with small offsets are not observed. Large faults appear to grow from smaller faults by simultaneously adding length and displacement. Our observations are not compatible with such simple theories of self-similar fault evolution. Such theories, however, usually assume crustal rocks to be homogeneous and defect-free prior to faulting, a dubious assumption. If this view is dropped, it is possible to envisage major faults evolving in a broadly self-similar, but irregular fashion, interposing periods of constant length and increasing slip with episodes of rapid growth by the addition of segments. Our observations are compatible with such a hypothesis.

The slip rate of the Corinth Rift appears to be 10 times faster than that for comparable features elsewhere in the world, including faults in western Anatolia and elsewhere in the Aegean. This rapid extension is associated with a very young (1 Ma) phase of faulting cutting an older extensional basin. Thus, whatever processes may occur as a result of material properties, when we place the evolution of the Corinth Rift in the context of its location near the propagating end of the North Anatolian Fault, it is clear that it has evolved under conditions of inhomogeneous loading.

At a larger scale, the long-wavelength spacing of the rift systems in the Aegean may be inherited from early stages of normal faulting. The development of periodic necking instabilities in the upper mantle is a possible explanation for lithospheric failure under extension, and for primary rift localization, as in Tibet. Deep-seated localization of the deformation may account for other features, such as the migration of the Corinth Rift edge into the hanging wall, the persistent asymmetry of major rifts in the Aegean, and the possible existence of extensional detachment zones below the brittle crust.

To explain the 'anomaly' of the Corinth Rift we propose that it owes its fast extension rate to its location in relation to the propagating North Anatolian Fault. The latter apparently

started propagating into the Aegean about 5 Myr ago, long after slow extension had already started. This earlier extensional process probably initiated a slower proto-Corinth Rift. As the NAF extended south and west we suggest that it progressively reactivated the older extensional structures. The Corinth Rift, reactivated about 1 Myr ago, appears to be the most recent such structure.

The rates of deformation for the whole of the Aegean, both now and in the past, are summarized in Fig. 25. These differ from the varied models proposed on the basis of summing seismic moments. We suggest that such models suffer from the difficulty of selecting spatial windows and from the short time interval over which seismicity can be integrated.

The role of the North Anatolian Fault shown in Fig. 25 is similar to that of main faults in the smaller fault-propagation model discussed for the Corinth Rift eastern end. The Corinth Rift itself is just one element within the large process zone of the extending NAF. The model provides a simple, unified interpretation of the kinematics of the Aegean from the Late Tertiary to the Present, accounting satisfactorily for palaeomagnetic rotations and the displacement field now observed with space geodesy. It also sheds light on the relationship between the apparently steady process of slow continental extension in Aegea and the transient mechanics of rapidly propagating faults associated with extrusion—a long-debated problem in continental tectonics.

ACKNOWLEDGMENTS

This work was funded by the European Community EPOCH contract CT-91-0043, by the French Centre National de la Recherche Scientifique (CNRS), the Institut National des Sciences de l'Univers (INSU), the program Dynamique et Bilans de la Terre (DBT), and the program ISIS of the Centre National d'Etudes Spatiales (CNES). We also benefited from ARCHAEOMEDES project DG XII-EV5V-0021. We acknowledge R. Lacassin for useful comments and P. Tapponnier for thoughtful discussions on continental tectonics and for suggesting improvements. Ross Stein and Peter Molnar are acknowledged for thorough critical reviews. We share with P. Molnar a liking for long self-contained papers. We thank G. Aveline for drafting the figures. This is IPGP contribution No. 1412.

REFERENCES

Ambraseys, N.N. & Jackson, J.A., 1990. Seismicity and associated strain of central Greece between 1890 and 1988, *Geophys. J. Int.*, **101,** 663–708.

Angelier, J., Lyberis, N., Le Pichon, X., Barrier, E. & Huchon, P., 1982. The tectonic development of the Hellenic arc and the Sea of Crete, a synthesis, *Tectonophysics,* **86,** 159–196.

Armijo, R., Lyon-Caen, H. & Papanastassiou, D., 1992. E–W extension and Holocene normal fault scarps in the Hellenic Arc, *Geology,* **20,** 491–494.

Armijo, R., Tapponnier, P., Mercier, J.L. & Tonglin, H., 1986. Quaternary extension in southern Tibet: field observations and tectonic implications, *J. geophys. Res.,* **91,** 13 803–13 872.

Barka, A., 1992. The North Anatolian fault zone, *Annales Tectonicae,* **6,** 164–195.

Barka, A.A. & Kadinsky-Cade, K., 1988. Strike-slip fault geometry in Turkey and its influence on earthquake activity, *Tectonics,* **7,** 663–684.

Bassinot, F.C., Labeyrie, L.D., Vincent, E., Quidelleur, X., Shackleton, N.J. & Lancelot, Y., 1994. The astronomical theory of climate and the age of the Brunhes–Matuyama magnetic reversal, *Earth planet. Sci. Lett.,* **126,** 91–108.

Bentham, P., Collier, R.E.L., Gawthorpe, R.L., Leeder, M.R., Prossor, S. & Stark, C., 1991. Tectono-sedimentary development of an extensional basin: the Neogene Megara basin, Greece, *J. geol. Soc. Lond,* **148,** 923–934.

Billiris, H., Paradissis, D., Veis, G., England, P., Featherstone, W., Parsons, B., Cross, P., Rands, P., Rayson, M., Sellers, P., Ashkenazi, V., Davison, M., Jackson, J. & Ambraseys, N., 1991. Geodetic determination of tectonic deformation in central Greece from 1900 to 1988, *Nature,* **350,** 124–129.

Bloom, A.L., Broecker, W.S., Chappell, J., Mathews, R.K. & Mesolella, K.J., 1974. Quaternary sea-level fluctuations on a tectonic coast: New $^{230}Th/^{234}U$ dates from the Huon Peninsula, New Guinea, *Quat. Res.,* **4,** 185–205.

Bousquet, B., Dufaure, J.J. & Péchoux, P.Y., 1977. Le rôle de la géomorphologie dans l'évaluation des déformations néotectoniques en Grèce, *Bull. Soc. géol. Fr.,* **19,** 685–693.

Boyer, S.E. & Elliot, D., 1982. Thrust systems, *Am. Assoc. Petrol. Geol. Bull.,* **66,** 1196–1230.

Briais, A., Patriat, P. & Tapponnier, P., 1993. Updated interpretation of magnetic anomalies and seafloor spreading stages in the South China Sea, implications for the Tertiary tectonics of SE Asia, *J. geophys. Res.,* **98,** 6299–6328.

Brooks, M. & Ferentinos, G., 1984. Tectonics and sedimentation in the Gulf of Corinth and the Zakinthos and Kefallinia channels, Western Greece, *Tectonophysics,* **101,** 25–54.

Buck, W.R., 1993. The effect of lithospheric thickness on the formation of high- and low-angle normal faults, *Geology,* **21,** 933–936.

Burov, E.B. & Diament, M., 1992. Flexure of the continental lithosphere with multilayer rheology, *Geophys. J. Int.,* **109,** 449–468.

Byrd, O.D., Smith, R.B. & Geissman, J.W., 1994. The Teton fault, Wyoming: Topographic signature, neotectonics, and mechanisms of deformation, *J. geophys. Res.,* **99,** 20 095–20 122.

Chappell, J., 1974. Geology of coral terraces, Huon Peninsula, New Guinea: A study of Quaternary tectonic movements and sea-level changes, *Geol. Soc. Am. Bull.,* **85,** 553–570.

Chappell, J. & Shackleton, N.J., 1986. Oxygen isotopes and sea level, *Nature,* **324,** 137–140.

Chappell, J.M., 1983. A revised sea-level record for the last 300,000 years from Papua New Guinea, *Search,* **14,** 99–101.

Collier, R.E.L., 1990. Eustatic and tectonic controls upon Quaternary coastal sedimentation in the Corinth Basin, Greece, *J. geol. Soc. Lond.,* **147,** 301–314.

Collier, R.E.L., Leeder, M.R., Rowe, R.J. & Atkinson, T.C., 1992. Rates of tectonic uplift in the Corinth and Megara basins, Central Greece, *Tectonics,* **11,** 1159–1167.

Courtillot, V., Armijo, R. & Tapponnier, P. 1987. Kinematics of the Sinai triple junction and a two-phase model of Arabia-Africa rifting, in *Continental Extensional Tectonics,* eds Coward, M.P., Dewey, J.F. & Hancock, P.L., *Geol. Soc. Spec. Publ.,* **28,** 559–573.

Cowie, P.A. & Scholz, C.H., 1992a. Displacement-length scaling relationship for faults: data synthesis and discussion, *J. struct. Geol.,* **10,** 1149–1156.

Cowie, P.A. & Scholz, C.H., 1992b. Growth of faults by accumulation of seismic slip, *J. geophys. Res.,* **97,** 11 085–11 095.

Cowie, P.A. & Scholz, C.H., 1992c. Physical explanation for the displacement-length relationship of faults using post-yield fracture mechanics model, *J. struct. Geol.,* **14,** 1133–1148.

Dawers, N.H., Anders, M.H. & Scholz, C.H., 1993. Growth of normal faults: Displacement-length scaling, *Geology,* **21,** 1107–1110.

DeMets, C., Gordon, R.G., Argus, D.F. & Stein, S., 1990. Current plate motions, *Geophys. J. Int.,* **101,** 425–478.

Depéret, C., 1913. Observations sur l'histoire géologique pliocène et quaternaire du golfe et de l'isthme de Corinthe, *C.R. Acad. Sci. Paris,* **156,** 1048–1052.

Dinter, D.A. & Royden, L., 1993. Late Cenozoic extension in northeastern Greece: Strymon Valley detachment system and Rhodope metamorphic core complex, *Geology,* **21,** 45–48.

DMAAC (Defense Mapping Agency Aerospace Center), 1984. *Tactical Pilotage Chart, scale 1:500,000,* TPC G-3A, St. Louis, MN.

Doutsos, T. & Piper, D.J.W., 1990. Listric faulting, sedimentation, and morphological evolution of the Quaternary eastern Corinth rift, Greece: First stages of continental rifting, *Geol. Soc. Am. Bull.,* **102,** 81–829.

Dufaure, J.J., 1977. Néotectonique et morphogenèse dans une péninsule méditerranéenne: Le Péloponnèse, *Rev. Géog. Phys. Géol. Dyn.,* **19,** 27–58.

Dufaure, J.J. & Zamanis, A., 1980. Styles néotectoniques et étagements de niveaux marins sur un segment d'arc insulaire, le Péloponnèse, in *Proc. Conf. Niveaux marins et Tectonique Quaternaire dans l'Aire Méditerranéenne,* pp. 77–107, CNRS, Paris, France.

Eddington, P.K., Smith, R.B. & Renggli, C., 1987. Kinematics of Basin Range intraplate extension, in *Continental Extensional Tectonics, Spec. Publ. geol. Soc. Lond.,* **28,** 371–392.

Ellis, M.A. & King, G.C.P., 1991. Structural control of flank volcanism in continental rifts, *Science,* **254,** 839–842.

Eyidogan, H. & Jackson, J.A., 1985. A seismological study of normal faulting in the Demirci, Alasehir and Gediz earthquakes of 1969–1970 in Western Turkey: implications for the nature and geometry deformation in the continental crust, *Geophys. J. R. astr. Soc.,* **81,** 569–607.

Fletcher, R.C. & Hallet, B., 1983. Unstable extension of the lithosphere: a mechanical model for Basin and Range structure, *J. geophys. Res.,* **88,** 7457–7466.

Francheteau, J., Jaupart, C., Shen, X.-J., Kang, W.-H., Lee, D.-L., Bai, J.-C., Wei, H.-P. & Deng, H.-Y., 1984. High heat flow in southern Tibet, *Nature,* **307,** 32–36.

Freyberg, B., 1973. Geologie des Isthmus von Korinth, *Erlanger Geol. Abh.,* **95,** 1–183.

Froidevaux, C., 1986. Basin and Range large-scale tectonics: constraints from gravity and reflection seismology, *J. geophys. Res.,* **91,** 3625–3632.

Garfunkel, Z. & Bartov, Y., 1977. The tectonics of the Suez Rift, *Bull. geol. Surv. Isr.,* **71,** 1–44.

Gaudemer, Y., Jaupart, C. & Tapponnier, P., 1988. Thermal control on post-orogenic extension in collision belts, *Earth planet. Sci. Lett.,* **89,** 48–62.

Gautier, P. & Brun, J.-P., 1994. Ductile crust exhumation and extensional detachments in the central Aegean (Cyclades and Evvia Islands), *Geodinamica Acta,* **7,** 57–85.

Goetze, C., 1978. The mechanisms of creep in Olivine, *Phil. Trans. R. Soc. Lond.,* **A288,** 99–119.

HAGS (Hellenic army geographical service), 1975a, 1975b, 1976. *Topographic map of Greece, scale 1:50,000,* sheets Xilokastron, Korinthos, and Nemea.

HAGS (Hellenic army geographical service), 1980. *Topographic map of Greece, scale 1:5,000.*

Heezen, B.C., Ewing, M. & Johnson, H.L., 1966. The Gulf of Corinth floor, *Deep-Sea Res.,* **13,** 381–411.

Higgs, B., 1988. Syn-sedimentary structural controls on basin deformation in the Gulf of Corinth, Greece, *Basin Res.,* **1,** 155–165.

Holcomb, D.J., 1981. Memory, relaxation, and microfracturing in dilatant rock, *J. geophys. Res.,* **86,** 6235–6248.

Hubert, A., King, G.C.P., Armijo, R. & Meyer, B., 1996. Fault reactivation, stress interaction and rupture propagation in the 1981 Corinth earthquake sequence, *Earth planet. Sci. Lett,* in press.

IGME (Institute of Geology and Mineral Exploration), 1983. *Geological map of Greece, scale 1:500,000.*

Imbrie, J., Hays, J.D., Martinson, D.G., McIntyre, A., Mix, A.C., Morley, J.J., Pisias, N.G., Prell, W.L. & Shackleton, N.J., 1984. The orbital theory of the Pleistocene climate: support from a revised chronology of the marine $\delta^{18}O$ record, in *Milankovitch and Climate, Part I,* pp. 269–305, ed. Berger A, *et al.* Reidel, Dordrecht.

Jackson, J.A. & McKenzie, D.P., 1988. The relationship between plate motions and seismic tensors, and the rate of active deformation in the Mediterranean and Middle East, *Geophys. J.,* **93,** 45–73.

Jackson, J.A. & White, N.J., 1989. Normal faulting in the upper continental crust: observations from regions of active extension, *J. struct. Geol.,* **11,** 1–36.

Jackson, J.A., Gagnepain, J., Houseman, G., King, G.C.P., Papadimitriou, P., Soufleris, C. & Virieux, J., 1982. Seismicity, normal faulting and the geomorphological development of the Gulf of Corinth (Greece): the Corinth earthquakes of February and March 1981, *Earth planet. Sci. Lett.,* **57,** 377–397.

Jackson, J.A., Haines, J. & Holt, W., 1992. The horizontal velocity field in the deforming Aegean Sea region determined from the moment tensor of earthquakes, *J. geophys. Res.,* **97,** 17 657–17 684.

Jackson, J.A., Haines, J. & Holt, W., 1994. A comparison of satellite laser ranging and seismicity data in the Aegean region, *Geophys. Res. Lett.,* **21,** 2849–2852.

Jaeger, J.C. & Cook, N.G.W., 1969. *Fundamentals of Rock Mechanics,* Chapman and Hall, London.

Jolivet, L., Brun, J.P., Gautier, P., Lallemant, S. & Patriat, M., 1994. 3D-kinematics of extension in the Aegean region from the early Miocene to the present, insights from the ductile crust, *Bull. Soc. Géol. Fr.,* **165,** 195–209.

Kelletat, D., Kowalczyk, G., Schröder, B. & Winter, K.P., 1976. A synoptic view of the neotectonic development of the Peloponnesian coastal regions, *Z. Dtsch. Geol. Ges.,* **127,** 447–465.

Keraudren, B., 1970. Les formations quaternaires marines de la Grèce (première partie), *Bulletin du Musée d'Anthropologie et de Préhistoire de Monaco,* **16,** 6–153.

Keraudren, B., 1971. Les formations quaternaires marines de la Grèce (deuxième partie), *Bulletin du Musée d'Anthropologie et de Préhistoire de Monaco,* **17,** 87–169.

Keraudren, B. & Sorel, D., 1987. The terraces of Corinth (Greece)—a detailed record of eustatic sea-level variations during the last 500,000 years, *Mar. Geol.,* **77,** 99–107.

King, G.C.P. & Ellis, M.A., 1990. The origin of large local uplift in extensional regions, *Nature,* **348,** 689–693.

King, G.C.P. & Yielding, G., 1984. The evolution of a thrust fault system: process of rupture initiation, propagation and termination in the 1980 El Asnam (Algeria) earthquake, *Geophys. J. R. astr. Soc.,* **77,** 915–933.

King, G.C.P., Ouyang, Z.X., Papadimitriou, P., Deschamps, A., Gagnepain, J., Houseman, G., Jackson, J.A., Soufleris, C. & Virieux, J., 1985. The evolution of the Gulf of Corinth (Greece): an aftershock study of the 1981 earthquakes, *Geophys. J. R. astr. Soc.,* **80,** 677–683.

King, G.C.P., Stein, R.S. & Rundle, J.B., 1988. The growth of geological structures by repeated earthquakes. 1. Conceptual framework, *J. geophys. Res.,* **93,** 13 307–13 318.

King, G., Oppenheimer, D. & Amelung, F., 1994a. Block versus continuum deformation in the Western United States, *Earth planet. Sci. Lett.,* **128,** 55–64.

King, G.C.P., Stein, R.S. & Lin, J., 1994b. Static stress changes and the triggering of earthquakes, *Bull. seism. Soc. Am.,* **84,** 935–953.

Kissel, C. & Laj, C., 1988. The Tertiary geodynamical evolution of the Aegean arc: a palaeomagnetic reconstruction, *Tectonophysics,* **146,** 183–201.

Kissel, C., Laj, C. & Müller, C., 1985. Tertiary geodynamical evolution of northwestern Greece: palaeomagnetic results, *Earth planet. Sci. Lett.,* **72,** 190–204.

Kissel, C., Laj, C. & Mazaud, A., 1986. First palaeomagnetic results from neogene formations in Evia, Skyros and the Volos region and the deformation of central Aegea, *Geophys. Res. Lett.,* **13,** 1446–1449.

Kissel, C., Laj, C., Sengor, A.M.C. & Poisson, A., 1987. Paleomagnetic evidence for rotation in opposite senses of adjacent blocks in northeastern Aegea and western Anatolia, *Geophys. Res. Lett.,* **14,** 907–910.

Kusznir, N.J., Marsden, G. & Egan, S.S., 1991. A flexural cantilever simple shear/pure shear model of continental lithosphere extension:

applications to the Jeanne d'Arc Basin, Grand Banks, and the Viking Graben, North Sea, in *The Geometry of Normal Faults,* eds Roberts, A.M., Yielding, G. & Freeman, B., *Spec. Publ. geol. Soc. Lond.,* **56,** 41–60.

Lajoie, K.R., 1986. Coastal tectonics, in *Active Tectonics,* pp. 95–124, National Academic Press, Washington DC.

Lawn, B.R. & Wilshaw, T.R., 1975. *Fracture of Brittle Solids,* Cambridge University Press, Cambridge.

Le Pichon, X. & Angelier, J., 1981. The Aegean Sea, *Phil. Trans. R. Soc. Lond.,* **A, 300,** 357–372.

Le Pichon, X. & Chamot-Rooke, N., 1991. Extension of the continental crust, in *Controversies in Modern Geology,* pp. 313–338, Academic Press, London.

Leeder, M.R., Seger, M.J. & Stark, C.P., 1991. Sedimentation and tectonic geomorphology adjacent to major active and inactive normal faults, southern Greece, *J. geol. Soc. Lond.,* **148,** 331–343.

Leloup, P.H., Lacassin, R., Tapponnier, P., Schärer, U., Dalai, Z., Xiaohan, L., Liangshang, Z., Shaocheng, J. & Trinh, P.T., 1995. The Ailao Shan-Red River shear zone (Yunnan, China), Tertiary transform boundary of Indochina, *Tectonophysics,* **251,** 3–84.

Lowry, A.R. & Smith, R.B., 1994. Flexural rigidity of the Basin and Range—Colorado Plateau—Rocky Mountains transition from coherence analysis of gravity and topography, *J. geophys. Res.,* **99,** 20 123–20 140.

Lyon-Caen, H., Armijo, R., Drakopoulos, J., Baskoutass, J., Delibassis, N., Gaulon, R., Kouskouna, V., Latoussakis, J., Makropoulos, K., Papadimitriou, P., Papanastassiou, D. & Pedotti, G., 1988. The 1986 Kalamata (South Peloponnesus) earthquake: detailed study of a normal fault, evidences for east–west extension in the Hellenic arc, *J. geophys. Res.,* **93,** 14 967–15 000.

Machette, M.N., Personius, S.F., Nelson, A.R., Schwartz, D.P. & Lund, W.R., 1991. The Wasatch fault zone, Utah: segmentation and history of Holocene earthquakes, *J. struct. Geol.,* **13,** 137–149.

Makris, J., 1978. The crust and upper mantle of the Aegean region from deep seismic sounding, *Tectonophysics,* **46,** 269–284.

Mascle, J. & Martin, L., 1990. Shallow structure and recent evolution of the Aegean Sea: a synthesis based on continuous reflection profiles, *Mar. Geol.,* **94,** 271–299.

Masek, J.G., Isacks, B.L. & Fielding, E.J., 1994. Rift flank uplift in Tibet: evidence for a viscous lower crust, *Tectonics,* **13,** 659–667.

McKenzie, D., 1972. Active tectonics of the Mediterranean region, *Geophys. J. R. astr. Soc.,* **30,** 109–185.

McKenzie, D.P., 1978. Active tectonics of the Alpine-Himalayan belt: the Aegean Sea and surrounding regions, *Geophys. J. R. astr. Soc.,* **55,** 217–254.

McKenzie, D. & Jackson, J.A., 1983. The relationship between strain rates, crustal thickening, palaeomagnetism, finite strain and fault movements within a deforming zone, *Earth planet. Sci. Lett.,* **65,** 182–202.

Mercier, J.L., Carey, E., Philip, H. & Sorel, D., 1977. La néotectonique plio-quaternaire de l'arc egéen externe et de la mer Egée et ses relations avec la sismicité, *Bull. Soc. geol. Fr.,* **18,** 159–176.

Mercier, J.L., Sorel, D. & Vergely, P., 1989. Extensional tectonic regimes in the Aegean basins during the Cenozoic, *Basin Res.,* **2,** 49–71.

Merritts, D. & Bull, W.B., 1989. Interpreting Quaternary uplift rates at the Mendocino triple junction, northern California, from uplifted marine terraces, *Geology,* **17,** 1020–1024.

Molnar, P. & Chen, W.P., 1983. Focal depths and fault plane solutions of earthquakes under the Tibetan Plateau, *J. geophys. Res.,* **88,** 1180–1196.

Molnar, P. & Lyon-Caen, H., 1988. Some simple physical aspects of the support, structure, and evolution of mountain belts, *Geol. Soc. Am. Spec. Paper,* **218,** 179–207.

Mouyaris, N., Papastamatiou, D. & Vita-Finzi, C., 1992. The Helice Fault?, *Terra Nova,* **4,** 124–129.

Noomen, R., Ambrosius, B.C.A. & Wakker, K.F., 1993. Crustal motions in the Mediterranean region determined from laser ranging to LAGEOS, in *Contribution of Space Geodesy to Geodynamics: Crustal Dynamics,* eds Smith, D.E. & Turcotte, D.L., *AGU Geodyn. Ser.,* **23,** 331–346.

Oral, M.B., Reilinger, R.E., Toksöz, M.N., King, R.W., Barka, A.A., Kinik, I. & Lenk, O., 1995. Global Positioning System offers evidence of plate motions in Eastern Mediterranean, *EOS, Trans. Am. geophys. Un.,* **76,** 9–11.

Ori, G.G., 1989. Geologic history of the extensional basin of the Gulf of Corinth (?Miocene–Pleistocene), Greece, *Geology,* **17,** 918–921.

Papazachos, C.B. & Kiratzi, A.A., 1992. A formulation for reliable estimation of active crustal deformation and its application to Central Greece, *Geophys. J. Int.,* **111,** 424–432.

Papazachos, B.C. & Papazachos, C.B., 1989. The Earthquakes of Greece, Ziti Publications, Thessaloniki, Greece (in Greek).

Peltzer, G. & Tapponnier, P., 1988. Formation and evolution of strike-slip faults, rifts, and basins during the India–Asia collision: an experimental approach, *J. geophys. Res.,* **93,** 15 085–15 117.

Perissoratis, C., Mitropoulos, D. & Angelopoulos, I., 1986. Marine geological research at the E. Korinthiakos Gulf, *Special issue of Geology and Geophysical Research,* Institute of Geology and Mineral Exploration, Athens, Greece.

Ricard, Y. & Froidevaux, C., 1986. Stretching intabilities and lithospheric boudinage, *J. geophys. Res.,* **91,** 8314–8324.

Rigo, A., 1994. Etude Sismotectonique et Géodesique du Golfe de Corinthe (Grèce), *Thèse d'Université,* Univ. Paris VII, France.

Rigo, A., Lyon-Caen, H., Armijo, R., Deschamps, A., Hatzfeld, D., Makropoulos, K. & Papadimitriou, P., 1996. A microseismic study in the western part of the Gulf of Corinth (Greece): implications for large-scale normal faulting mechanisms, *Geophys. J. Int.,* in press.

Roberts, S. & Jackson, J., 1991. Active normal faulting in central Greece: an overview, in *The Geometry of Normal Faults,* eds Roberts, A.M., Yielding, G. & Freeman, B., *Spec. Publ. geol. Soc. Lond.,* **56,** 125–142.

Sauvage, J. & Dufaure, J.J., 1976. Sur une flore pré-Tiglienne dans la série marno-conglomératique corinthienne (Péloponèse, Grèce), *C.R. Acad. Sci. Paris,* **282,** 687–690.

Schlische, R.W., 1991. Half-graben basin filling models: new constraints on continental extensional basin development, *Basin Res.,* **3,** 123–141.

Schmidt, J.F.J., 1881. Studien über Vulcans und Erdbeben, Carl Scholtze, Leipzig.

Scholz, C.H., Dawers, N.H., Yu, J.-Z., Anders, M.H. & Cowie, P.A., 1993. Fault growth and fault scaling laws: preliminary results, *J. geophys. Res.,* **98,** 21 951–21 961.

Sébrier, M., 1977. Tectonique récente d'une transversale à l'Arc Egéen: le Golfe de Corinthe et ses régions périphériques, *Thèse 3ème cycle,* Univ. Paris-Sud, France.

Sengör, A.M.C., 1979. The North Anatolian transform fault: its age, offset and tectonic significance, *J. geol. Soc. Lond.,* **136,** 269–282.

Seyitoglu, G., Scott, B.C. & Rundle, C.C., 1992. Timing of Cenozoic extensional tectonics in west Turkey, *J. geol. Soc. Lond.,* **149,** 533–538.

Shackleton, N.J., 1987. Oxygen isotopes, ice volume and sea level, *Q. Sci. Rev.,* **6,** 183–190.

Smith, D.E., Kolenkiewicz, R., Robbins, P.J., Dunn, P.J. & Torrence, M.H., 1994. Horizontal crustal motion in the central and eastern Mediterranean inferred from SLR measurements, *Geophys. Res. Lett.,* **21,** 1979–1982.

Stein, R.S., King, G.C.P & Rundle, J.B., 1988. The growth of geological structures by repeated earthquakes. 2. Field examples of continental dip-slip faults, *J. geophys. Res.,* **95,** 13 319–13 331.

Stein, R., King, G.C.P & Lin, J., 1992. Change in failure stress on the southern San Andreas fault system caused by the 1992 magnitude = 7.4 Landers earthquake, *Science,* **258,** 1328–1332.

Stein, R.S., King, G.C.P. & Lin, J., 1994. Stress triggering of the 1994 M = 6.7 Northridge, California, earthquake by its predecessors, *Science,* **265,** 1432–1435.

Tapponnier, P., Peltzer, G. & Armijo, R., 1986. On the mechanics of

the collision between India and Asia, in *Collision Tectonics,* eds Coward, M.P. & Ries, A.C., *Geol. Soc. Spec. Publ.,* **19,** 115–157.

Tapponnier, P., Lacassin, R., Leloup, P.H., Schärer, U., Dalai, Z., Xiaohan, L., Shaocheng, J., Lianshang, Z. & Jiayou, Z., 1990. The Ailao Shan/Red River metamorphic belt: Tertiary left-lateral shear between Indochina and South China, *Nature,* **343,** 431–437.

Taymaz, T., Jackson, J.A. & McKenzie, D.P., 1991. Active tectonics of the north and central Aegean Sea, *Geophys. J. Int.,* **106,** 433–490.

Thatcher, W. & Rundle, J.B., 1979. A model for the earthquake cycle in underthrust zones, *J. geophys. Res.,* **84,** 5540–5556.

Turcotte, D.L. & Schubert, G., 1982. *Geodynamics: Applications of Continuum Physics to Geological Problems,* John Wiley, New York, NY.

UNESCO, 1981. *International bathymetry chart of the Mediterranean, scale 1:1,000,000,* Paris.

Valensise, G. & Pantosti, D., 1992. A 125 kyr-long geological record of seismic source repeatability: the Messina Straits (southern Italy) and the 1908 earthquake (Ms 7½), *Terra Nova,* **4,** 472–483.

Valensise, G. & Ward, S., 1991. Long-term uplift of the Santa Cruz coastline in response to repeated earthquakes along the San Andreas fault, *Bull. seism. Soc. Am.,* **81,** 1694–1704.

Vita-Finzi, C. & King, G.C.P., 1985. The seismicity, geomorphology and structural evolution of the Corinth area of Greece, *Phil. Trans. R. Soc. Lond.,* **314,** 379–407.

Wallace, R.E., 1981. Active faults, palaeoseismology, and earthquake hazards in the western United States, in *Earthquake Prediction: An international review,* Maurice Ewing Series, eds Simpson, D.W. & Richards, P.G., *Am. Geophys. Un.,* **4,** 209–216.

Walsh, J.J. & Watterson, J., 1988. Analysis of the relationship between displacements and dimensions of faults, *J. struct. Geol.,* **10,** 239–247.

Ward, S.M., 1986. A note on the surface volume change of shallow earthquakes, *Geophys. J. R. astr. Soc.,* **85,** 461–466.

Westaway, R., 1994. Evidence for dynamic coupling of surface processes with isostatic compensation in the lower crust during active extension of western Turkey, *J. geophys. Res.,* **99,** 20 203–20 223.

Zuber, M.T., Parmentier, E.M. & Fletcher, R.C., 1986. Extension of continental lithosphere: A model for two scales of Basin and Range deformation, *J. geophys. Res.,* **91,** 4826–4838.